MULTICOMPONENT GAS DIFFUSION AND ADSORPTION IN COALS FOR ENHANCED METHANE RECOVERY

A THESIS SUBMITTED TO THE DEPARTMENT OF ENERGY RESOURCES ENGINEERING

OF STANFORD UNIVERSITY

IN PARTIAL FULFILLMENT OF THE REQUIREMENTS FOR THE DEGREE OF MASTER OF SCIENCE

By
Abhishek Dutta
June 2009

I certify that I have read this report and that in my opinion it is fully adequate, in scope and in quality, as partial fulfillment of the degree of Master of Science in Petroleum Engineering.

_____

Prof. Anthony R. Kovscek
(Principal Advisor)

I certify that I have read this report and that in my opinion it is fully adequate, in scope and in quality, as partial fulfillment of the degree of Master of Science in Petroleum Engineering.

_____

Dr. Louis Castanier

Abstract

Selective adsorption and transport of gases in coal is important for enhanced natural gas recovery and carbon sequestration in depleted coal seams. Enhanced coalbed methane (ECBM) recovery by injection of CO_2 or mixtures of CO_2 and N_2 is an attractive method to recover additional natural gas resources while at the same time sequestering CO_2 in the subsurface. Transport and adsorption of $CH_4/CO_2/N_2$ within coal is investigated from a simulation perspective.

This thesis presents a numerical model of multicomponent (ternary) gas diffusion and adsorption in coal beds, focusing on CO_2, N_2-CH_4 counter diffusion and simultaneous adsorption associated with CO_2 sequestration enhanced coal bed methane (CO_2-ECBM) recovery. In this simulation study, we present, for the first time, consistent models to incorporate adsorption along with diffusion of multicomponent (ternary) gas mixtures. The diffusion model was developed based on Fick's diffusion, integrated with Maxwell-Stefan (MS) diffusion theory. The Maxwell-Stefan (MS) diffusion formulation deals rigorously with the interactions between multicomponent gas molecules. Many of the simulation models assume the linearized theory of diffusion. We avoid this deficiency by making the Fickian diffusivities as functions of MS diffusivities and composition. The extended Langmuir and Ideal Adsorbate Solution (IAS) models are used to model the adsorption phenomenon in ternary gas mixtures. From the literature, it has been found that the extended Langmuir model is inadequate to describe the behavior of ternary $CH_4/CO_2/N_2$ displacements. A sorption model more sophisticated than the Extended Langmuir model is needed to represent the dynamics of multicomponent systems. We use the IAS model and compare the predicted behavior against the extended Langmuir model. The numerical simulations in one-dimensional (1D) coal-bed are performed using a finite difference discretization method. Spatial discretization is performed using an implicit second-order centered scheme. The numerical scheme is unconditionally stable and guarantees convergence.

The comparative study suggests that the multicomponent sorption equilibria described using IAS and extended Langmuir models are quite different. IAS prediction however is strongly dependent upon the choice of pure gas isotherm equation. The results also show a significant effect of composition on diffusivities. Thus, concentration dependent diffusivities need to be taken into account in modeling the coalbed methane recovery, particularly for a multicomponent domain.

Acknowledgments

First and foremost, I offer my sincerest gratitude to my advisor Prof. Anthony R. Kovscek, who has supported me throughout my research with his patience and knowledge whilst allowing me room to work in my own way. This research would not have been possible without his constant input and moral support. I would like to thank Bolivia Vega for her guidance, time and strong encouragements with the CT scan experiments. I also wish to acknowledge Prof. Hamdi Tchelepi and Dr. Louis Castanier for making many useful suggestions.

Special thanks to all my friends and officemates for their friendship and co-operation and for making my stay at Stanford a wonderful and unforgettable experience. Finally, I am forever indebted to my fiancée and family for their countless support and encouragement when it was most required.

Financial support from the Department of Energy Resources Engineering, the Global Climate and Energy Project (GCEP) of Stanford University, affiliates of SUPRI-A and the Edmund Wattis Littlefield Fellowship is greatly acknowledged.

Contents

List of Tables

List of Figures

Chapter 1

1. Introduction

With rapid industrialization and growth in world population, energy demand is on the rise. Fossil fuels are the conventional sources of energy and their widespread consumption has lead to emission of vast amounts of greenhouse gases. One of the methods to reduce carbon dioxide (CO_2) concentration in the atmosphere is by sequestering it in geologic formations such as coalbed seams, depleted oil reservoirs and saline aquifers (IPCC, 2005). To be economically viable, geologic sequestration activities should be considered in conjunction with enhanced recovery of oil and natural gas.

Storage of CO_2 in coal seams is a potentially attractive carbon sequestration technology because it enhances methane (natural gas) production from coalbeds as well as has the potential to be carbon neutral and perhaps a carbon sink (Wong et al., 2000; Harris et al., 2008). In some cases, this can be cost effective as the additional CH_4 recovery from coal can either partially or completely offset the operational costs incurred.

Coal beds have large internal surface area and show a strong affinity towards methane (CH_4) and CO_2. In coal bed methane (CBM) reservoirs, most of the CH_4 is present in an adsorbed state at liquid like density, within the micropores. Only a small fraction of the gas is in a free phase. Primary recovery of this CBM involves dewatering the coalbeds, leading to reduced pressures. CH_4 then desorbs from the coal surfaces. Unfortunately, the primary recovery techniques recover less than half of the CBM in place (Stevens and Spector, 1998) and the costs of dewatering are significant. Injection of nitrogen (N_2) and CO_2, so called as enhanced coal bed methane (ECBM) recovery is a means to improve the ultimate recovery. The gas injection serves to reduce the partial pressure of CH_4, thereby leading to desorption from the coalbed but at the same time, maintains the coalbed reservoir pressure. In practice, ECBM injection gases are N_2 and/or CO_2. N_2 injection generally leads to a more rapid response whereas CO_2 injection leads to a more complete and better sweep. Moreover the coalbed surface shows a greater affinity towards CO_2 than CH_4 or N_2 (see Figure 1-3). As a result, the CH_4 is readily desorbed from the coalbed in the presence of CO_2 as the injectant (Tang et al., 2005).

Moving away from the big picture, there is a genuine lack of understanding of the mechanism of ECBM. This is partly because of the complicated structure of coalbed matrix. There are intricate networks of pore structures, as well as the coupled adsorption-transport mechanisms that take place as CO_2 is injected. Broadly categorizing, the physical mechanisms that dominate CO_2-ECBM recovery are multicomponent diffusion and adsorption. It is this interplay between the adsorption properties of coal surfaces and the advance of individual gas species that makes the theoretical and numerical modeling

such a difficult task. Apart from this, the heterogeneity of the coalbed and sorption induced permeability changes are other factors that contribute to the complexity. (Shi and Durucan, 2003; Lin et al., 2007).

This lack of understanding motivated us to undertake a simultaneous experimental and numerical model validation study of the CO_2-ECBM recovery process. There are several models that have been proposed for modeling multicomponent sorption on coal. The more popular ones are the extended Langmuir model (Ruthven, 1984 and Yang, 1987) and Ideal Adsorbate Solution (IAS) model (Myers and Prausnitz, 1965).

With this big picture in mind, the ensuing work is based on developing coupled adsorption-diffusion models for multicomponent systems. The modeling effort is complemented by a simultaneous experimental study of the CO_2- ECBM process. The experimental study concentrates on the use of X-ray Computed Tomography (CT) for observing single phase fluid flow within coal. The basic principle underlying CT scanning is the differential attenuation of a beam of X-rays as they pass through layers of varying thickness and density. The CT scans generate cross- sectional images of the coalpack and thereby assist in transient front tracking and flow profiling that otherwise is practically undetectable. The CT scanning also determines the dynamic phase saturation. Xenon was injected into the coalpack as the tracer gas because it is dense and gives good image resolution.

Technology development and application for CO_2- ECBM recovery is still at a nascent stage. The numerical simulation model is a useful tool for exploitation of CO_2 sequestration for ECBM recovery. The experimental study further aids in validating the simulation results. A complete description of the process is challenging because of the extreme complexity of the process. Nevertheless, the CO_2-ECBM process is technically and commercially viable. CO_2 enhances the CBM production rates, increases the overall recovery and offers important possibilities for making further use of fossil fuels more compatible with climate change and mitigation policies (Sengul, 2006). The Weyburn and Sleipner projects have demonstrated the feasibility of large scale CO_2 injection projects (Stevens and Spector, 1998; Sengul, 2006).

1.1. Pore structure of coal

The pore structure of coal is highly heterogeneous and varies with coal type and rank (Laxminarayana and Crosdale, 1990). Coalbeds are often characterized by two distinctive porosity systems: a uniformly distributed network of natural fractures and porous blocks between the cleats (King et al., 1986). The natural fractures (also known as cleats) can be subdivided into the face and butt cleat. The face cleat is continuous throughout the reservoir whereas the butt cleat is discontinuous and terminates at intersections with the face cleat (Figure 1-1). The cleat spacing is very uniform and ranges from the order of millimeters to centimeters (King et al., 1986).

The heterogeneous pore structure of coal offers pore sizes varying from a few Angstroms to over a micrometer in size, see Figure 1-2. According to the International Union of Pure and Applied Chemistry (IUPAC) classification (1994), pores may be classified into macropores (> 50 nm), transient or mesopores (between 2 and 50 nm) and micropores (< 2 nm). Determination of pore volumes and their distribution in coals is important to understand the storage and gas transport behavior of gases such as CO_2, CH_4 and/or N_2 in coalbeds.

Coalbed gas is retained in coals in the following ways: 1) physical adsorption upon internal surfaces (in micropores); 2) absorption into the molecular structure of coal; 3) as free gas in voids, cleats and fractures; and 4) as a solute in groundwater present within the coal seam (e.g., Rice, 1993). Gas adsorption upon the internal surface of the coal is considered, by far, the most important mechanism of gas retention and accounts for approximately 95-98% of the gas in coal seams (Clarkson and Bustin, 1999; Shi and Durucan, 2008). A significant portion of the pore volume is located in micropores (Sharkey and McCartney, 1981) and thus the potentially available sites for adsorption.

1.2. Adsorption in coal

Coalbeds have a large internal surface area and serve as favorable sites for adsorption of gases, particularly CH_4 and CO_2. In CBM reservoirs, most of the gas is present in an adsorbed state at liquid-like density (Tang et al., 2005). The CBM recovery process involves desorption of CH_4 gas from the coal matrix. The desorption phenomena is promoted by reduction in partial pressure of CBM in free gas.

Primary recovery using depressurization induces desorption by lowering the overall pressure of the reservoir. The depressurization is achieved by dewatering the reservoir. Unfortunately, such primary methods typically recover less than half of the CH_4 in a coalbed (Stevens et al., 1998).

On the other hand, enhanced recovery of coalbed methane (ECBM) by injecting a second gas or a mixture of gases is a means to increase the ultimate recovery. The gas injection maintains the overall pressure of the reservoir, while lowering the partial pressure of CBM in the free gas. The gas injectants also sweep the desorbed CH_4 through the reservoir. N_2 is a natural choice for ECBM due to its availability and the fact that it tends to yield a greater initial recovery rate (Zhu et al., 2003). CO_2 injection also has advantages in that CO_2 tends to adsorb to coal surfaces more strongly than either CH_4 or N_2, see Figure 1-3 (Tang el at., 2005).

Thus, one important aspect of ECBM is the adsorption and desorption behavior of gas mixtures on coalbeds. The extended Langmuir model (ELM) and IAS theory (Myers and Prausnitz, 1965) are most commonly used for the prediction of mixed gas adsorption on coal. The simplest model for prediction of multicomponent adsorption isotherms is the ELM:

$$a_i = \frac{\rho_i \rho_r V_{mi} B_i P_i}{1 + \sum_{j=1}^{n_C} B_j P_j} \tag{1-1}$$

where a_i is the molar concentration of the adsorbed component i (mol/l), ρ_r is the density of the coalbed, ρ_i is the molar density of component i at standard condition, and V_{mi} and B_i the pure gas isotherm Langmuir constants for component i at a given temperature and are normally expressed with units of psi^{-1} and scf/ton, respectively. The partial pressure, P_i of component i in the free gas phase is

$$P_i = y_i P \tag{1-2}$$

where y_i is the mole fraction of species i. The gas phase composition (C_i) is related to the total pressure (P) by the gas law

$$P_i = Z C_i R_g T \tag{1-3}$$

where Z is the gas compressibility ratio which takes into account the non-ideality.

Langmuir parameters for pure component isotherms are used to predict component adsorbed volumes for gas mixtures at any gas pressure and free gas composition. A convenient method for expressing the relative adsorption of components in an adsorption system is through the calculation of a separation factor. The separation factor, or selectivity ratio, for a binary gas adsorption system is defined as (Ruthven, 1984)

$$\alpha_{ij} = \frac{(x/y)_i}{(x/y)_j} \tag{1-4}$$

For the ELM, the separation factor is simply the ratio of the adsorption equilibrium constants for the pure component isotherms (Ruthven, 1984) and is independent of concentration and total pressure, see Figure 1-4 . The assumption of a constant separation factor is not necessarily accurate for all systems (Ruthven, 1984). An increasing selectivity for the most strongly adsorbed component with decreasing concentration of that component is generally observed (Myers, 1968). The assumptions associated with the derivation of the fundamental Langmuir equation, such as one molecule- one site interaction, no interaction among adsorbate molecules and constant heat of adsorption with loading are too restrictive and hence very often it does not describe well multicomponent adsorption equilibria.

Although fairly accurate in describing adsorption/desorption coupled with transport of a two component system (Tang et al., 2005, Jessen et al., 2007), the ELM is inadequate to describe the behavior of ternary $CH_4/CO_2/N_2$ displacements. The inaccuracy of the ELM

is especially evident in the work of Tang et al. (2005) who applied this adsorption model in flow simulations to interpret experimental observations from displacements of CH_4 by mixtures of CO_2 and N_2 in packs of dry, ground coal from the Powder River Basin. A sorption model more sophisticated than the extended Langmuir model is needed to represent the dynamics of multicomponent systems (Jessen et al., 2007).

The IAS theory (Myers and Prausnitz, 1965) is derived from the general theory of vapor-liquid equilibrium where the fugacity of a component in the vapor phase must be equal to that in the adsorbate phase. The IAS model is based upon the assumption that the adsorbed mixture behaves like an ideal, adsorbed solution (unit activity coefficient) and the gas phase behaves like an ideal gas (unit fugacity coefficient). This results in the following equilibrium relation between the gas phase mole fraction of a component and the adsorbed phase mole fraction (analogous to Raoult's law for bulk solutions):

$$y_i P = x_i P_i^o(\pi) \tag{1-5}$$

where P_i^o is the hypothetical gas (vapor) pressure of the pure component adsorbed at the same temperature and spreading pressure (π) as the solution. The spreading pressure for the pure components is determined through integration of the Gibbs adsorption isotherm to the vapor pressure of the pure component, P_i^o:

$$\pi_i^* = \frac{\pi_i A}{R_g T} = \int_0^{P_i^0} \frac{n(P)}{P} dP \tag{1-6}$$

where n(P) is the pure component adsorption isotherm. The spreading pressure (π) is defined as the reduction in surface tension of a surface due to the spreading of the adsorbate over the surface (Ruthven, 1984). At equilibrium, the spreading pressure evaluated for each component at the corresponding reference pressure (P_i^o) must be equal. Thus, for an n_C component mixture, this equilibrium relation is given as

$$\pi^* = \frac{\pi A}{R_g T} = \int_0^{P_1^0} \frac{n(P_1)}{P_1} dP_1 = \int_0^{P_2^0} \frac{n(P_2)}{P_2} dP_2 = \ldots = \int_0^{P_{n_C}^0} \frac{n(P_{n_C})}{P_{n_C}} dP_{n_C} \tag{1-7}$$

where n is the specific amount adsorbed. The total amount of adsorbed gas in the mixture (for an ideal solution) is given by

$$\frac{1}{n_t} = \sum_{i=1}^{n_C} \frac{x_i}{n_i^o} \tag{1-8}$$

The actual amount of each component adsorbed in the mixture is given by

$$n_i = n_t x_i \tag{1-9}$$

The IAS theory is thermodynamically consistent and takes into account the intermolecular interactions in a multicomponent sorption domain. Unlike the ELM, the IAS adsorption isotherm is sensitive to changes in concentration and pressure (i.e. separation factor is not constant), see Figure 1-4.

1.3. Gas transport in coal

Coalbeds presents a highly heterogeneous pore structure with a wide varying scale of pore sizes. It is generally assumed that the flow of gas (and water) through the cleats is laminar and obeys Darcy' law. On the other hand, gas transport through the porous coal matrix is controlled by diffusion (Shi and Durucan, 2008), see Figure 1-5. Three mechanisms have been identified for diffusion of an adsorbing gas in the matrix. They are molecular/bulk diffusion (molecule-molecule collisions dominate), Knudsen diffusion (molecule-wall collisions dominate) and surface diffusion (transport through physically adsorbed layer) (Saulsberry et al. 1996; Shi and Durucan, 2008). Gas diffusion in coals is significantly influenced by coal rank and lithotype, microstructure and secondary mineralization (Gamson et al., 1993; Gamson et al., 1996; Crosdale et al., 1998). As a result, the net effective diffusivity often includes contributions from more than one mechanism.

1.3.1. Molecular/Bulk diffusion

Molecular/bulk diffusion is significant for large pore sizes and high system pressures in which gas molecule-molecule collisions dominate over gas molecule-wall collisions. In this mode of transport, different species move relative to each other. The parameter characterizing this relative motion between species of different type is the binary diffusion coefficient, D_{ij} where the subscripts i and j denote the species i and j respectively. The expression of the molecular diffusion flux for the above case is given by

$$J_i = -D_{ij} \nabla C_i \tag{1-10}$$

where J_i is the molecular diffusion flux of i with respect to the binary mixture and D_{ij} is the Fickian diffusivity of component i with respect to j.

The above expression is the vector form of Fick's first law of diffusion. Concentration gradient is the driving force. We will be using the above formulation, wherein the diffusion is driven by concentration gradient. This is referred to as concentration diffusion or ordinary diffusion. There can, however be other kinds of diffusion based on the driving force, such as: thermal diffusion, which results from temperature gradient; pressure diffusion, resulting from a pressure gradient; and forced diffusion, which is caused by unequal external forces on the chemical species (Bird et al., 2002).

For non-ideal n_C component mixtures, there are $(n_C\text{-}1)$ independent diffusion fluxes expressed by the generalized Fick's law, and $(n_C\text{-}1)^2$ diffusion coefficients (Cussler, 1984; Taylor and Krishna, 1993). The expression of the molecular diffusion flux for the n_C component mixture is given by

$$\mathbf{J} = -[\mathbf{D}]\nabla \mathbf{C} \tag{1-11}$$

$$\mathbf{J} = \begin{pmatrix} J_1 \\ J_2 \\ \vdots \\ J_{n_C-1} \end{pmatrix} \quad \mathbf{C} = \begin{pmatrix} C_1 \\ C_2 \\ \vdots \\ C_{n_C-1} \end{pmatrix} \text{ and } [\mathbf{D}] = \begin{pmatrix} D_{1,1} & D_{1,2} & \cdots\cdots D_{1,n_C-1} \\ D_{2,1} & D_{2,2} & \cdots\cdots D_{2,n_C-1} \\ \vdots & \ddots & \\ D_{n_C-1,1} & & \cdots\cdots D_{n_C-1,n_C-1} \end{pmatrix} \tag{1-12}$$

The matrix $[\mathbf{D}]$ of Fick's diffusion coefficients is of dimension $(n_C\text{-}1) \times (n_C\text{-}1)$. Eq (1-11) in expanded form is

$$J_i = \sum_{j=1}^{n_C-1} D_{i,j} \nabla x_j \ , \ i = 1, \ 2, \ldots\ldots, \ n_C - 1 \tag{1-13}$$

The diagonal entries $D_{i,i}$; i=1,2,….., n_c-1 are known as the main diffusion coefficients and the off diagonal entities $D_{i,j}$; i,j=1,2,…, n_c-1 (i≠j) are known as the cross diffusion coefficients. Each cross term gives a measure of flux of one species that is engendered by the concentration gradient of a second solute. The cross diffusion coefficients are usually non zero and can be of either sign (Ghorayeb and Firoozabadi, 1999). In fact it is possible to alter the sign of these cross coefficients by altering the numbering of the components (Taylor and Krishna, 1993).

The matrix [**D**] is generally non symmetric ($D_{i,j} \neq D_{j,i}$), except for special cases. There are circumstances when the matrix [**D**] is diagonal and the diffusion flux of i is independent of the composition gradients of the other species. This happens for the case of a mixture of chemically similar species such as toluene-chlorobenzene-bromobenzene (Burchard and Toor, 1962) and in the case of infinite dilution (Taylor and Krishna, 1993). Thus for n_C-1 components infinitely diluted, the cross diffusion terms vanish.

For an n_C component mixture, Eq. 1-11 contains $(n_C\text{-}1)^2$ diffusion coefficients. This implies that one component must be arbitrarily designated as the solvent n_C (Cussler, 1984). The n_C^{th} component diffusion flux J_{nc} is not independent and is obtained from the constraint equation (Cussler, 1984; Taylor and Krishna, 1993):

$$\sum_{i=1}^{n_C} J_i = 0 \tag{1-14}$$

Fick's law of diffusion is widely used to describe the coal bed gas diffusion process because of its simplicity. If used in its actual form, its validity is severely restricted and even misleading in many practical situations where the diffusion coefficients of the fluid species depend on composition.

The Maxwell-Stefan (MS) diffusion formulation better applies to multicomponent (n_C>2) fluid diffusion and deals rigorously with the interactions between multicomponent gas molecules (Wei et al., 2007). The MS approach basically involves the concept of force and friction between molecules of different types. The driving force F_i on a component i surrounded by other components j is given by

$$F_i = \sum_{j \neq i} \zeta_{i,j} y_j (u_i - u_j) \tag{1-15}$$

where $\zeta_{i,j}$ is the friction coefficient between i and j, y_j is the mole fraction of j and u_i and u_j are the diffusive species velocities. The friction coefficients $\zeta_{i,j}$ are closely related to the MS diffusivities ($Đ_{ij}$). The simple relation between the two is

$$Đ_{i,j} = RT / \zeta_{i,j} \tag{1-16}$$

The above is the classical expression of the MS approach. The more commonly used expression for the MS formulation is given as (Taylor and Krishna, 1993; Bird et al., 2002)

$$d_{F,i} = \left(\frac{1}{P}\right) \nabla P_i = -\sum_{j=1}^{n_C} \frac{y_i y_j (u_i - u_j)}{Đ_{i,j}} \tag{1-17}$$

where $d_{F,i}$ is the driving force for diffusion of species i in an ideal gas mixture at constant temperature and pressure. The above expressions are more useful when written in terms of molar fluxes $N_i = C_i u_i$. For a mixture of ideal gases, the $Đ_{ij}$ are composition independent and $Đ_{ij}$>0 (Taylor and Krishna, 1993). For the non ideal case, the $Đ_{ij}$'s are composition dependent. Based on the second postulate of irreversible thermodynamics, the coefficients $Đ_{ij}$ are symmetric (Onsager reciprocal relation; Muckenfuss, 1973, Leahy-Dios and Firoozabadi, 2007):

$$Đ_{i,j} = Đ_{j,i} \tag{1-18}$$

For an n_C component mixtures, there are $n_C(n_C-1)/2$ MS diffusion coefficients (Leahy-Dios and Firoozabadi, 2007). In the limiting case for some simple diffusion cases, the MS

equation does yield Fick's equation (Wesselingh and Krishna, 2000). Even in a binary mixture, the Fickian and MS diffusivity are close in magnitude but these have a different meaning and a different behavior (Wesselingh and Krishna, 2000).

The Maxwell-Stefan (MS) diffusion formulation deals rigorously with the interactions between multicomponent gas molecules and better applies to multicomponent fluid diffusion (Wei et al., 2007; Wesselingh and Krishna, 2000). In our case, the simplicity of the Fickian diffusion expression has been retained but at the same time the MS approach is incorporated to describe the transient multicomponent gas diffusion dynamics. The MS diffusivities ($Đ_{ij}$) are used to compute the Fickian diffusivities.

For a binary gas mixture, the gas diffusivities are estimated quite well from the kinetic theory of gases. The Chapman-Enskog theory (Chapman and Cowling, 1970) is the most common method for theoretical estimation of gaseous diffusion coefficients. The equation is as follows

$$D_{AB} = \frac{1.86\times10^{-3}T^{3/2}(1/M_1 + 1/M_2)^{1/2}}{P\sigma_{AB}^2\Omega_D} \tag{1-19}$$

where D_{AB} is the binary diffusion coefficient in cm^2/s, T is temperature in K, P is pressure in atm, M_A and M_B are molecular weights of A and B in gm/mol, σ_{AB} is the collision diameter in Å and Ω_D is the diffusion collision integral.

The above formulation is accurate up to pressures of 1 MPa (Wesselingh and Krishna, 2000) beyond which the assumptions of the kinetic theory of only binary collisions and a "mean free path" much larger than the molecule diameter are not correct. The predictions from the Chapman-Enskog kinetic theory tend to be limited in two ways (Cussler, 1984). Firstly they require estimates of σ_{AB} and Ω_D that are not available for all gases and secondly, the theory assumes non polar gases. In order to cope with this complexity, many empirical correlations have been developed. These include the method by Wilke and Lee (1955):

$$D_{AB} = \frac{[3.03 - (0.98/M_{AB}^{1/2})](10^{-3})T^{3/2}}{PM_{AB}^{1/2}\sigma_{AB}^2\Omega_D} \tag{1-20}$$

where D_{AB} is the binary diffusion coefficient in cm^2/s, T is temperature in K, P is pressure in bar, M_A and M_B are the molecular weights of A and B in gm/mol, σ_{AB} is the collision diameter in Å and Ω_D is the diffusion collision integral. $M_{AB} = 2[(1/M_A) + (1/M_B)]^{-1}$.

A correlation due to Fuller et al. (1966, 1969) is recommended by Reid at al. (1987) and by Danner and Daubert (1983).

$$D_{AB} = \frac{0.00143T^{1.75}}{PM_{AB}^{1/2}[(\sum_v)_A^{1/3} + (\sum_v)_B^{1/3}]^2} \quad (1\text{-}21)$$

where D_{AB} is the binary diffusion coefficient, cm^2/s, T is temperature in K, P is pressure in bar, M_A and M_B are the molecular weights of A and B in gm/mol, σ_{AB} is the collision diameter in Å, Ω_D is the diffusion collision integral and Σ_V is the sum of atomic diffusion volumes for each component (Tabulated by Fuller et al., 1969). $M_{AB} = 2[(1/M_A) + (1/M_B)]^{-1}$.

A detailed example for estimating binary diffusion coefficients using the above correlations is given in Appendix A. Multicomponent effects are most significant when the system is concentrated and contains interacting species (Cussler, 1984). So for the case of mixture of ideal gases at low to moderate pressures with more than two components, one can simply use the above binary diffusion coefficients (Wesselingh and Krishna, 2000). In the past, attempts to measure multicomponent diffusion coefficients have been limited. Most correlation for multicomponent diffusion coefficients are mainly based on data for binary diffusion coefficients (Mathur and Thodos, 1965; Dawson et al. 1970; Takahasi et al. 1974; Sigmund 1976a, 1976b; Riazi and Whitson, 1993). But almost all these correlations neglect the cross diffusion coefficients at non-ideal conditions and assume effective diffusivity, meaning the diffusion flux of component i depends only on its composition gradient (Hoteit and Firoozabadi, 2006).

1.3.2. Knudsen diffusion

If the pores are very small, a particular gaseous molecule will collide more often with the pore walls and not very frequently with other molecules. This type of transport is called Knudsen diffusion (Knudsen, 1950). It is important when the mean free path (distance between molecular collisions) is greater than the pore diameter. This normally occurs at very low pressures and channels of small size, usually of order of 10nm to 100 nm (Do, 2008). Under such conditions, the molecules bounce from wall to wall, rather than colliding with themselves. The driving force for such a transport is the concentration gradient and the parameter characterizing this transport is called the Knudsen diffusivity $D_{K,i}$ for the species i (Eq. 1-23)

$$J_i = -D_{Ki}\nabla C_i \quad (1\text{-}22)$$

During Knudsen flow, the intermolecular interactions are less as the diffusing molecules predominantly bounce from wall to wall. As a result, unlike the case of molecular/bulk diffusion, the Knudsen diffusion for a component in a multicomponent gas mixture is driven only by its own concentration gradient (Cussler, 1984; Fathi and Akkutlu, 2008). The Knudsen diffusion coefficient D_{Ki} can be found for dilute gases from (Evans et al., 1961) as

$$D_{Ki} = 4850d\sqrt{T/M} \tag{1-23}$$

where d is pore diameter in cm, T is temperature in K, M is molecular weight and D_{Kn} is in cm^2/s.

The Knudsen flow is quantified using the Knudsen number (Cunnigham and Williams, 1980) defined as Kn = λ/d, where λ is the mean free path and d is the pore diameter. When this number is much larger than unity, we have Knudsen flow. According to Yang (1997), Knudsen diffusion may be assumed when the mean free path is greater than ten times the pore diameter. In the intermediate zone, both wall collisions and intermolecular collisions contribute to diffusional resistance, and the net diffusivity depends on both molecular and Knudsen diffusivities. In order to calculate the Knudsen number, one must first estimate the mean free path (λ) of the diffusing species. This is done using the given expression (Cunnigham and Williams, 1980):

$$\lambda = \frac{k_B T}{\sqrt{2}(\pi\sigma^2_{ii} P)} \tag{1-24}$$

where σ_{ii} is the collision diameter of the diffusing species and k_B is the Boltzmann constant.

The mean free path for CO_2, N_2 and CH_4 has been calculated (see Appendix A.2 for details) for a set of pressure-temperature conditions found in-situ Powder River Basin, Wyoming (Moore, 2003). It is of the order of 2.5 nm. This means that for the given in situ temperature and pressure conditions of Wyoming coal, the Knudsen domain will be dominant for pore diameters much smaller than 2 nm. But, because of the dependence of mean free path on pressure, there can be a transition from Knudsen flow at low pressures to molecular diffusion at high pressures (Smith and Williams, 1984). Generally speaking, the contribution of Knudsen diffusion in the gas transport within coal matrix is expected to be lesser compared to molecular/bulk diffusion.

1.3.3. Surface diffusion

Surface diffusion involves the transport of molecules through the physically adsorbed layer along the pore wall surface. Owing to its complexity, this mode of transport is undergoing extensive research to better understand the diffusion phenomenon. This mechanism of transport becomes dominant for micro-pores and for strongly adsorbed species. The reason is that in very fine micropores (<1nm), the diffusing molecules never escape the potential field of the adsorbing surface and the transport involves the adsorbed molecules “hopping” across adsorption sites (Do, 1998).

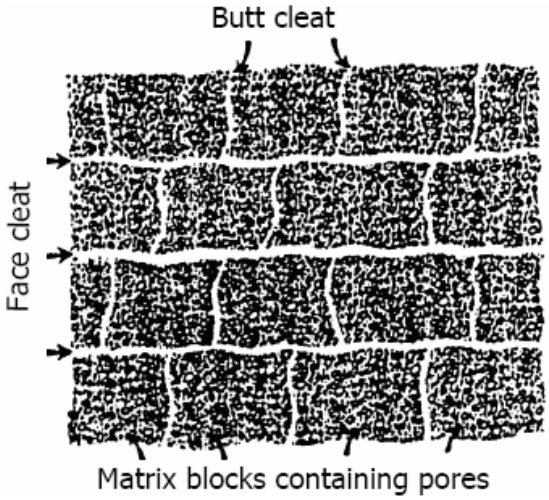

Figure 1-1: A schematic of coal structure (after King et al., 1986).

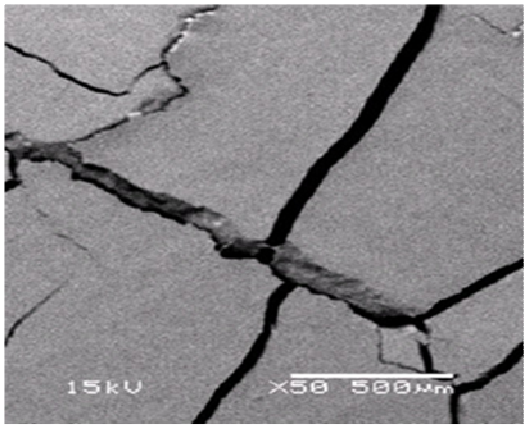

(a)

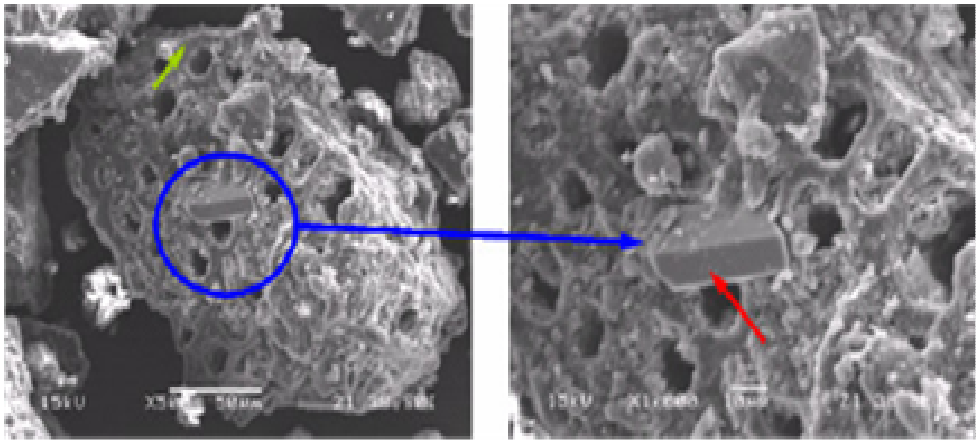

(b) (c)

Figure 1-2: SEM analysis of bituminous coal showing (a) cleats and fractures (b) coal matrix and (c) micropores (Liu, 2008).

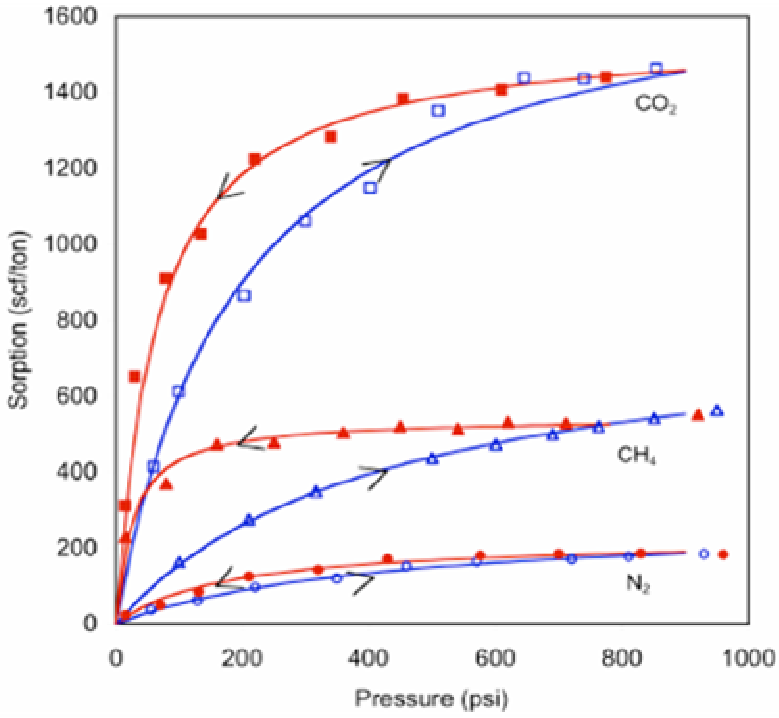

Figure 1-3: Sorption characteristics of Wyoming coal. Adsorption shown by open symbols and desorption with closed symbols (Tang et al., 2005).

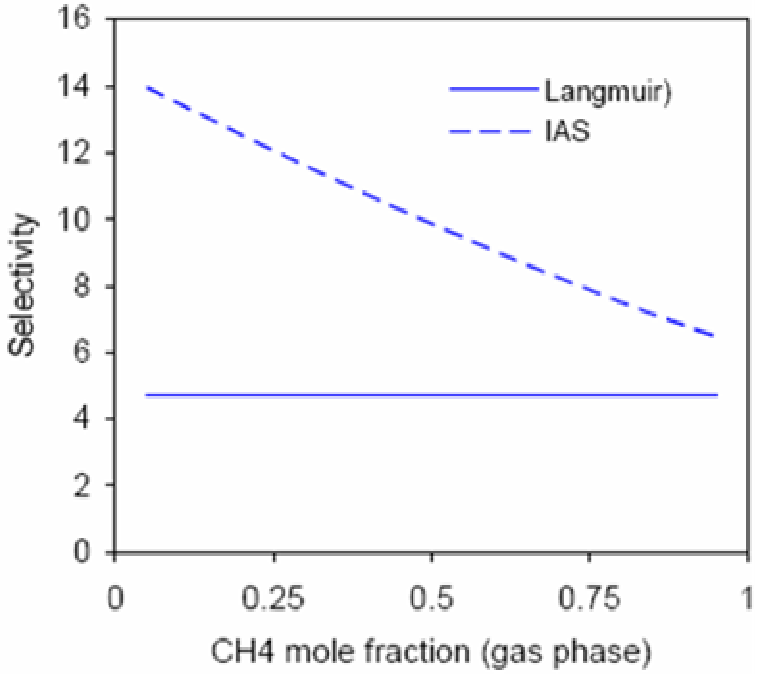

Figure 1-4: Selectivity of CH_4-CO_2 binary gas mixture at 600 psia and 22 ˚C predicted by IAS and Langmuir models (Jessen et al., 2007).

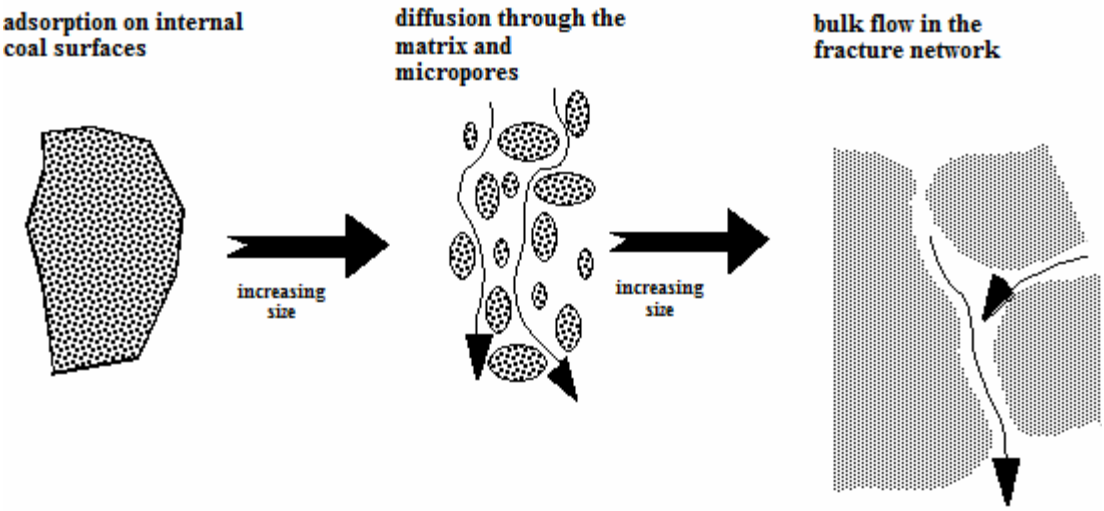

Figure 1-5: Schematic of CH_4 flow dynamics in coal seams (Kovscek, 2008). CH_4 desorbs from the internal coal surface, diffuses through the bulk matrix, and flows into and through the cleats. The pathway for CO_2 and/or N_2 is reversed.

Chapter 2

2. Modeling of gas transport in coalbeds

In Chapter 1.3 we have described how coalbeds present a highly heterogeneous pore structure with a wide varying scale of pore sizes. The gas flow in such geological formations involves two physically different set of transport processes; one is related to flow within fractures and cleats and the other is associated with much fine scale pore structures in matrix blocks between these fractures (Remner at al., 1984; King et al., 1986; Saulsberry et al. 1996; Gasem et al. 2003), see Figure 1-5. The transport of gases through coal seams is generally a two-stage process (Cervik, 1967). With water production (primary CBM recovery) or with gas injection (ECBM recovery), CH_4 is desorbed from the matrix blocks and migrates through the interconnected micropores to the cleats and fractures. Then the gas is transported along with brine through the cleats to drainage wells.

The gas transport within large scale fractures and cleats is driven by pressure gradients and described using Darcy law; while within small scale pore structures in matrix blocks, transport is diffusion dominated. Several kinds of diffusion mechanisms may be present, subject to in-situ pressure conditions and pore sizes (Saulsberry et al. 1996; Shi and Durucan, 2008). For these diffusion processes, the concentration gradient is the primary driving force (Lu and Connell, 2005).To deal with the transport problem of two greatly different spatial scales, dual-porosity models have been developed following the concept proposed by Barenblatt et al. (1960) and Warren and Root (1963). The Warren-Root model (Warren and Root, 1963) is a popular approach and most commonly used in a wide variety of commercial reservoir simulation codes. Also in case of coal, there is a strong interplay between adsorption and diffusion. The adsorption processes play a major role since CH_4 is primarily present in an adsorbed phase within coal matrix.

Significant gas storage (approximately 95-98%) in the coal seams, through the mechanism of physical adsorption, occurs in coal matrix (Clarkson and Bustin, 1999; Shi and Durucan, 2008).Gas adsorption takes place primarily in the micropores of the coal matrix. Thus, a detailed modeling of gas transport in the matrix blocks is important for accurate prediction of ECBM recovery. Keeping this fact in mind, in the ensuing modeling task a significant amount of work has been invested to model the complicated gas transport occurring in the pores within the matrix blocks. Once the gas transport within the matrix pores is modeled and verified, we go ahead and model the matrix-fracture transfer functions. The matrix-fracture transfer functions couple the diffusive gas transport within the matrix blocks with the bulk flow in cleats and fractures.

2.1. Modeling gas transport in coalbed matrix

The Warren-Root approach (Warren and Root, 1963) is the industry standard procedure for representing gas transport in dual-porosity media and implemented in many petroleum reservoir simulators. As a reservoir rock, coalbeds are characterized by two distinctive porosity systems: a well defined and almost uniformly distributed network of natural fractures and porous matrix blocks between the cleats (King at al., 1986). As a result in coalbed reservoirs, similar to naturally fractured petroleum reservoirs, an immediate extension of the Warren and Root (1963) model combining a pseudo-steady-sate assumption of adsorption behavior on the surface of the matrix blocks is used. With this approach, the Warren and Root model is applied to each individual gaseous component. For each component representation, an independent constant, called characteristic "adsorption time" or "diffusion time" is introduced that takes into account the matrix geometry and diffusion characteristics. The equation for the mass transfer between the cleat and matrix is given by (Shi and Durucan, 2005)

$$\frac{dV}{dt} = -\frac{1}{\tau}\left[V - V_E(P)\right] \tag{2-1}$$

where V and V_E are, respectively the average remaining gas content in the coal matrix and the gas content in equilibrium with cleat gas pressure P, and τ is the diffusion time constant/sorption time of the coal matrix. The sorption time (τ) is given by

$$\tau = \frac{1}{\sigma D_{eff}} \tag{2-2}$$

where D_{eff} is the effective diffusion coefficient of gas in coal matrix, and σ is the shape factor (Warren and Root, 1963).

The above is referred to as "unipore diffusion model" and is widely used in conventional dual-porosity coalbed reservoir simulators. The unipore models assume that there is negligible free gas in the coal matrix and that the gas only exists in an adsorbed state (Shi and Durucan, 2005). The assumption of no free gas in the matrix blocks is not true as in some low rank coals, it has been reported that free gas in the macropores of a coal matrix could comprise up to 70% of the total storage capacity (Bustin and Clarkson, 1999).

Unipore diffusion models when implemented in conventional coalbed reservoir simulators are found to be applicable only to some bright coals (coal consisting of alternating layers of clarain and vitrain; Smith and Williams, 1984; Clarkson and Bustin, 1999). There is strong laboratory evidence which suggests that many coals exhibit bimodal (such as micropores and macropores) or multimodal pore structure (Shi and Durucan, 2005). This motivated the development and implementation of the "bidisperse pore diffusion model" in coalbed reservoir simulators. In the bidisperse pore diffusion model, the coal seam is characterized using a triple porosity porous medium (Shi and

Durucan, 2005): (1) micropores, where gas sorption takes place; (2) macropores, where only free gas exits; and (3) cleats, where both gas and water phases are present, see Figure 2-30. In the bidisperse model, molar concentrations of free gas in the cleats and macropores and the adsorbed phase in the micropores are used as dependent variable. Just like the unipore quasi steady state sorption model, now there are two diffusion/adsorption time constants, similar to Eq. 2-2, defined for the micropores and macropores respectively (Shi and Durucan, 2005).

Both the bidisperse and unipore models invoke certain assumptions in the treatment of the diffusive mass transport, which in a multicomponent domain are questionable. In the formulation of the bidisperse and unipore model (such as Eq. 2-1,2-2), it was assumed that the diffusion could be modeled by a simple extension of Fick's law for mixed gases, and the diffusion of an individual gas component is independent of the other components in the system. An "effective diffusivity" parameter (D_{eff}) is defined, that is mathematically equivalent to considering the "self diffusion" process of each component in the porous medium, thereby omitting the interactions between gases (Taylor and Krishna, 1993; Lu and Connell, 2006). Theoretically, these interactions between gases can have significant impacts to flow (Cussler, 1984; Ghorayeb and Firoozabadi, 1999; Wesselingh and Krishna, 2000; Hoteit and Firoozabadi, 2006). Acknowledging these intermolecular interactions will result in non zero "cross diffusion" coefficients to appear in the diffusivity matrix [**D**]. Lu and Connell (2006) have shown that even if the cross diffusion coefficients are smaller by one order of magnitude than their self diffusion counterparts, the effect on model predictions can be as high as 10~35%.

Motivated by the above theoretical background, in our modeling approach the simplicity of the Fick's diffusion expression has been retained but at the same time the MS approach has been incorporated to describe the transient multicomponent gas diffusion dynamics. The MS diffusivities ($Đ_{ij}$) are used to compute the Fickian diffusivities. During ECBM recovery, a mixture of gases such as N_2 and CO_2 are co-injected to displace CH_4 gas that is otherwise not recovered by primary recovery methods. In the later stages of ECBM recovery, CH_4 concentration near the exit declines substantially. Because diffusion is driven by concentration gradient, this drop in gradient hinders the production of CH_4 from the pores. Our modeling effort is targeted towards capturing the physics of the ternary (three component) gas adsorption-diffusion dynamics. The idea is to understand the impact of intermolecular interactions and mass transfer limitations on the CH_4 production prediction. The strong interplay between adsorption and diffusion in the multicomponent (n_C>2) domain, greatly adds to the complexity. In order to the keep the problem simple, a model very similar to the unipore diffusion model has been implemented. The only difference is that in this case, unlike the unipore diffusion model, gas can co-exist as a free gas and as an adsorbed state in the coal matrix.

2.1.1. General mathematical model

The following assumptions are used to model the multicomponent gas diffusion and transport in coal matrix:

- The coal matrix is treated as rectangular block surrounded by well defined cleats and fractures (Warren and Root, 1963), see Figure 2-1.

- The matrix has a homogeneous uniform pore structure. As a result, the coalbed is treated as a fractured media having a dual-porosity.

- The gas in the matrix exists in an adsorbed state and as a free gas stored within the pore structure. The free gas behaves like an ideal gas. There is no water phase inside the coal matrix.

- The transport mechanism is molecular/bulk diffusion in the coal matrix. Based on the theoretical background stated in Chapter 1.3.2, Knudsen diffusion has been ignored.

- The MS approach has been incorporated into Fickian diffusion expression to describe the transient multicomponent (n_C=3) gas diffusion dynamics. The Fickian diffusivities are functions of gas compositions (non linearized theory of diffusion).

- Adsorption in the coal matrix is modeled using the ELM (Ruthven, 1984 and Yang, 1987) and IAS theory (Myers and Prausnitz, 1965).

- The gas phase is at constant pressure and mobile whereas the adsorbed phase is immobile.

- Pores are incompressible and the system is isothermal.

2.1.2. Simulation of ternary gas adsorption-diffusion

In the multicomponent (n_C>2) domain, it is the diffusion of gases that is the most intriguing part. The MS diffusion formulation better applies to multicomponent fluid diffusion and deals rigorously with the interactions between multicomponent gas molecules**.** The mathematical model stated in Chapter 2.1.1 is implemented in this case.

Eqs. 1-10, 1-11, 1-12 and 1-13 represent the molecular diffusion flux of an n_C multicomponent mixture. In our case, we have three components that are numbered as follows: component 1 is CO_2, component 2 is N_2 and component 3 is CH_4. The diffusion and adsorption of gases takes place inside a linear 1 D geometry, initially saturated with CH_4. CO_2 and N_2 diffuses from one end while CH_4 diffuses countercurrent to the flow of injectant gases, see Figure 2-2. In this case, there are two independent diffusion and four diffusion coefficients (Cussler, 1984; Taylor and Krishna, 1993). Choosing component 1 and 2 as the independent variables with respect to modeling diffusive flux, the diffusivity matrix [**D**] in this case is given by

$$[\mathbf{D}] = \begin{pmatrix} D_{11} & D_{12} \\ D_{21} & D_{22} \end{pmatrix} \tag{2-3}$$

The Fickian diffusivities in this case are not constant. They are functions of MS diffusivities ($Đ_{ij}$) and gas compositions. For the ternary (three components) case, the elements of the matrix [**D**] are given as (Taylor and Krishna, 1993)

$$\begin{aligned} D_{11} &= Đ_{13}\left(y_1 Đ_{23} + (1-y_1)Đ_{12}\right)/S \\ D_{12} &= y_1 Đ_{23}(Đ_{13} - Đ_{12})/S \\ D_{21} &= y_2\ Đ_{13}\left(Đ_{23} - Đ_{12}\right)/S \\ D_{22} &= Đ_{23}\left(y_2 Đ_{13} + (1-y_2)Đ_{12}\right)/S \\ S &= y_1 Đ_{23} + y_2 Đ_{13} + y_3 Đ_{12} \end{aligned} \tag{2-4}$$

The expression of the molecular/bulk diffusion flux for 1 and 2 is given by

$$J_1 = D_{11}\frac{\partial C_1}{\partial x} + D_{12}\frac{\partial C_2}{\partial x} \tag{2-5}$$

$$J_2 = D_{21}\frac{\partial C_1}{\partial x} + D_{22}\frac{\partial C_2}{\partial x} \tag{2-6}$$

The diffusion flux of component 3 is not independent. Based on the constraint relation given by Eq. 1-14 (Cussler, 1984; Taylor and Krishna, 1993), it is expressed as

$$J_3 = -\left(J_1 + J_2\right) \tag{2-7}$$

For the 3 component adsorption-diffusion problem, there are two species balance equation (Eqs. 2-8 and 2-9) and one overall mass balance relation (Eq. 2-10).

$$\phi\frac{\partial C_1}{\partial t} + (1-\phi)\frac{\partial a_1}{\partial t} = \phi\frac{\partial J_1}{\partial x} \tag{2-8}$$

$$\phi\frac{\partial C_2}{\partial t} + (1-\phi)\frac{\partial a_2}{\partial t} = \phi\frac{\partial J_2}{\partial x} \tag{2-9}$$

$$\phi\frac{\partial (C_1 + C_2 + C_3)}{\partial t} + (1-\phi)\frac{\partial (a_1 + a_2 + a_3)}{\partial t} = 0 \tag{2-10}$$

where C_1, C_2 and C_3 are the free gas compositions of CO_2, N_2, and CH_4 respectively and a_1, a_2 and a_3 are the adsorbate phase compositions of CO_2, N_2, and CH_4 respectively.

The ELM (Ruthven, 1984 and Yang, 1987) and IAS theory (Myers and Prausnitz, 1965) are most commonly used for the prediction of mixed gas adsorption on coal. In Part (I), the ELM is used and later on the IAS model is used in Part (II), and the results compared against the extended Langmuir model.

Part (I): Adsorption modeled using ELM

Eq. 1-1 represents the extended Langmuir model for an n_C component gas mixture. In our case, we have three adsorbing species and the amount adsorbed for component i is given as

$$a_i = \frac{\rho_i \rho_r V_{mi} B_i P_i}{1 + B_1 P_1 + B_2 P_2 + B_3 P_3} \tag{2-11}$$

Choosing the gas compositions as the dependent variables in the transport equations 2-8, 2-9 and 2-10, the partial pressure (P_i) is expressed as an explicit function of gas composition (C_i) using the ideal gas law. The adsorption term now reads

$$a_i = \frac{\alpha_i' C_i}{1 + \beta_1' C_1 + \beta_2' C_2 + \beta_3' C_3} \tag{2-12}$$

In the above expression for a_i, all the variables other than gas compositions are lumped together into the new variables α' and β' (modified Langmuir constants). Substituting the adsorption and diffusive flux terms in the transport equations (Eqs. 2-8, 2-9 and 2-10) results in the following coupled non linear partial differential equations:

$$\phi \frac{\partial C_1}{\partial t} + (1-\phi) \frac{\partial}{\partial t} \left(\frac{\alpha_1' C_1}{1 + \beta_1' C_1 + \beta_2' C_2 + \beta_3' C_3} \right) = \phi \left[\frac{\partial}{\partial x} \left(D_{11} \frac{\partial C_1}{\partial x} + D_{12} \frac{\partial C_2}{\partial x} \right) \right] \tag{2-13}$$

$$\phi \frac{\partial C_2}{\partial t} + (1-\phi) \frac{\partial}{\partial t} \left(\frac{\alpha_2' C_2}{1 + \beta_1' C_1 + \beta_2' C_2 + \beta_3' C_3} \right) = \phi \left[\frac{\partial}{\partial x} \left(D_{21} \frac{\partial C_1}{\partial x} + D_{22} \frac{\partial C_2}{\partial x} \right) \right] \tag{2-14}$$

$$\phi \frac{\partial (C_1 + C_2 + C_3)}{\partial t} + (1-\phi) \frac{\partial}{\partial t} \left(\frac{\alpha_1' C_1 + \alpha_2' C_2 + \alpha_3' C_3}{1 + \beta_1' C_1 + \beta_2' C_2 + \beta_3' C_3} \right) = 0 \tag{2-15}$$

The partial differential equations (PDE) describing the model are non-linear and solved numerically. The continuum equations were solved in the x-coordinate using the finite difference approximation. This leads to a set of coupled discretized equations that were solved for different spatial locations integrated in time using the non-linear form of Newton Raphson (NR) iteration technique. The fully implicit discretization method is used to solve the PDE's. The unknown C_i^{n+1} is now implicitly related to unknowns of the

neighbor grid points. The set of equations for all the grid points forms a tri-diagonal system of equations that needs to be solved at each time step.

For the ternary adsorption-diffusion transport problem, there are 3 primary variables (C_1, C_2 and C_3). Eqs. 2-17 and 2-18 describe the NR iterative procedure used to solve the coupled non linear PDE's.

$$[J]^{v}\,\delta y^{v+1} = -F^{v} \tag{2-16}$$

$$F = \begin{pmatrix} R_{11} \\ R_{21} \\ R_{31} \\ \vdots \\ \vdots \\ R_{1N} \\ R_{2N} \\ R_{3N} \end{pmatrix} \qquad \delta y = \begin{pmatrix} C_{11} \\ C_{21} \\ C_{31} \\ \vdots \\ \vdots \\ C_{1N} \\ C_{2N} \\ C_{3N} \end{pmatrix} \qquad [J] = \begin{pmatrix} & & \\ \frac{\partial R_{1,1}}{\partial C_{1,1}} & \frac{\partial R_{1,1}}{\partial C_{2,1}} & \cdots\cdots \frac{\partial R_{1,1}}{\partial C_{3,N}} \\ \frac{\partial R_{2,1}}{\partial C_{1,1}} & \frac{\partial R_{2,1}}{\partial C_{2,1}} & \cdots\cdots \frac{\partial R_{2,1}}{\partial C_{3,N}} \\ \vdots & & \\ \frac{\partial R_{3,N}}{\partial C_{1,1}} & \ddots & \cdots\cdots \frac{\partial R_{3,N}}{\partial C_{3,N}} \end{pmatrix} \tag{2-17}$$

where v is the iteration index, N is the number of discretized grid points, F is the residual vector, δ is the correction (update) vector and [J] is the Jacobian matrix. In our case, because we have three primary variables (C_1, C_2 and C_3) and a 1D rectangular model, [J] is a 3×3 block tri-diagonal matrix. All the Jacobian terms are derived by analytical differentiations of the residual equations.

As an example, Eq. 2-19 is the residual equation (R_{1i}) obtained upon discretizing the species balance PDE (Eq. 2-13). The structure of the residual equation (R_{2i}) for the other species balance equation (Eq. 2-14) is the same as R_{1i}, but with C_{2i} as the primary variable. The residual equation (R_{3i}) for the overall mass balance (Eq. 2-15) is shown in Eq. 2-20.

$$\phi\left(\frac{C_{1,i}^{n+1}-C_{1,i}^{n}}{\Delta t}\right)+\frac{(1-\phi)}{\Delta t}\left\{\frac{\alpha_1' C_{1,i}^{n+1}}{1+\beta_1' C_{1,i}^{n+1}+\beta_2' C_{2,i}^{n+1}+\beta_3' C_{3,i}^{n+1}}-\frac{\alpha_1' C_{1,i}^{n}}{1+\beta_1' C_{1,i}^{n}+\beta_2' C_{2,i}^{n}+\beta_3' C_{3,i}^{n}}\right\}-$$

$$\frac{\phi}{\Delta x^2}\left\{\begin{array}{l}\dfrac{Đ_{23}(C_{1,i}^{n+1}-C_{1,i}^{n})\left\{C_{1,i+1}^{n+1}(Đ_{23}-Đ_{12})+(C_{1,i+1}^{n+1}+C_{2,i+1}^{n+1}+C_{3,i+1}^{n+1})Đ_{12}\right\}}{(C_{1,i+1}^{n+1}Đ_{23}+C_{2,i+1}^{n+1}Đ_{13}+C_{3,i+1}^{n+1}Đ_{12})}-\\ \dfrac{Đ_{13}(C_{1,i}^{n+1}-C_{1,i-1}^{n+1})\left\{C_{1,i}^{n+1}(Đ_{23}-Đ_{12})+(C_{1,i}^{n+1}+C_{2,i}^{n+1}+C_{3,i}^{n+1})Đ_{12}\right\}}{(C_{1,i}^{n+1}Đ_{23}+C_{2,i}^{n+1}Đ_{13}+C_{3,i}^{n+1}Đ_{12})}+\\ \dfrac{Đ_{23}(Đ_{13}-Đ_{12})C_{1,i+1}^{n+1}(C_{2,i+1}^{n+1}-C_{2,i}^{n+1})}{(C_{1,i+1}^{n+1}Đ_{23}+C_{2,i+1}^{n+1}Đ_{13}+C_{3,i+1}^{n+1}Đ_{12})}-\dfrac{Đ_{23}(Đ_{13}-Đ_{12})C_{1,i}^{n+1}(C_{2,i}^{n+1}-C_{2,i-1}^{n+1})}{(C_{1,i}^{n+1}Đ_{23}+C_{2,i}^{n+1}Đ_{13}+C_{3,i}^{n+1}Đ_{12})}\end{array}\right\}=0 \qquad (2\text{-}18)$$

$$\phi\left\{\frac{(C^{n+1}{}_{1,i}+C^{n+1}{}_{2,i}+C^{n+1}{}_{3,i})-(C^{n}{}_{1,i}+C_{2,i}^{n}+C_{3,i}^{n})}{\Delta t}\right\}-$$

$$\frac{(1-\phi)}{\Delta t}\left\{\frac{\alpha_1' C^{n+1}{}_{1,i}+\alpha_2' C^{n+1}{}_{2,i}+\alpha_3' C^{n+1}{}_{3,i}}{1+\beta_1' C^{n+1}{}_{1,i}+\beta_2' C^{n+1}{}_{2,i}+\beta_3' C^{n+1}{}_{3,i}}-\frac{\alpha_1' C_{1,i}^{n}+\alpha_2' C_{2,i}^{n}+\alpha_3' C_{3,i}^{n}}{1+\beta_1' C^{n}{}_{1,i}+\beta_2' C^{n}{}_{2,i}+\beta_3' C^{n}{}_{3,i}}\right\}=0 \qquad (2\text{-}19)$$

The initial and boundary conditions are as follows. Initially, the coal matrix is saturated with CH_4 (C_3) while the concentrations of CO_2 (C_1) and N_2 (C_2) are very low (almost zero). Constant supply of injectants (CO_2 and N_2) is maintained at the inlet (x=0) while a no flux boundary condition is enforced at x=L. The numerical values associated with the above initial and boundary conditions are

- At t=0 $[C_1] = [C_2] = 0.02$ mol/l ; $[C_3] = 0.96$ mol/l for all x
- At x=0 $[C_1] = [C_2] = 1$ mol/l; $[C_3] = 0$ mol/l
- At x=L No flux

Figure 2-3, 2-4 and 2-5 illustrate the concentration profiles for CO_2, N_2 and CH_4 generated using a grid size (Δx) of 1mm and a time-step size (Δt) of 0.1s. The MS diffusivities used in this case are $Đ_{13}=0.05$ mm^2/s; $Đ_{12}=0.06$ mm^2/s; $Đ_{23}=0.03$ mm^2/s. The length of the domain in this case is 20 mm and the total time of simulation run is 625 seconds.

The simulation code is sensitive to the input MS diffusivity values with respect to stability. The set of runs are performed using large MS diffusivities in order to test the robustness of the numerical model. These values are: $Đ_{13}=0.2$ mm^2/s; $Đ_{12}=0.3$ mm^2/s; $Đ_{23}=0.1$ mm^2/s. Figure 2-6, 2-7 and 2-8 illustrate the concentration profiles for CO_2, N_2 and CH_4 generated using a grid size (Δx) of 1mm and a time-step size (Δt) of 0.1s. The length of the domain in this case is 10 mm and the total time of simulation run is 60 seconds. The fully implicit numerical scheme is found to be stable and it converges for a wide range of MS diffusivity inputs.

The high MS diffusivities result in rapid build up or decay of concentration profiles. One of the interesting observations from the concentration profile of CH_4 is the presence of very small concentration gradient in the vicinity of the CH_4 gas exit (x=0). Because the molecular diffusion is driven by concentration gradient, these low CH_4 concentrations near the boundary create potential mass transfer resistance, thus hindering the production of CH_4.

Unlike many of the simulation models that assume the linearized theory of diffusion, the Fickian diffusivities in our case are computed rigorously from MS diffusivities and composition (Eq.2-11). Figure 2-9, 2-10, 2-11 and 2-12 illustrate the variation of diffusivity parameters with time for the case when high MS diffusivity values were taken as input. For some cases, this variation is quite significant and has an important bearing on the gas adsorption-diffusion dynamics. For instance in this case, D_{21} varies by a factor of about 10 in Figure 2-11.

Part (II): Adsorption modeled using IAS theory

In Chapter 1.2 it was mentioned that the ELM shows no selectivity/sensitivity to changes in pressure and compositions, which according to Myers (1968) generally increases for the most strongly adsorbed component with decreasing concentration of that component. Because of the fundamental assumptions associated with the derivation of the ELM, it is often considered inadequate to describe well multicomponent adsorption equilibria (Tang et al., 2005). The IAS adsorption model on the other hand is sensitive to changes in pressure and compositions (Figure 1-4) and could possibly prove to be a better adsorption model for the case of multicomponent gas mixtures. We incorporate the IAS adsorption model into the numerical model and compare the predicted behavior against the extended Langmuir model.

The equations describing the IAS model are presented in Chapter 1.2. Eq. 1-5 is the fundamental IAS equation that relates the amount adsorbed (x) with the gas phase composition (y). Unlike the ELM, however the introduction of additional variable P_i^o (pure adsorbate pressure) makes the IAS model more complicated because now the adsorbate composition cannot be expressed directly in terms of the gaseous phase composition (Eq. 1-5). A nested iterative procedure was developed in order to solve for the case when the IAS model is incorporated. In order to cope with the seemingly complex adsorption-diffusion transport problem, the development of the algorithm was divided into two stages. This approach is similar to the flash in a conventional fully compositional simulator.

Stage 1:

The first stage deals with formulating the algorithm to compute the adsorbate composition (x_i) given the pressure and gas phase composition (Figure 22). It is based on the procedure outlined by Do (1998) and Jessen et al. (2007). It invokes NR iterations to

solve the non-linear transport problem. The algorithm is referenced as NR-1 and is used in stage 2 to solve the complete adsorption-diffusion transport problem.

At equilibrium, the spreading pressure evaluated for each component at the corresponding reference pressure (P_i^o) must be equal (Eq. 1-7). This equilibrium criterion is used as a constraint to frame the objective function for the NR solver. The NR solver iterates until the spreading pressures for all the components are equal, and when this is achieved, the adsorbate composition can be found using Eq. 1-5. The details of the algorithm are as follows:

Step 1: We calculate the spreading pressure for each pure component using Eq. 1-6. The integral in Eq. 1-6 can be simplified by assuming that the pure component adsorption behavior is represented sufficiently accurately by the Langmuir isotherm. Rewriting Eq.1-1 in terms of specific amount (scf/ton or mol/kg) and for a single component gives the following expression for the pure component Langmuir isotherm:

$$n_i = \frac{V_{mi} B_i P_i}{1 + B_i P_i} \tag{2-20}$$

Now substituting the above expression in Eq. 1-6 allows us to rewrite the integral for each component as

$$\pi_i^* = V_{mi} \ln(1 + B_i P_i^o) \tag{2-21}$$

The above equation gives the spreading pressures for each component, all of which are not necessarily equal. At equilibrium, the spreading pressures for each component are equal.

Step 2: The initial estimate of spreading pressure at equilibrium (π^*) is calculated by taking the molar average of the spreading pressures and assuming that the pure adsorbate pressure (P_i^o) for each component is equal to its partial pressure (P_i).

$$\pi^* = \sum_{i=1}^{n_C} y_i V_{mi} \ln(1 + B_i P_i) \tag{2-22}$$

Step 3: At equilibrium the spreading pressures of each component are equal ($\pi_1 = \pi_2 = \ldots = \pi_{nc} = \pi^*$). This means that by using the estimated reduced spreading pressure at equilibrium (π^*) from step 1 we can calculate the pure component pressure P_i^o at equilibrium. In order to do so, we solve Eq. 2-29 which results in the following expression for P_i^o:

$$P_i^o = \frac{\exp(\pi^* / V_{mi}) - 1}{B_i} \tag{2-23}$$

Step 4: Next, using Eq. 1-5 we formulate the objective function (residual) and solve for π^* using NR iterations.

$$F(\pi^*) = \sum x_i - 1 = \sum_{i=1}^{n_c} \frac{Py_i}{P_i^o(\pi^*)} - 1 = 0 \tag{2-24}$$

The residual (Eq. 2-32) is a function of only the spreading pressure (π^*) as the hypothetical pressure (P_i^o) is a function of the spreading pressure. The NR iteration formula for the reduced spreading pressure is

$$\pi^{*(v+1)} = \pi^{*(v)} - \frac{F(\pi^{*(v)})}{F'(\pi^{*(v)})} \tag{2-25}$$

where v is the NR iteration counter.

Step 5: Using the converged value of π^*, we compute the pure component pressure P_i^o using Eq. 2-31 and then the adsorbate composition (x_i) using Eq. 1-5.

Stage 2:

This part solves the ternary adsorption-diffusion transport problem (Eqs. 2-8, 2-9 and 2-10) using the IAS model. Unlike the previous case (Stage 1), the pressure and gas phase compositions are not known apriori. This makes the numerical solution strategy rather complicated and consequently, an iterative procedure has been developed to solve the transport problem. The fully implicit discretization technique is used to solve numerically the non-linear PDE's. Figure 2-14 illustrates the flowchart of the solution algorithm.

Step 1: Using the previous time step gas phase composition (y^n), we find the adsorbate composition (x^n) using the NR iterative procedure (NR-1) already developed in stage 1. This y^n and x^n serve as the initial guess for the next NR iteration (referenced as NR-2) to solve for y^{n+1} and x^{n+1} (concentrations at the next time step).

Step 2: The adsorption term using IAS model is a function of two variables, the gas phase composition and pure adsorbate pressure. In order to deal with this, we use the chain rule of differentiation, and express the adsorption term as:

$$\frac{\partial a_1}{\partial t} = \frac{\partial a_1}{\partial C_1}\frac{\partial C_1}{\partial t} \approx \left.\frac{\partial a_1}{\partial C_1}\right|^n \left(\frac{C_{1,i}^{n+1} - C_{1,i}^n}{\partial t}\right) \tag{2-26}$$

where, a_1 is the amount adsorbed for component 1 (CO_2) and the same being true for a_2. The above derivative is computed numerically and NR-1 function is invoked to do so. All of this done each time before the transport equations are solved.

Step 3: Once the initial guess values of x_i and y_i are known and the derivative of adsorption terms with respect to time numerically evaluated, we solve the discrete form of the transport equations using Newton-Raphson iterations.

Step 4: Once the gas phase compositions (y_i^{n+1}) converge, evaluate the adsorbate mole fraction (x_i^{n+1}) by doing a final NR-1 iterative flash.

Step 5: This completes the computation for a particular time step, after which we move to the next time step and repeat steps 1-4.

The initial and boundary conditions are as follows. Initially, the coal matrix is saturated with CH_4 (C_3) while the concentrations of CO_2 and N_2 are very low (almost zero). Constant supply of injectants (CO_2 and N_2) is maintained at the inlet (x=0) while a no flux boundary condition is enforced at x=L. The numerical values associated with the above initial and boundary conditions are

- At t=0 $[C_1] = [C_2] = 0.02$ mol/l ; $[C_3] = 0.96$ mol/l for all x
- At x=0 $[C_1] = [C_2] = 1$ mol/l; $[C_3] = 0$ mol/l
- At x=L No flux

Figure 2-15, 2-16 and 2-17 compare the concentration profiles for CO_2, N_2 and CH_4 generated using a grid size (Δx) of 1mm and a time-step size (Δt) of 0.5s. In order to show the robustness of the numerical model, high MS diffusivities are used for comparison purpose. In our case, these are: $Đ_{13}$=0.3 mm^2/s; $Đ_{12}$=0.3 mm^2/s; $Đ_{23}$=0.3 mm^2/s. The length of the core in this case is 10 mm and the total time of simulation run is 50 seconds.

From the concentration profiles one can see that there is substantial mismatch in prediction in the early transient phase. The mismatch is more prominent for the most strongly adsorbed components which in this case are CO_2 and CH_4. This suggests that probably the IAS model is more sensitive to dynamic changes in pressure and composition than the extended Langmuir model.

2.1.3. Sensitivity study

It is interesting to probe further into the fully implicit numerical solution technique. This is achieved by perturbing the simulation model and analyzing the impact on the simulation output.

The first part of the sensitivity study deals with the MS diffusivity input values. It was observed that for some high diffusivity values, the concentration of CH_4 goes negative

(aphysical solution). In order to circumvent this issue, the numerical model was modified based on the following two approaches:

Shoe-Horn Technique

The following is the shoe-horn tuning procedure. For each NR iteration, if the NR update results in a negative C_i^{n+1}, then the update is approximated in an exponential fashion.

- Calculate ΔC and C^{n+1}using NR iteration
- Check if ($C_i^{n+1}<0$) for any i
  $C^{n+1} = C^n \exp(\Delta C/C^n)$
  else
  $C^{n+1} = C^n + \Delta C$

Constrained NR Technique

The constrained NR technique is analogous to the penalty factor approach. In the penalty factor approach, penalty functions are included that give a strong penalty to any solution that tends to "wander" out of the dictated solution space. In our case, we introduce additional solution constraints that are based on our physical understanding of the problem. This is a commonly used simulation strategy involving NR iterative solver. Like in the previous case, if the NR update results in a negative concentration, the constrained NR technique sets that result to some positive value and thereby narrows down the search domain for the NR solver. This serves as the new guess to the NR solver for the next set of iterations.

- Calculate ΔC and C^{n+1}using NR iteration
- Check if the update results in $C_i^{n+1}<0$, then set it equal to some positive value
- This serves as the new guess for the NR solver
- Continue iterating and updating the C values

Figure 2-18 illustrates the impact of tuning based on the above two approach on the CH_4 concentration profile and compares it against the untuned model. ELM is used to model the adsorption behavior. The concentration profiles are for the same initial and boundary conditions as stated in the last case. A grid size (Δx) of 1mm and a time-step size (Δt) of 0.1s was chosen in this case. The MS diffusivity input values are $D_{13}=D_{12}=D_{23}=0.1$ mm^2/s. The shoe-horn tuning procedure was made to be default part of the simulation code to circumvent aphysical solutions at very long times or for very high MS diffusivity values.

Impact of MS diffusivity parameters

In this part of the sensitivity study, we study the adsorption-diffusion dynamics in ECBM under varying MS diffusivity parameters. The model takes the MS diffusivity parameters as input and then implicitly calculates the Fickian diffusivities (Eq. 2-4), however

because of lack of experimental data in the literature, the exact value of MS diffusivities are not known. With this understanding, we proceed by varying the magnitudes of MS diffusivity parameters and study their impact on the concentration profiles of ECBM gases inside the matrix.

The concept of self-similar solution of PDE's is invoked to plot the concentration profiles. The self-similarity method reduces the number of independent variables by introducing the so-called "similarity variable". Although our case is not exactly the pure parabolic diffusion case, we can still use the self-similar variable ξ (Eq. 3-3) defined in Chapter 3.2. This is made partially dimensionless by dividing ξ with the length of domain, L. As a result, the concentration profiles are transformed into characteristic curves that fall onto each other by plotting the concentration vs. the self similar variable ξ. From Figures 2-19 and 2-20, it is seen that with increasing MS diffusivity, there is improved influx of ECBM gases and a rapid depletion of CH_4 gas composition inside the matrix.

Impact of ELM adsorption parameters

In the ELM adsorption model, adsorption is defined via Langmuir parameters α and β (Eqs. 2-11 and 2-12). These adsorption parameters when substituted in the ELM formulation (Eq. 2-11) dictate the adsorbing capacity of gas specie. The α, β values for the base case are tabulated in Table 1. In this set of sensitivity runs, we study the impact of ELM adsorption parameters on the concentration profiles of ECBM gases. Keeping everything else the same, in one case the adsorption parameters are made half while in the other case, it is made double as that in the base case for all components. Note that the relative loading of the surface for a given species is unchanged.

Again the concentration profiles have been plotted against the dimensionless self similar variable ξ. From Figures 2-21 and 2-22, one can see that the gas adsorption-diffusion dynamics is not that sensitive to the ELM adsorption parameters. This is contingent, however, upon the fact that the values of the adsorbing species in the base case must be representative of the adsorption capacity of that gas species.

Impact of ECBM gas composition on CH_4 recovery

All the concentration profiles presented so far dealt with injection of an equimolar mixture of CO_2 and N_2. During ECBM recovery, usually a mixture of N_2 and CO_2 is co-injected and the gas composition is chosen in such a fashion so as to be able to maximize the CH_4 recovery. For this sensitivity study, we have taken different injection gas compositions and study the cumulative recovery (per unit volume) of CH_4 from the coal matrix.

From Figure 2-23 it is seen that with increasing concentration of N_2, there is rapid production of CH_4. The reason is explained based on the varying adsorption tendencies of N_2 and CO_2. The latter strongly adsorbs to the coal surface, as a result it is not able to

penetrate the system quickly. The concentration of N_2 on the other hand rapidly builds up within the coal matrix, which results in lowering the partial pressure of CH_4 and thereby leading to rapid desorption. Although the figure suggests that N_2 leads to a more rapid response, it has been found that CO_2 leads to a more complete displacement (Jessen et al., 2007).

Grid size and time step size sensitivity

The final part of the sensitivity study deals with the impact of time step size and grid size on the simulation convergence. The discretization of the differential equations yields a set of algebraic equations whose solution gives an approximate response at discrete points in the domain. In our case, Taylor series expansion was used to discretize the differential terms. But, while doing the above expansion, we take just a few a few terms and ignore the rest. This introduces a truncation error which is a function of the block size. In practice, the number of blocks is limited principally by the cost of calculations. For the grid sensitivity study, we start with a coarse grid model with 10 grid blocks and subsequently refine the grid (20 and 40 grid blocks), keeping the time step the same in all the cases (0.1 s). The length of the domain in this case was 20mm. Figure 2-24 shows the CO_2 concentration profile after 20s using MS diffusivities: $Đ_{13}$=0.09 mm^2/s; $Đ_{12}$=0.08 mm^2/s; $Đ_{23}$=0.07 mm^2/s. As the grid is made finer, the discretization truncation errors are reduced and the simulation results approach the exact analytical solution for the system under consideration. The coarse grid profiles almost overlap each other but differ slightly from the fine grid solution.

The discrete form of the transport equations involves a first order approximation in the time discretization. This means that for smaller time step sizes, the truncation error decreases; thus, resulting in more accurate concentration profiles. This is illustrated by Figure 2-25. Figure 2-25 shows the CH_4 concentration profile after 20s using MS diffusivities: $Đ_{13}$=0.09 mm2/s; $Đ_{12}$=0.08 mm2/s; $Đ_{23}$=0.07 mm^2/s. The length of the core in this case is 10mm. For larger time step sizes (0.3s and 0.5s), the concentration profiles exactly overlap but as the time step size is made smaller (0.1s), the truncation errors associated with time discretization reduce and the solution converges to the exact solution. Convergence is guaranteed for large time step sizes and this goes to show that the fully implicit solution method developed is unconditionally stable.

2.1.4. Model validation

The ternary adsorption-diffusion problem is complicated and the transport equations describing it are coupled non-linear PDE's. The non linear interplay between the adsorption and diffusion makes the analytical solution of the governing equations almost impossible. From the literature survey, it has been found that most of the research pertaining to transport of gases inside the coal matrix have assumptions of some kind that do not fit our mathematical model. Most of the transport models assume the linearized theory of diffusion such that the diffusivities are constant (Lu and Connell, 2006).

In our case, we have rigorously incorporated the MS approach along with Fick's diffusion, to take into account the intermolecular interactions. We thereby have the Fickian diffusivities as functions of composition and MS diffusivities. Also in the past, attempts to measure multicomponent diffusion coefficients have been limited. Most correlation for multicomponent diffusion coefficients are mainly based on data for binary diffusion coefficients (Mathur and Thodos, 1965; Dawson et al. 1970; Takahasi et al. 1974; Sigmund 1976a, 1976b; Riazi and Whitson, 1993). But almost all these correlations neglect the cross diffusion coefficients at non-ideal conditions and assume effective diffusivity, meaning the diffusion flux of component i depends only on its composition gradient (Hoteit and Firoozabadi, 2006). In our case, based upon the order of magnitude of some binary gas diffusivities, we have used synthetic MS diffusivities as the input. Because of lack of published literature and analytical solutions pertaining to our transport model, we have to resort to numerical techniques in order to validate the numerical model. The validation in done in two parts, both of which are completely different and mutually exclusive.

Part I: Reduction to a single component diffusion case

In order to verify the model developed for the ternary gas adsorption-diffusion case, the parameters in that model were changed appropriately to represent a single component diffusion process. The reduced order transport problem represents the diffusion (no adsorption) of CO_2 (no CH_4 and N_2) into a coal matrix. Keeping the coalbed geometry the same (Figure 2-2), the initial and boundary conditions are changed as follows

- At t=0 $[CH_4] = [N_2] = 0$ mol/l ; $[CO_2] = 0.02$ mol/l for all x
- At x=0 $[CH_4] = [N_2] = 0$ mol/ l; [CO] = 1 mol/l
- At x=L No flux

Specification of the above boundary and initial conditions reduces the model developed for multicomponent gas diffusion-adsorption case to a single component (in this case CO_2) case. However, by doing so the Jacobian matrix in the NR solver goes singular. For the case of N discretized grid blocks, the Jacobian for the model is of dimension 3N×3N and reducing the model results in zero values in the rows corresponding to concentration of CH_4 and N_2. In order to circumvent these issues, Jacobian reduction was performed and the non-zero rows related to concentration of CO_2 (C_1) are extracted. We thereby construct a Jacobian of dimension N×N.

The results generated by the reduced model were matched against the numerical code (representing the actual case) specifically written for the single component gas diffusion process. The transport problem specifically pertaining to the above case is mathematically represented as

$$\frac{\partial C}{\partial t} = D\frac{\partial^2 C}{\partial t^2} \tag{2-27}$$

where C is the concentration of CO_2 and D is the single component Fickian diffusivity.

Based upon the MS formulation given by Eq. 2-4, the Fickian diffusivity (D) in this case is equal to $Đ_{13}$ (MS diffusivity input in the model) and is a constant value. The above equation (Eq. 2-28) is discretized in an implicit fashion and results in a set of linear discrete equations represented in the form of Ay=b. The concentration value in the next time step (y) is solved by directly multiplying b vector with the inverse of A matrix (tri-diagonal matrix).

Figure 2-26 and 2-27 compare the concentration profiles generated by the reduced model against the actual case for two different input diffusivity values. A grid size (Δx) of 1mm and a time-step size (Δt) of 0.1s has been used. The length of the core in this case is 10 mm and the total time of simulation run is 500s. The profiles show an almost exact match for both the cases, thus verifying the simulation code developed for the ternary multicomponent gas adsorption-diffusion transport problem.

Part II: Perturbation technique to numerically construct the Jacobian

A more rigorous validation of the numerical model is to solve the full multicomponent transport problem using "numerical perturbation" technique. The derivatives required in the Jacobian of the fully coupled implicit system are approximated by numerical differences. In order to keep it simple, the following explanation of the perturbation technique is for a 1D single component case. For a 1D system discretized into N grid blocks, [J] is a N×N matrix, and from Eq. 2-18 it is seen that its elements are defined as

$$J_{i,j} = \frac{\partial F_i}{\partial (\delta y)_j} = \frac{\partial F_i(C)}{\partial C_j} \qquad i, j = 1, 2, ..., N \tag{2-28}$$

The element $J_{i,j}$ is approximated using a second order accurate central finite difference quotient

$$J_{i,j} \cong \frac{\Delta F_i(C)}{2\Delta C_j} \tag{2-29}$$

where

$$\Delta F_i(C) = F_i(C_1, ..., C_j + \Delta C_j, ..., C_N) - F_i(C_1, ..., C_j - \Delta C_j, ..., C_N) \tag{2-30}$$

ΔC_j is a small quantity (perturbation) and its choice has significant impact on the convergence, accuracy and stability of numerical methods. Decreasing the perturbation size reduces the truncation errors, but this would come at a price of computational cost. In our case, an adaptive algorithm is implemented to decide upon the optimal perturbation size. We initially start with a small perturbation (10^{-4}) and evaluate $J_{i,j}$. The algorithm then bisects this perturbation into half and re-computes $J_{i,j}$. If the difference between the two values is within the acceptable tolerance limit, then the algorithm steps out of the loop, otherwise it goes on bisecting and reducing the perturbation size. There, however, is

a minimum threshold size (user defined) beyond which the perturbation is no longer reduced. The decision of this threshold value is based on the computational cost constraint. In our case, this was kept equal to 10^{-10}. A sample of the MATLAB code implementing the above algorithm is given in Appendix B.1.

Figure 2-28 and 2-29 compare the concentration profiles for the two cases. A grid size (Δx) of 1mm and a time-step size (Δt) of 0.1s has been used. The length of the domain in this case is 10 mm and the total time of simulation run is 40s. In both the cases, different set of input MS diffusivity values have been used and from the figures one can see that both the models match almost exactly for the two different cases. Each time during a NR iteration, the Jacobian needs to be reconstructed. The perturbation technique involves a lot of numerical difference calculations for the derivatives in the Jacobian and for a much finer grid resolution, slows down the simulator immensely. The analytical Jacobian on the other hand is much faster even under fine scale grid resolution.

2.2. Modeling matrix-fracture interactions

Coalbeds are naturally fractured reservoirs (NFR) comprising of an interconnected fracture system that forms larger scale porous structures through which permeability flow travels according to Darcy's law and matrix blocks between those fractures with fine pores within which diffusion takes place. Although cleats and fractures are the main flow paths with considerably higher permeability, the matrix blocks have a much higher storage capacity for CH_4 gas (Beckner, 1990). As a result, flow between the matrix block and fracture is fundamental to the productivity of CH_4 gas from coal seams.

The Warren and Root (1963) dual-porosity model is used for characterization of coalbed reservoirs and implemented in conventional coalbed methane simulators. This is because the cleats are distributed uniformly in between the matrix blocks, and as a result coalbeds conform more to the idealized dual-porosity model (King et al., 1986) than NFR's. The following is the dual-porosity model for a 2D fracture defined by Warren and Root (1963) for a NFR:

$$\frac{k_{fx}}{\mu}\frac{\partial^2 p_f}{\partial x^2}+\frac{k_{fy}}{\mu}\frac{\partial^2 p_f}{\partial y^2}-\phi_m c_m\frac{\partial p_m}{\partial t}=\phi_f c_f\frac{\partial p_f}{\partial t} \tag{2-31}$$

where subscript f stands for fracture parameters and m for matrix parameters and c stands for compressibility of fluid.

In the dual-porosity model matrix-fracture interaction governing mass transfer between matrices and fractures is modeled through a "transfer function" (Barenblatt et al., 1960; Warren and Root, 1963) incorporating a "shape factor" (σ). For a NFR, this interaction has been defined in the following way

$$\phi_m c_m \frac{\partial p_m}{\partial t} = \frac{\sigma k_m}{\mu_f}(p_f - p_m) \tag{2-32}$$

In the derivation of the above equation, it was assumed that pseudo-steady state exists in the matrix and that the flow in it obeys Darcy's law. For the case of coalbed reservoirs, the above two equations need to be modified. This is because diffusion is the mode of mass transfer inside the coal matrix. Eq. 2-1 represents the matrix-fracture interactions during CBM recovery, assuming that pseudo-steady state condition exists. Eq. 2-2 describes the shape factor that quantifies the sorption/diffusion time within coal. The shape factor, σ, reflects the geometry of the matrix elements and is time independent for pseudo-steady state conditions. In the bidisperse model described by Shi and Durucan (2005), the coal matrix is treated as a cylindrical cell surrounded by main fractures, see Figure 2-30. Pseudo-steady state approach is used in formulating the two (since bidisperse) matrix fracture transfer functions, one for the macropore (σ_{macro}) and other for the micropore (σ_{micro}). The shape factors in their case are given by

$$\sigma_{micro} = \frac{15}{r_c^2} \tag{2-33}$$

$$\sigma_{macro} = \frac{15}{R_p^2} \tag{2-34}$$

where r_c and R_p are the radius of a microporous particle (crystal) and macroporous particle (pellet) respectively.

The above formulation by Shi and Durucan (2005) is implemented in most conventional CBM simulators. But for cases where rectangular geometry is assumed (Figure 2-31) for the matrix blocks (such as in ECLIPSE), a separate formulation of shape factor is used. This is given by (Kazemi et al., 1976)

$$\sigma = 4\left(\frac{1}{L_x^2} + \frac{1}{L_y^2} + \frac{1}{L_z^2}\right) \tag{2-35}$$

where L_x, L_y, and L_z are the typical X, Y and Z dimensions of the matrix blocks.

The classical pseudo-steady state approach for describing matrix-fracture transfer leads to constant shape factors. But many authors have reported that this is not true during the early transient times and result in discrepancies in experimental and simulation results. Rangel-German and Kovscek (2006) performed water imbibition experiments in a fractured porous media and found that the shape factor is time dependent when the fractures do not fill rapidly with water. Sarma and Aziz (2006) also reported that a constant value of shape factor cannot be used to get a good match at all times. As a result, alternate derivations of the shape factor have evolved that have avoided, at least partially

the pseudo-steady state assumption by combining the geometrical aspects of the systems with analytical solutions of the matrix transport equation. Lim and Aziz (1995) derived matrix fracture shape factors by truncating the infinite series solution to their pressure diffusion equation after the first term to obtain

$$\sigma = \frac{\pi^2}{(k_x k_y k_z)^{1/3}} \left[\frac{k_x}{L_x^2} + \frac{k_y}{L_y^2} + \frac{k_z}{L_z^2} \right] \tag{2-36}$$

where k_x, k_y, k_z are the permeabilities in X,Y and Z and L_x, L_y, and L_z are the typical X, Y and Z dimensions of the matrix blocks.

Although the pseudo-steady state assumption was not used explicitly in the derivation of Eq. 2-37, truncating the infinite series leads to inaccurate pressure distribution at early times. Chang (1993) also avoided the pseudo-steady state assumption and for 1D flow driven by pressure depletion in isotropic medium, the shape factor reads as

$$\sigma = \frac{\pi^2}{L_x^2} \frac{\sum_{m=0}^{\infty} \exp\left[-(2m+1)^2 \pi t_{DC} \right]}{\sum_{m=0}^{\infty} \frac{1}{(2m+1)^2} \exp\left[-(2m+1)^2 \pi t_{DC} \right]} \tag{2-37}$$

where

$$t_{DC} = \frac{k_x t}{L_x^2 \phi \mu c} \tag{2-38}$$

With time the above shape factor converges to that for 3D flow in fractured rock consistent with the result of Lim and Aziz (1995). Thus, from the preceding discussions it can be concluded that the matrix-transfer shape factor for dual-porosity simulators is a parameter encompassing both the geometry of the system and the physics of mass transfer in the matrix (Lim and Aziz, 1995).

With respect to CBM models, the standard industry practice is to assume a constant shape factor. The conventional CBM simulators define a sorption/diffusion time (such as Eq.2-2) which involves a constant effective diffusivity and a constant shape factor (Eqs. 2-34, 2-35), both of which are not true in complete sense. Wei et al. (2006) through their case study on numerical simulation of ECBM found that the gas diffusion rate cannot be described accurately using the Warren and Root model based on a pseudo-steady state assumption. They concluded that a more rigorous multicomponent diffusion model needs to be incorporated in CBM models.

The multicomponent CBM model that we have developed takes into account these intermolecular interactions by incorporating MS approach along with Fick's diffusion

(Eq. 2-4). In a multicomponent gas mixture, it is not accurate to assume a constant diffusivity (such as D_{eff}, Eq. 2-2) and in some simulation runs we found that there was significant variation of the Fickian diffusivity (Figure 2-11). In Chapter 2.1, we developed and validated the numerical model for mass transfer in coal matrix. We now go ahead and model the matrix-fracture transfer function. In our derivation of shape factor, we do not invoke the pseudo-steady state assumption and thereby, attempt to capture the transient matrix-fracture interactions. The coupled PDE's that describe the transport phenomena of mass transport in matrices (Eqs. 2-15, 2-16 and 2-17) are non linear and do not have any analytical solutions. As a result, in the results to follow, we don't really have an analytical expression for shape factor. Our idea is to be able to compute numerically the shape factor which can then be coupled with the fracture/cleat Darcy flow equations.

Methodology

- Solve the above matrix transport equations to obtain the gas composition C^{n+1}.

- Compute the volume averaged accumulation term Θ_{av} for the matrix block.

$$\Theta_{av} = \phi C_{av} + (1 - \phi - \phi_f)\, a_{av} \tag{2-39}$$

  where ϕ is the matrix porosity , ϕ_f is the fracture porosity and a is the adsorbate compostion.

- The volume average gas phase and adsorbate composition are approximated by numerical integration across the domain as

$$C_{av} = \frac{\sum_{i=1}^{N} V_i C_i}{\sum_{i=1}^{N} V_i} \qquad a_{av} = \frac{\sum_{i=1}^{N} V_i a_i}{\sum_{i=1}^{N} V_i} \tag{2-40}$$

  where N is the number of grid blocks, V_i, C_i and a_i, respectively, are the volume, gas composition and adsorbate composition of block i.

- In a dual-porosity media, all mass flow is from the matrix to fracture or vice versa. Therefore, the rate of matrix-fracture transfer is related to the rate of mass accumulation in the matrix as follows

$$q = -\frac{\partial \Theta_{av}}{\partial t} \tag{2-41}$$

- The derivative of the average accumulation term (Θ_{av}) is computed numerically as

$$\frac{\partial \Theta_{av}}{\partial t} \sim \frac{\Theta_{av}^{n+1} - \Theta_{av}^{n}}{\Delta t} \tag{2-42}$$

- The shape factor is then calculated from the following matrix-fracture mass transfer relation as a function of time:

$$\frac{\partial \Theta_{av}}{\partial t} = \phi \sigma D \left(C_f - C_{av} \right) \tag{2-43}$$

where C_f is the gas composition in the fracture.

- For the case of multicomponent gas mixtures, it is inappropriate to assume a single (effective) diffusivity for the gas component. Eq. 2-1 is the standard expression used in commercial CBM models. In our case, we retain the above expression but express D as a function of the Fickian diffusivities. For a ternary gas mixture, D for each component is given by

$$D_1 = D_{11} + D_{12} \frac{\nabla C_2}{\nabla C_1} \tag{2-44}$$

$$D_2 = D_{22} + D_{21} \frac{\nabla C_1}{\nabla C_2} \tag{2-45}$$

$$D_3 = -\frac{1}{\nabla C_3} \left[D_1 \nabla C_1 + D_2 \nabla C_2 \right] \tag{2-46}$$

where components that are numbered as follows: component 1 is CO_2, component 2 is N_2 and component 3 is CH_4.

- The inlet boundary condition for the matrix block serves as the fracture composition (C_f). Here, it is assumed that these values remain constant in the fracture and thus we do not solve the fracture flow equations simultaneously.

Based on the above methodology, we go ahead and investigate the shape factor for the following cases:

2.2.1. Single component diffusion

We start with the simple case and do a sensitivity analysis of the parameters on which the shape factor depends. The transport equation in 1D for a single component diffusing into a matrix (no adsorption) described using Fick's law, is given by Eq. 2-28. Figure 2-32 illustrates the geometry of the coalbed with the matrix block and single vertical fracture aligned perpendicular to the length of the block. The initial and boundary conditions for the base case are as follows

- At t=0 [Gas] = 0 mol/l for all x
- At x=0 [Gas] = 1 mol/l
- At x=L No flux

The length of the matrix block for the base case is 10 mm and the gas composition in the fracture is always assumed to be constant. The Fickian diffusivity in all cases is 0.1 mm^2/s unless otherwise mentioned. In the following sensitivity study, fine grid simulations were performed using a grid size of 0.1mm and time step size of 0.1s. The simulation study does not take into account the pseudo-steady state assumption while computing the shape factors.

Impact of length of matrix block

The shape factor depends on the geometry of the system. Based on the geometry, a characteristic length scale is defined. From literature survey, it has been found that the shape factor at late times is inversely proportional to the square of the characteristic length. Even during the early time period, the shape factor behaves qualitatively in a similar manner being greatest for the matrix block with the smallest dimension (Figure 2-33). At late times when pseudo-steady state commences, the shape factor is some constant multiple of the square of that characteristic length, see Figure 2-34. In our case at late times, the dimensionless parameter, σL^2, for various lengths of matrix blocks converge to a constant value of approximately 2.443.

Impact of Fickian diffusivity

For this sensitivity study, the input Fickian diffusivity was varied. Based on the shape factor formulation presented in Eq. 2-44, it is inversely proportional to the Fickian diffusivity, see Figure 2-35. Also from the figure, one can observe that varying the diffusivity impacts the shape factor only in the early transient times.

Impact of initial and boundary conditions

This part of the sensitivity study investigates the impact of initial and boundary conditions (gas composition in the fracture) on the shape factor. From Figure 2-36 and 2-37, one can observe that varying the initial and boundary condition has no impact on the shape factor even during the early transient phase (also mentioned by Sarma and Aziz, 2006).

Thus, from the above sensitivity study it becomes clear that the shape factor solely reflects the geometry of matrix elements and is time independent only under pseudo-steady state conditions. At early times, however, the shape factor is not a constant value and from Figures 2-34, 2-35, 2-36 and 2-37 one can see that depending on the diffusivity value and length of the matrix block, it rapidly drops to the constant pseudo-steady state value. In the early phases of mass transfer, the shape factor is much larger than the

constant stabilized value because the concentration gradient driving mass into the matrix from fracture is maximum, progressively decreasing with time. In all the sensitivity runs, we found that at late times the product of the shape factor and square of the length of matrix block (σL^2) for the given coalbed geometry and for the single component diffusion case comes out to be around **2.443**.

Regarding the early transient time, the initial and boundary conditions do not affect the shape factor. For the case that we have considered, it is only a function of diffusivity, characteristic length (length of matrix block) and time. A deeper investigation into the early transient behavior of shape factor reveals that the log-log plot of σL^2 with time results in straight lines with a -1/2 log slope, see Figure 2-38 and 2-39.

2.2.2. Single component diffusion and adsorption

In coal seams, the bulk of the CH_4 gas (approximately 95-98%) is stored in the coal matrix through the mechanism of physical adsorption (Clarkson and Bustin, 1999; Shi and Durucan, 2008). As a consequence, during a CBM recovery, there is a strong interplay between adsorption and diffusion. The transfer function quantifying CH_4 productivity thereby becomes a function of both adsorption and diffusion parameters.

Here, we investigate the shape factor for the case when an adsorbing species (such as CO_2, CH_4 or N_2) undergoes simultaneous adsorption and diffusion. We retain the same matrix-fracture coalbed geometry as above (Figure 2-32) and study the matrix-fracture interactions for a single gas component diffusing into a matrix from the fracture and undergoing adsorption as the same time. The initial and boundary conditions for the base case are as follows

- At t=0 [Gas] = 0 mol/l for all x
- At x=0 [Gas] = 1 mol/l
- At x=L No flux

The length of the matrix block for the base case is 20mm and the gas composition in the fracture is always assumed to be constant. The Fickian diffusivity in all cases is 0.1 mm^2/s unless otherwise mentioned. In the following sensitivity study, fine grid simulations were performed using a grid size of 0.1mm and time step size of 0.1s. The simulation study doesn't take into account the pseudo-steady state assumption while computing the shape factors. Adsorption is modeled using the extended Langmuir adsorption isotherm.

The transfer function takes into account the amount of mass transfer between the fracture and matrix. The shape factor quantifying this mass transport is a measure of rate at which the matrix gets saturated with incoming gas (for flow from fracture to matrix). With time, as the gas concentration in the matrix block builds up, the driving force for fracture-matrix mass transfer drops down and this is reflected by a decline in shape factor values. In case of adsorption, the gas molecules inside the matrix block can now exist both as a

free gas and as an adsorbate phase. This suggests that the rate of accumulation of an adsorbing gas species is higher than the pure diffusion case.

Figure 2-40 compares the shape factor for the pure diffusion case against the adsorption-diffusion case. For this comparative study, the dimensions of the coal matrix, the initial and boundary conditions are kept the same as the current base case. From the figure, one can see that when adsorption occurs, the shape factor value is greater and there is a prolonged transition period (gradual slope) before attaining pseudo-steady state. At late times, however, the shape factor appears to converge to the pure diffusion value. Also, comparing the shape factor for gases with varying adsorption capacities (by varying the Langmuir parameters), we observe that the gas with a strong adsorption tendency will induce greater matrix-fracture mass transport than a weakly adsorbing gas species, see Figure 2-41. As in the previous case, we now perform sensitivity runs on some key parameters and study their impact on the shape factor.

Impact of length of matrix block and Fickian diffusivity

From Figure 2-42 one can see that the shape factor follows the same trend as the pure diffusion case, being inversely related to the length of matrix block. At late times, the product of shape factor and square of length (dimensionless) appears to stabilize and converge for varying matrix lengths, see Figure 2-43. This means that under pseudo-steady state conditions, the shape factor can still be assumed to be a function of geometry of the matrix block.

Again as expected, the shape factor being inversely related to the Fickian diffusivity is highest for the gas with the lowest diffusivity and goes through a much prolonged transient phase (Figure 2-44). A gas with smaller diffusivity value takes longer to saturate the coal matrix.

Impact of initial and boundary conditions

This part of the sensitivity study investigates the impact of initial and boundary conditions (gas composition in the fracture) on the shape factor for the adsorption-diffusion case. We have seen that for a gas undergoing pure diffusion, the initial and boundary conditions have no impact on the shape factor values. But, this is not true anymore when adsorption phenomenon comes into play; see Figure 2-45 and 2-46. From both the figures, it appears that the shape factor shows an inverse relationship with initial gas concentration inside the matrix and the concentration in the fracture. This means that during transient times, in addition to matrix length and diffusivity value, the shape factor is also a function of initial and boundary conditions for adsorption-diffusion case.

The above sensitivity study reveals that including adsorption in the gas transport mechanism has a marked impact on the shape factor, especially during the early transient phase. Initially, the shape factor is huge and with time it gradually drops down. During this transient phase, the shape factor is now also a function of initial and boundary

conditions. The log-log plot of σL^2 with time during the early transient phase again results in straight lines with a -1/2 log slope, see Figures 2-47 and 2-48.

At late times, the σL^2 value for the different sensitivity runs appears to converge to the diffusion σL^2 value. Adsorption phenomenon substantially prolongs the commencement of pseudo-steady state conditions. This means that the assumption of constant shape factor based on the geometric parameters of the matrix block can presumably lead to significant deviations in the gas productivity prediction in conventional CBM models (based on constant shape factors). The deviations would be more significant for strongly adsorbing gas species such as CO_2 and/or CH_4.

The above sensitivity study underlines the dependence of shape factor on some key parameters and brings forth the difference in shape factor behavior for the case when adsorption phenomenon comes into play as against a pure diffusion scenario. It would be also interesting to study the impact of two component adsorption-diffusion on the shape factor magnitudes, considering the fact that now the two adsorbing species compete against each other for adsorbing space. In order to investigate this, we run a fine grid simulation using a grid size of 0.1mm and time step size of 0.1s on a core of length 10mm. For the sake of comparison, the diffusivity of both gases is kept the same (0.1 mm^2/s), but one of them is strongly adsorbing (gas A) and the other weakly adsorbing (gas B). We then compare this with the single component (gas A) adsorption-diffusion case. The diffusivity in this case is kept equal to the two component adsorption-diffusion case (0.1 mm^2/s). Figure 2-49 shows that the presence of another adsorbing species (in this case gas B) brings down the shape factor for the other component (gas B) from what it was in the single component adsorption-diffusion case. This is because the presence of another adsorbing gas lowers the overall adsorption capacity with respect to individual gas components.

Table 2.1: Base case ELM adsorption parameters for the ELM parameters sensitivity study.

Component	**α (mol/l-atm)**	**β (atm^{-1})**
CO_2	0.2232	0.0766
N_2	0.0148	0.0356
CH_4	0.0442	0.0348

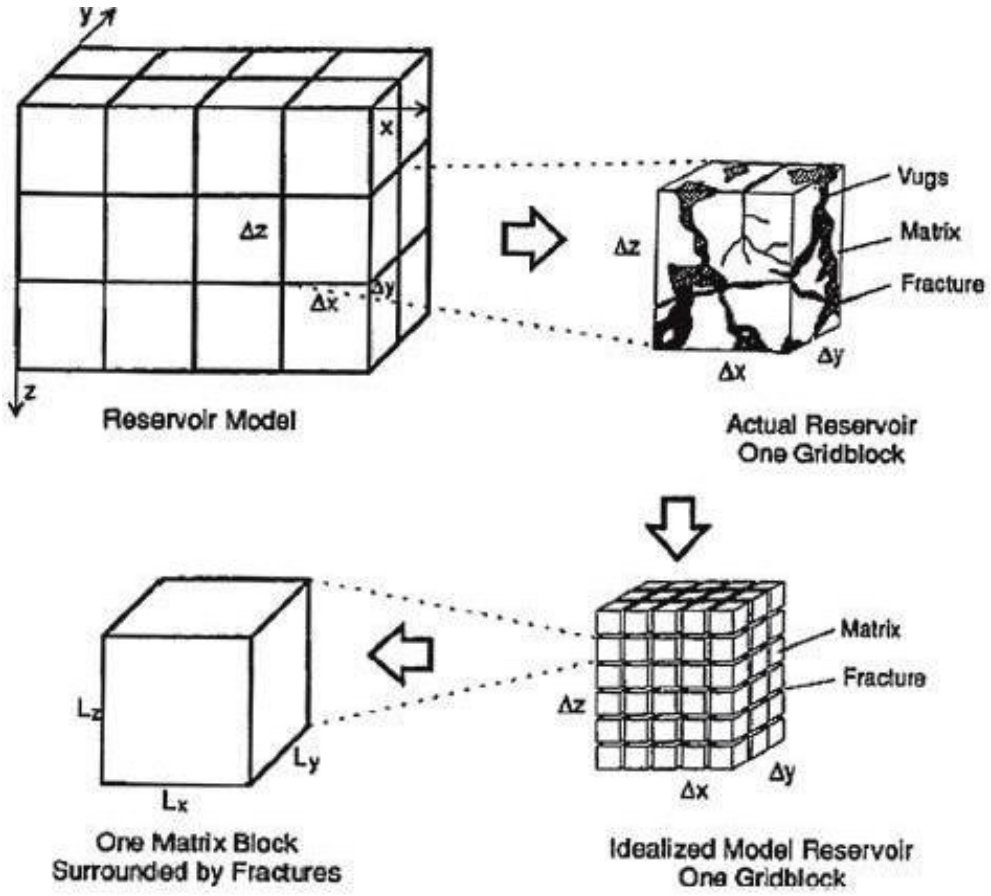

Figure 2-1: Idealization of the dual-porosity fractured porous media (Warren and Root, 1963).

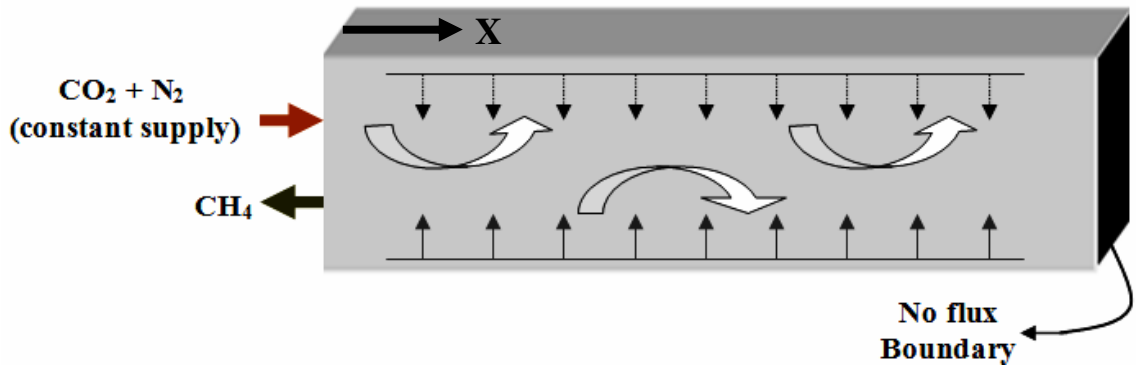

Figure 2-2: Schematic of a model coal matrix undergoing simultaneous adsorption and diffusion. Arrows indicate the direction of influx of CO2 and N2 and desorption of CH4.

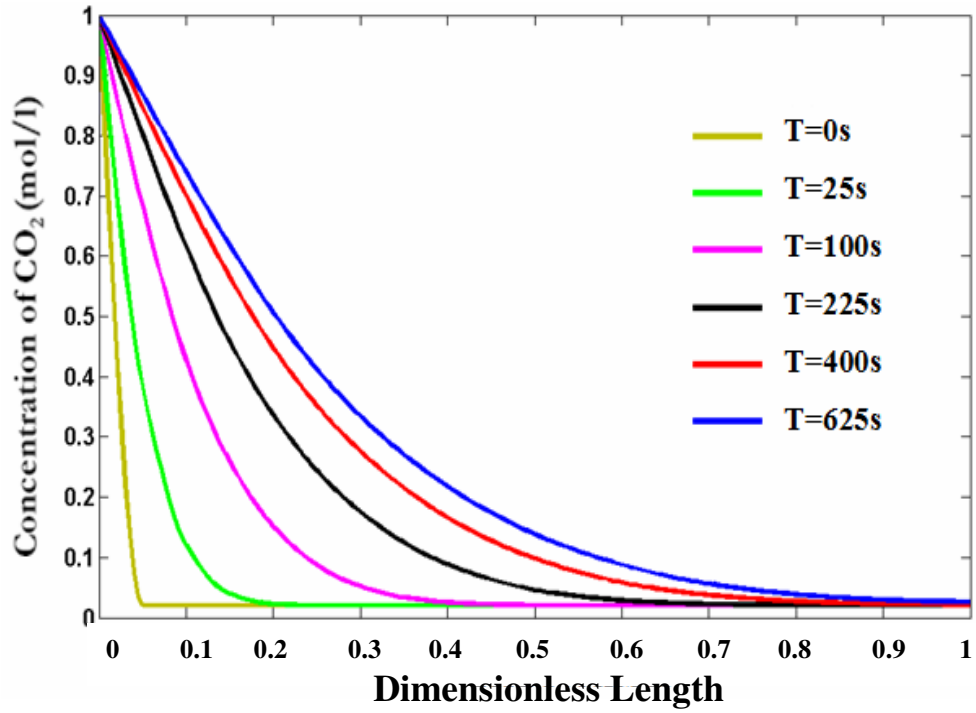

Figure 2-3: CO_2 concentration distribution as a function of space and time, ELM; $Đ_{13}$=0.05 mm^2/s; $Đ_{12}$=0.06 mm^2/s; $Đ_{23}$=0.03 mm^2/s.

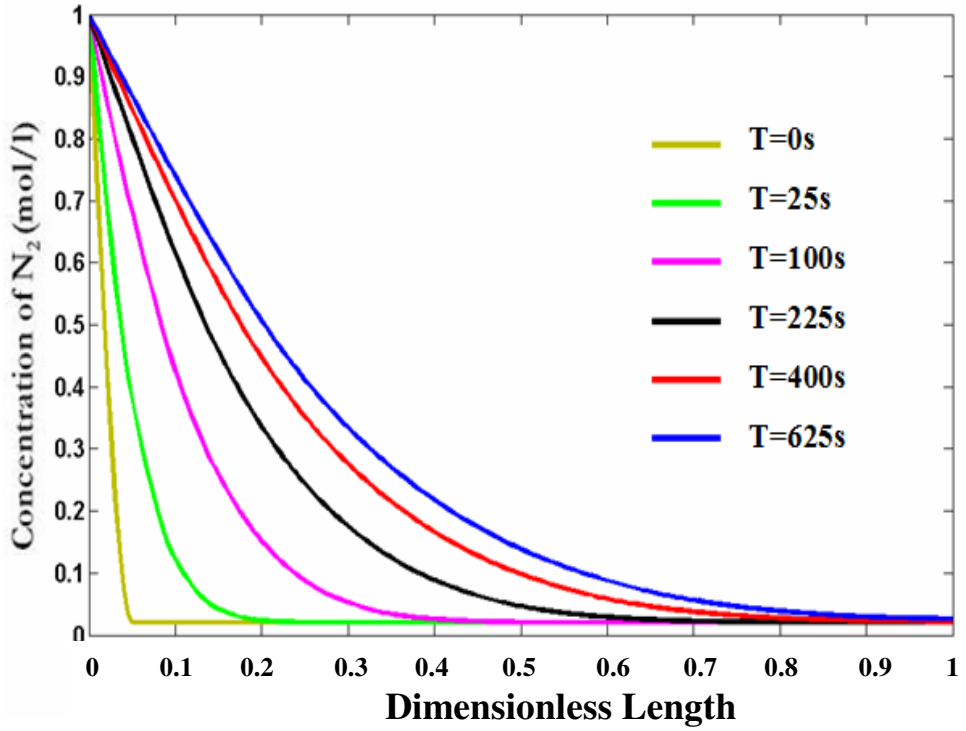

Figure 2-4: N_2 concentration distribution as a function of space and time, ELM; $Đ_{13}$=0.05 mm^2/s; $Đ_{12}$=0.06 mm^2/s; $Đ_{23}$=0.03 mm^2/s.

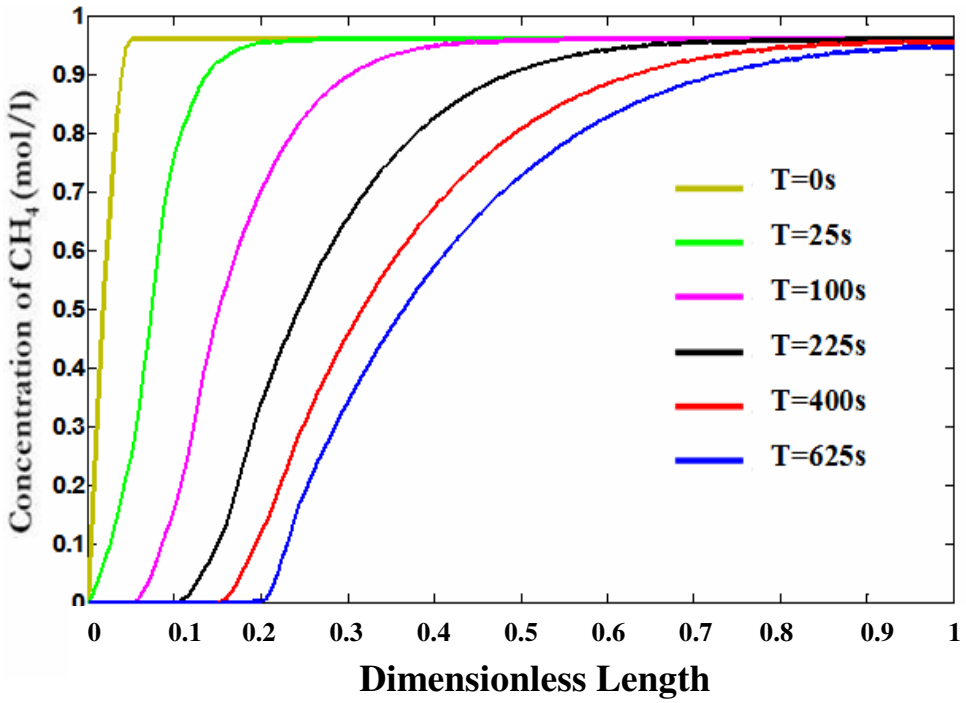

Figure 2-5: CH_4 concentration distribution as a function of space and time, ELM; $Đ_{13}$=0.05 mm^2/s; $Đ_{12}$=0.06 mm^2/s; $Đ_{23}$=0.03 mm^2/s.

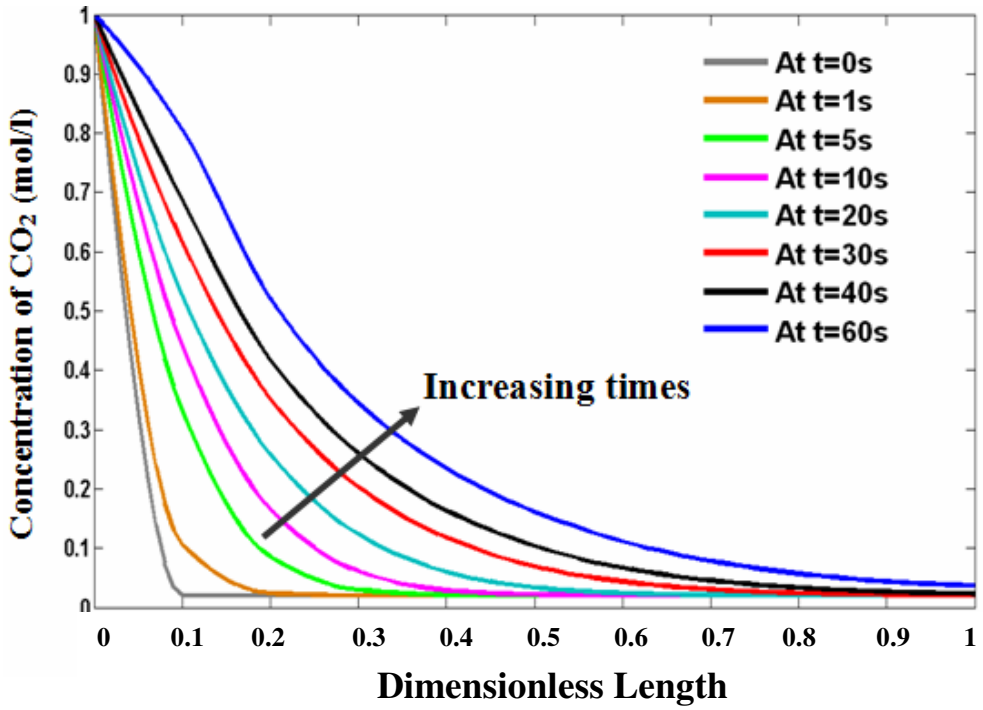

Figure 2-6: CO_2 concentration distribution as a function of space and time, ELM; $Đ_{13}$=0.2 mm^2/s; $Đ_{12}$=0.3 mm^2/s; $Đ_{23}$=0.1 mm^2/s.

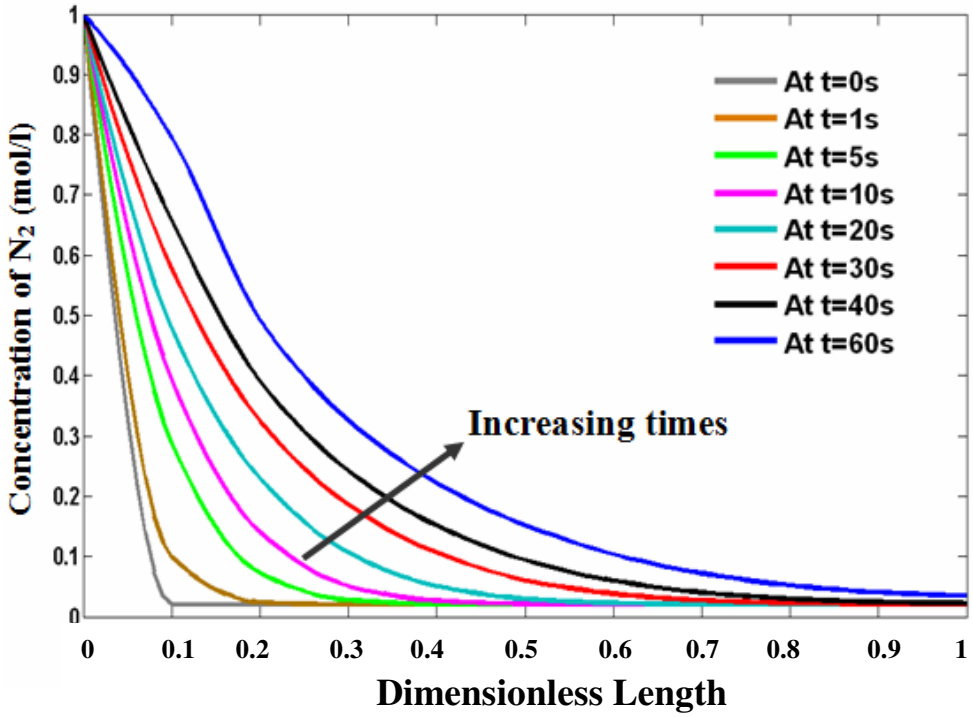

Figure 2-7: N_2 concentration distribution as a function of space and time, ELM; $Đ_{13}$=0.2 mm^2/s; $Đ_{12}$=0.3 mm^2/s; $Đ_{23}$=0.1 mm^2/s.

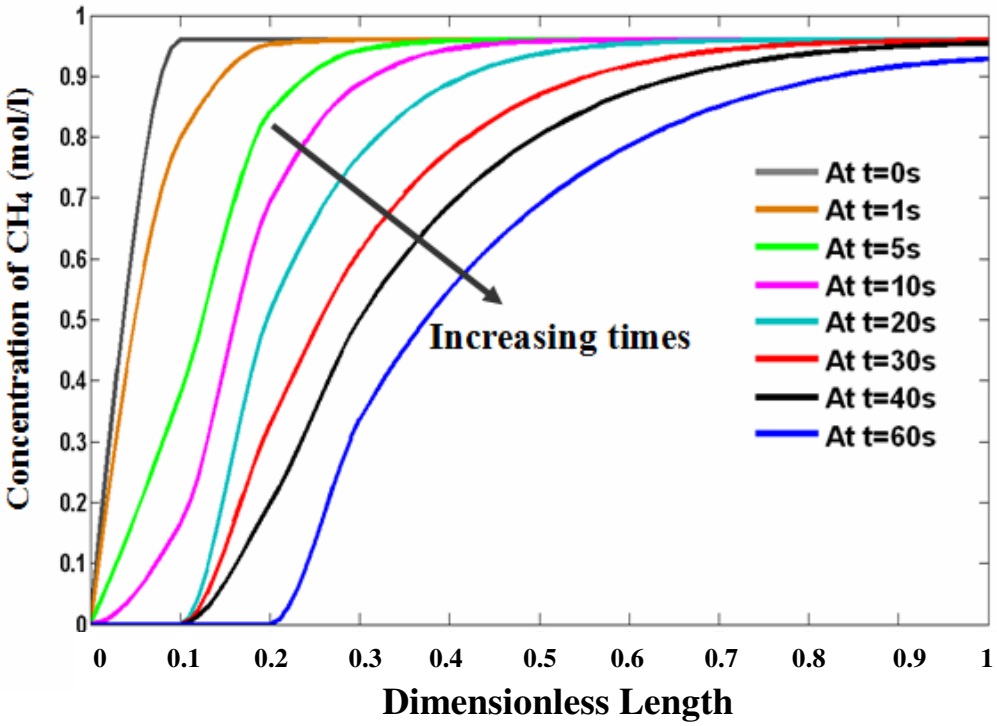

Figure 2-8: CH_4 concentration distribution as a function of space and time, ELM; $Đ_{13}$=0.2 mm^2/s; $Đ_{12}$=0.3 mm^2/s; $Đ_{23}$=0.1 mm^2/s.

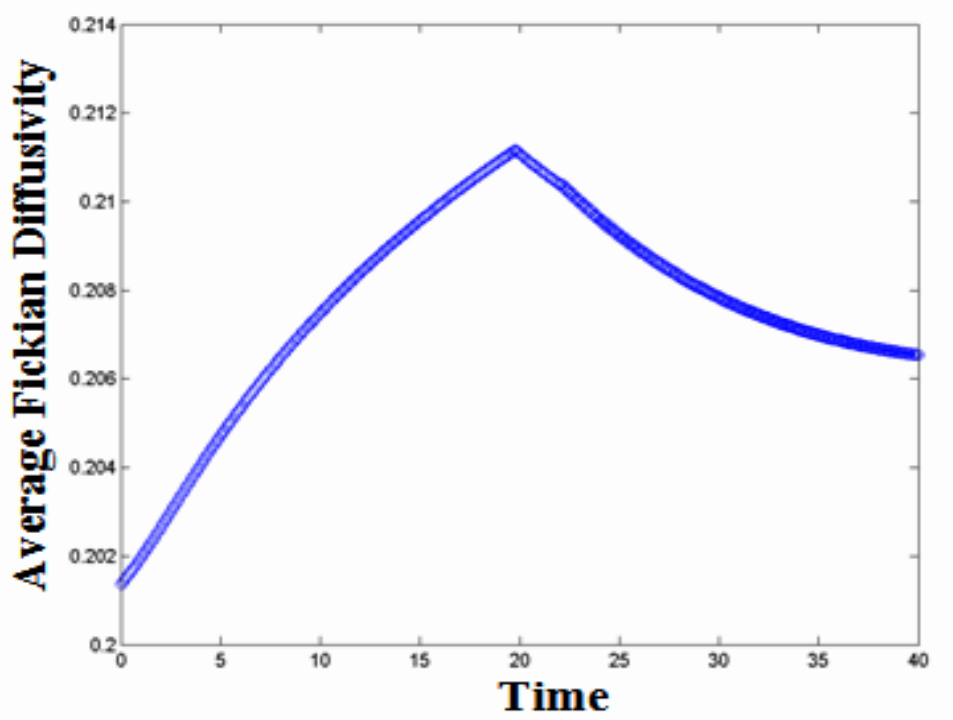

Figure 2-9: Variation of grid averaged D_{11} (mm^2/s) with time (s), ELM; $Đ_{13}$=0.2 mm^2/s; $Đ_{12}$=0.3 mm^2/s; $Đ_{23}$=0.1 mm^2/s.

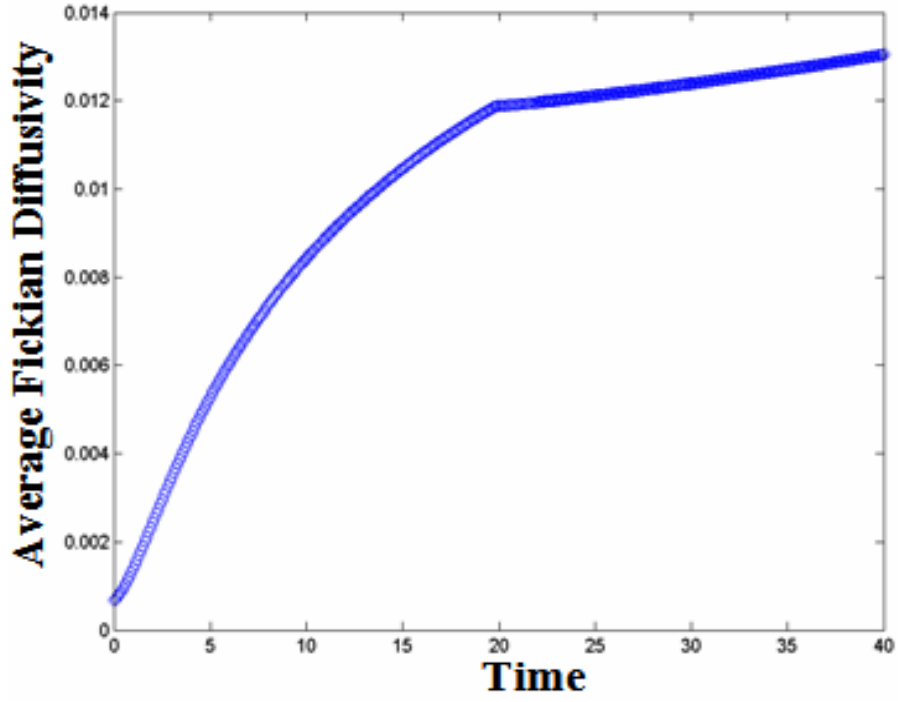

Figure 2-10: Variation of grid averaged D_{12} (mm^2/s) with time (s), ELM; $Đ_{13}$=0.2 mm^2/s; $Đ_{12}$=0.3 mm^2/s; $Đ_{23}$=0.1 mm^2/s.

.

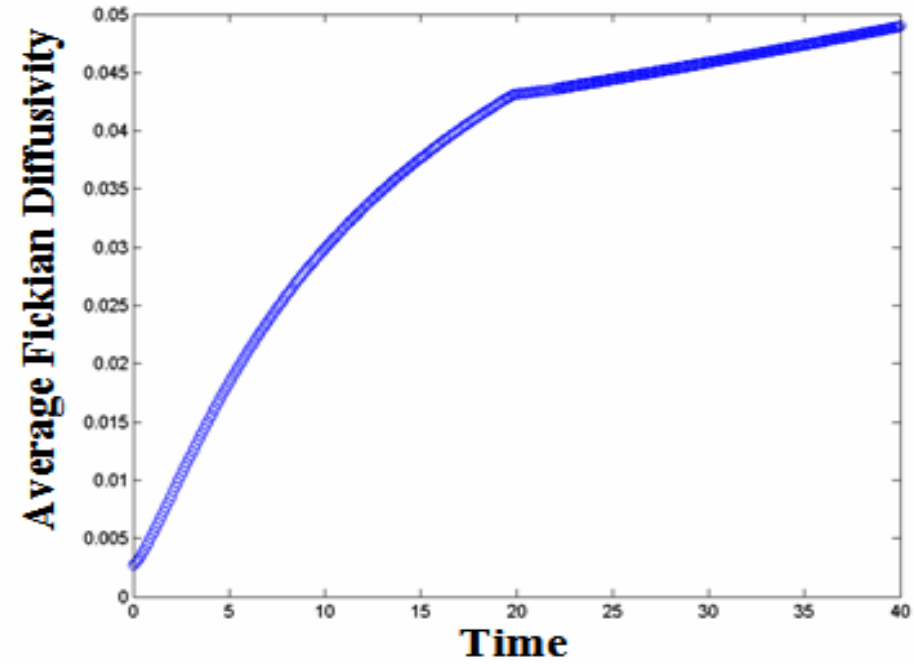

Figure 2-11: Variation of grid averaged D_{21} (mm^2/s) with time (s), ELM; $Đ_{13}$=0.2 mm^2/s; $Đ_{12}$=0.3 mm^2/s; $Đ_{23}$=0.1 mm^2/s.

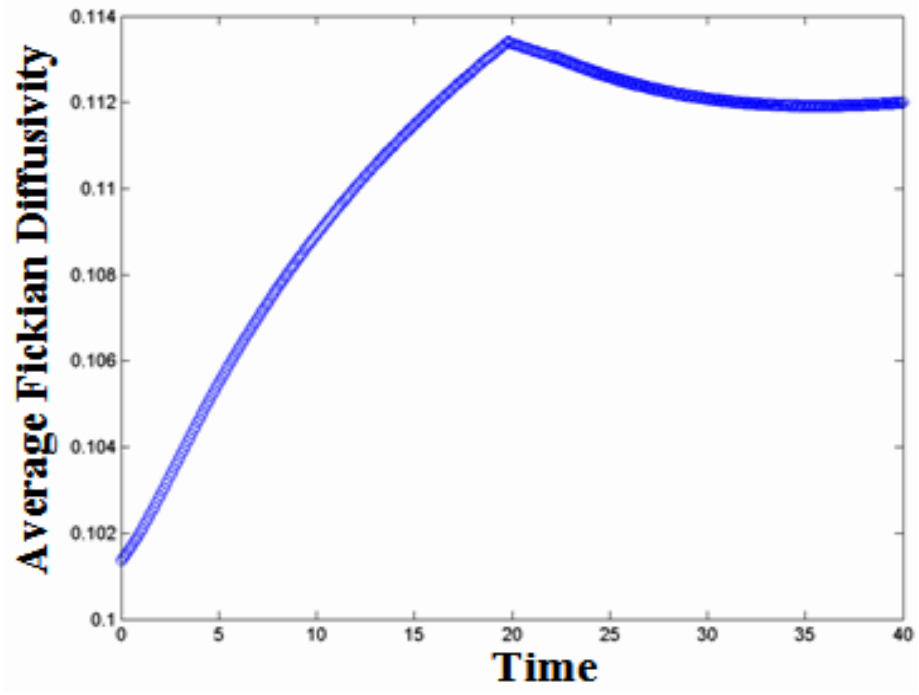

Figure 2-12: Variation of grid averaged D_{22} (mm^2/s) with time, ELM; $Đ_{13}$=0.2 mm^2/s; $Đ_{12}$=0.3 mm^2/s; $Đ_{23}$=0.1 mm^2/s.

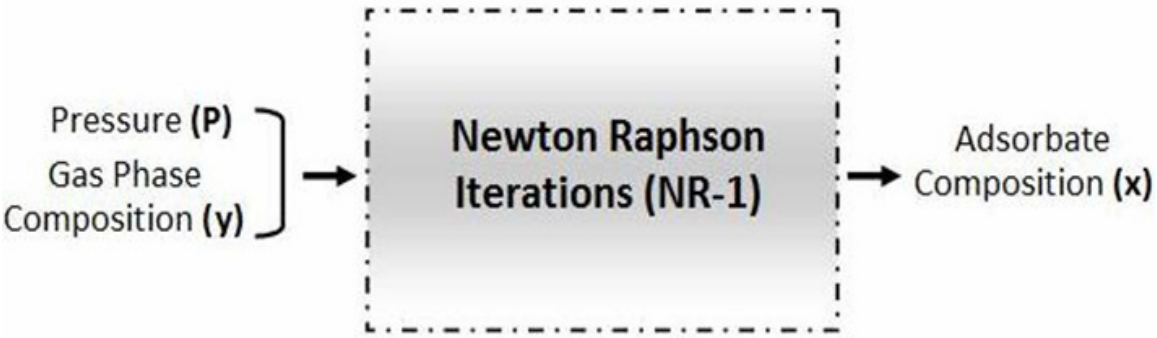

Figure 2-13: Objective of the algorithm developed in stage 1.

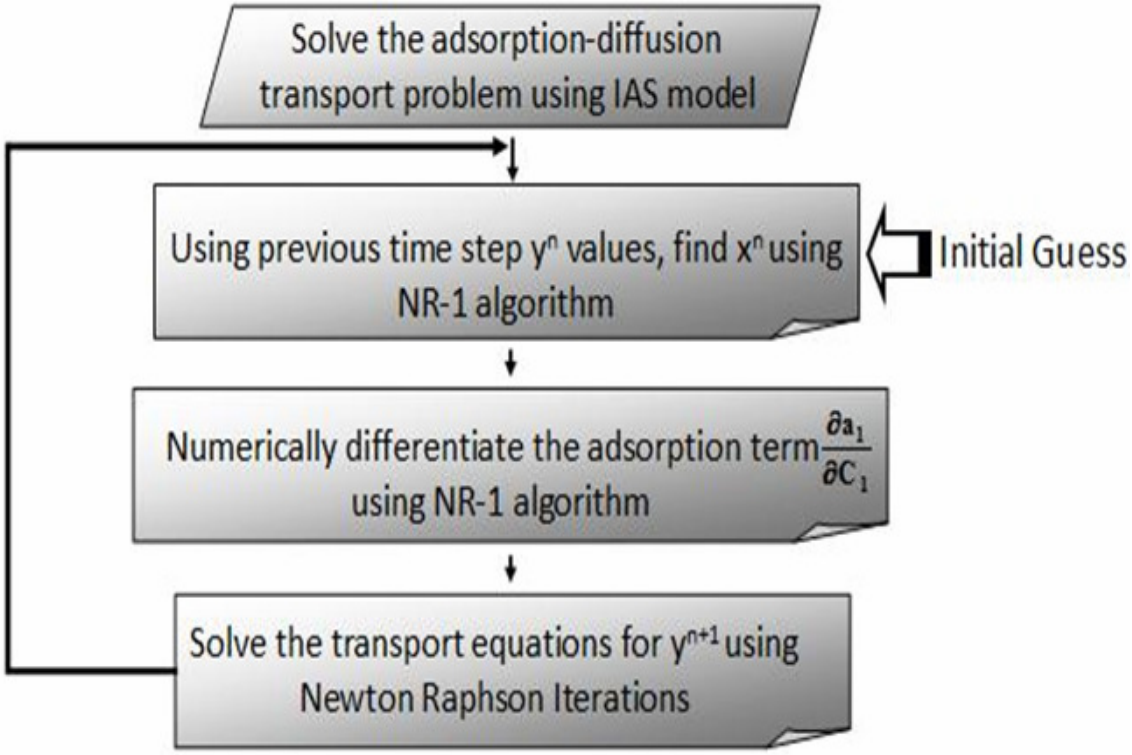

Figure 2-14: Flowchart of the solution strategy for the ternary adsorption-diffusion problem using the IAS adsorption model.

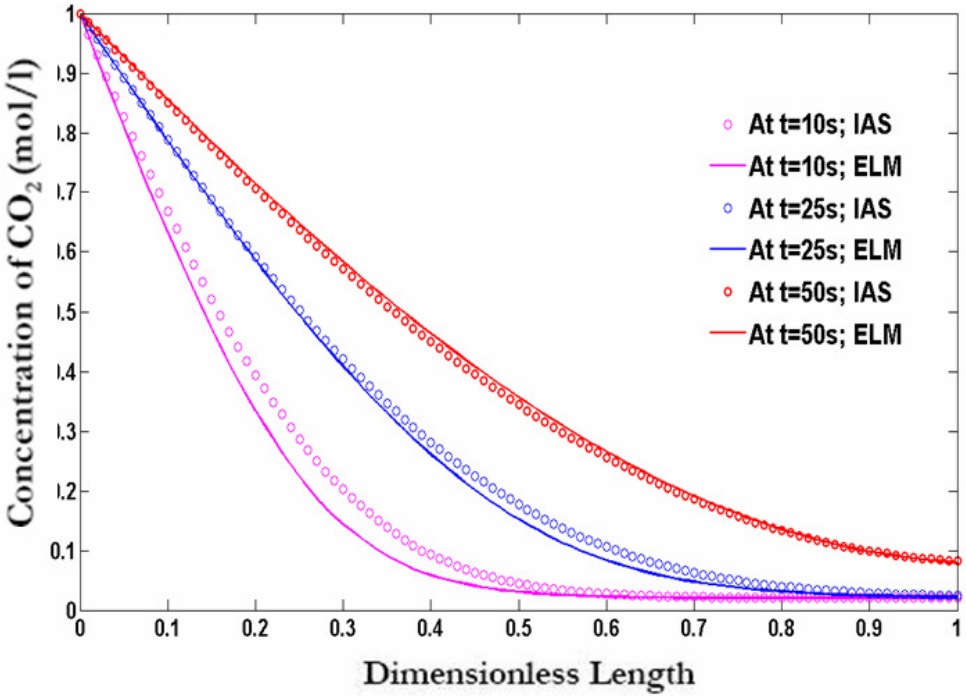

Figure 2-15: Comparison of concentration profiles for CO_2 using the ELM and IAS model; $Đ_{13} = Đ_{12} = Đ_{23}$=0.3 mm^2/s.

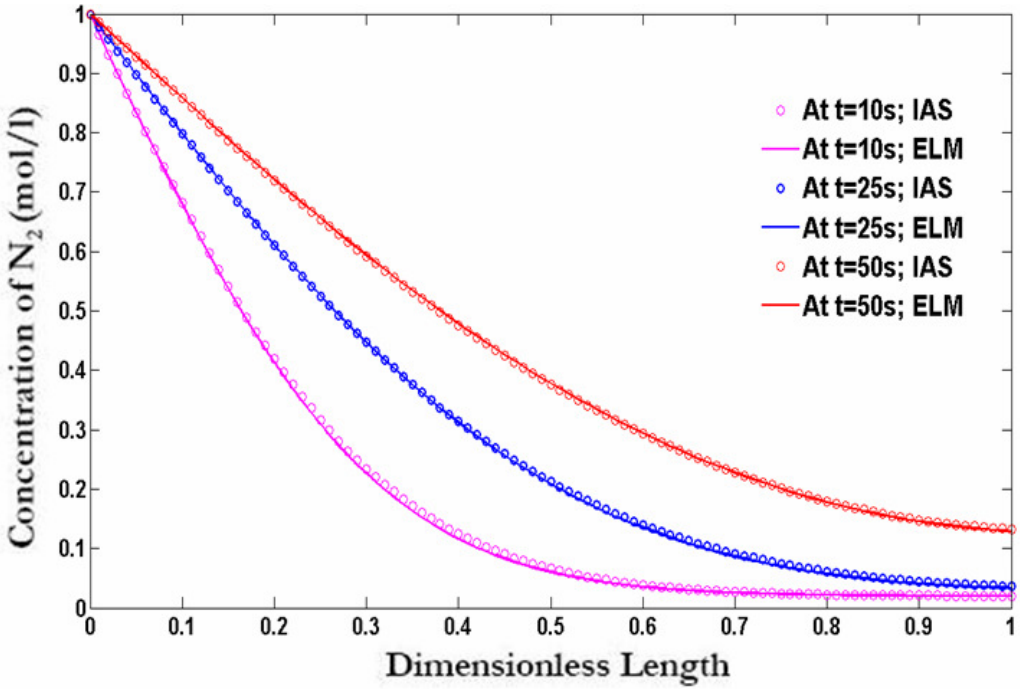

Figure 2-16: Comparison of concentration profiles for N_2 using the ELM and IAS model; $Đ_{13} = Đ_{12} = Đ_{23}$=0.3 mm^2/s.

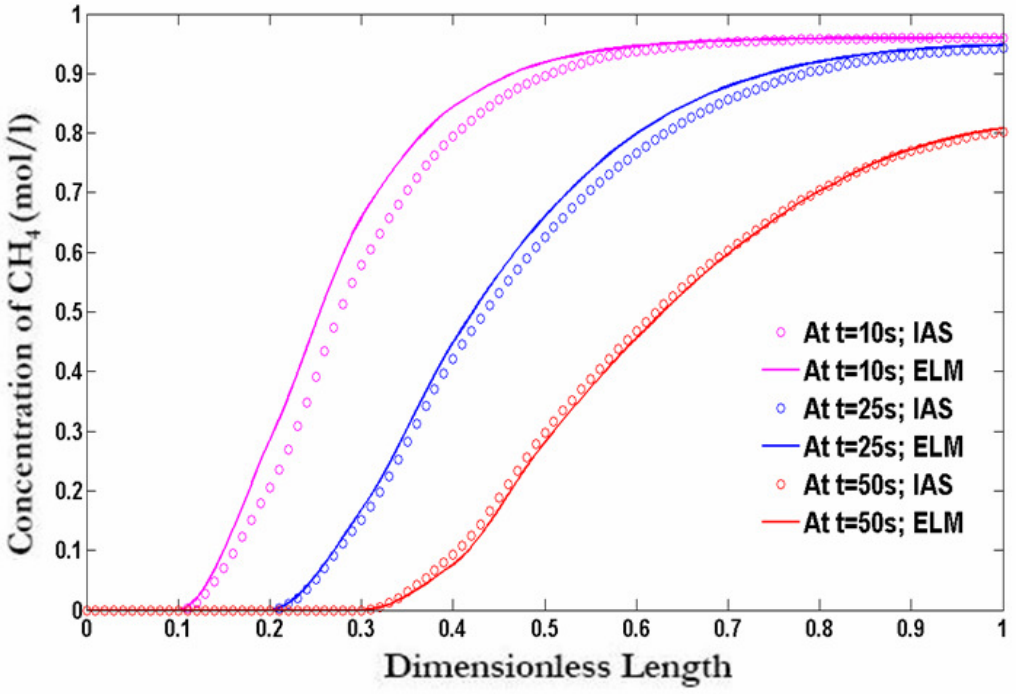

Figure 2-17: Comparison of concentration profiles for CH_4 using the ELM and IAS model; $Đ_{13} = Đ_{12} = Đ_{23}$=0.3 mm^2/s.

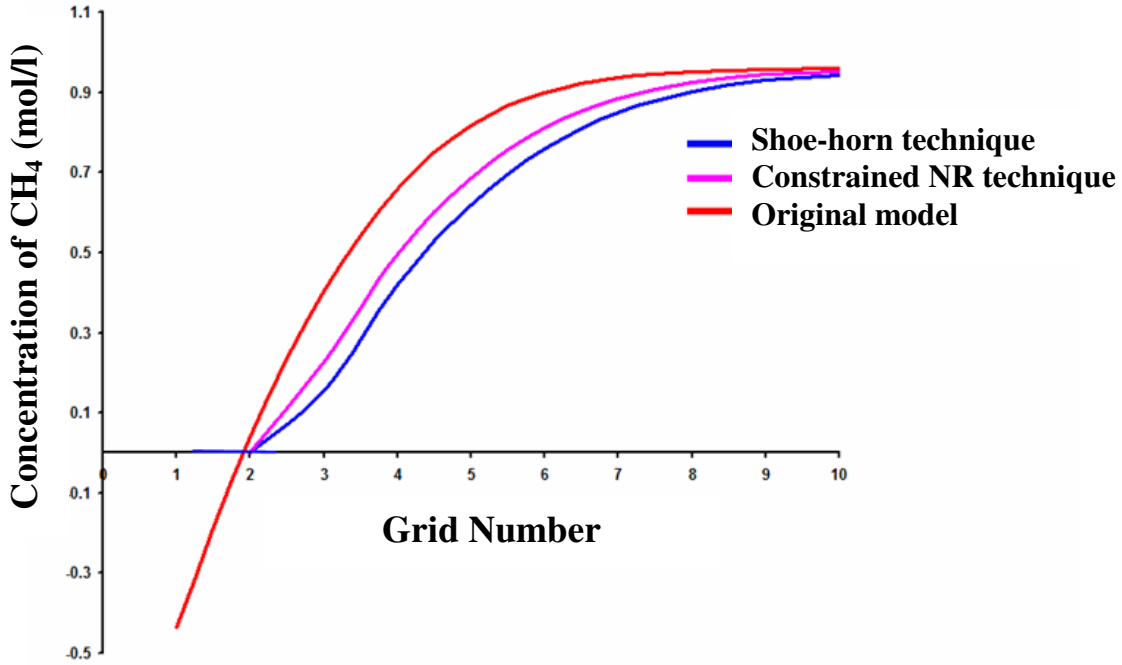

Figure 2-18: Effect of tuning on the CH_4 concentration profile at 40 s using the ELM; $D_{13}=D_{12}=D_{23}$=0.1 mm^2/s.

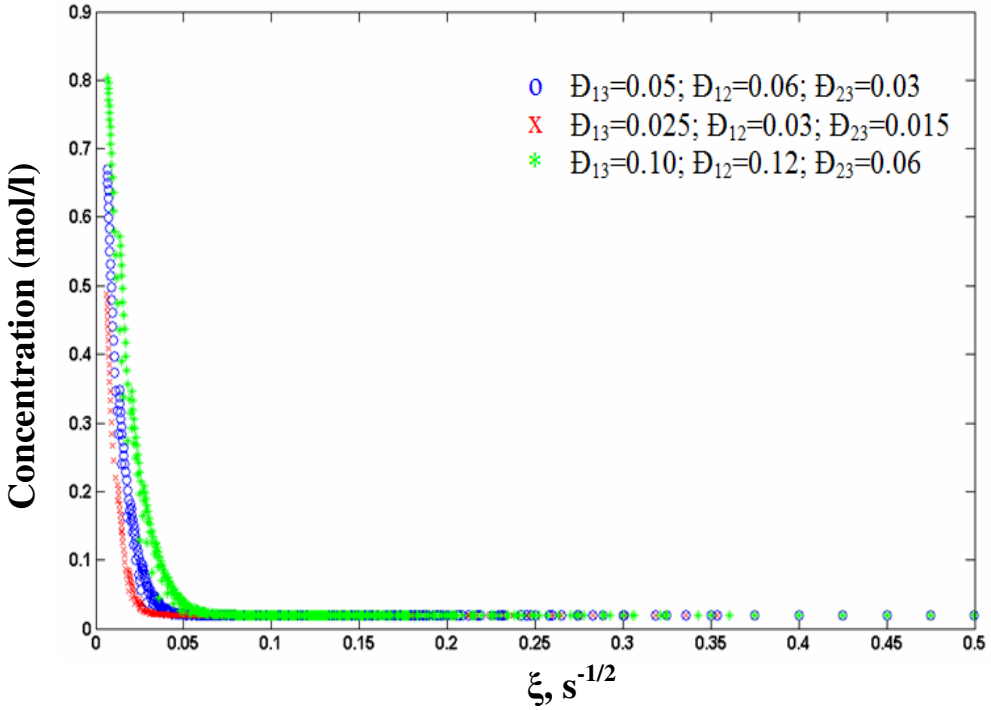

Figure 2-19: Impact of MS diffusivity (in mm^2/s) on the characteristic curves for CO_2 using ELM; L=10mm.

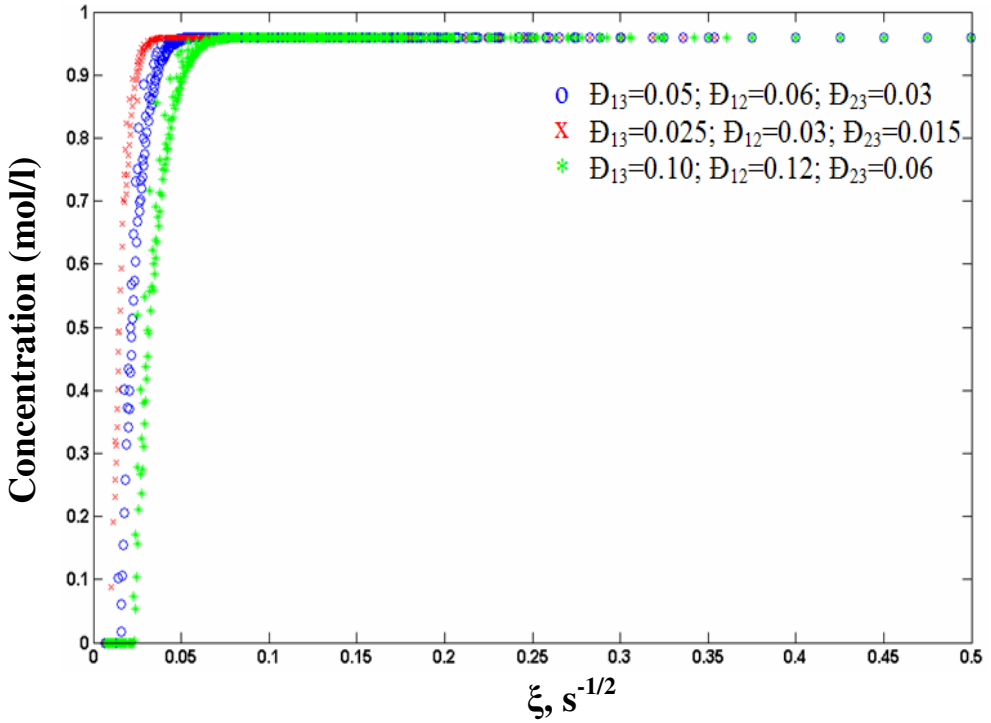

Figure 2-20: Impact of MS diffusivity (in mm^2/s) on the characteristic curves for CH_4 using ELM; L=10mm.

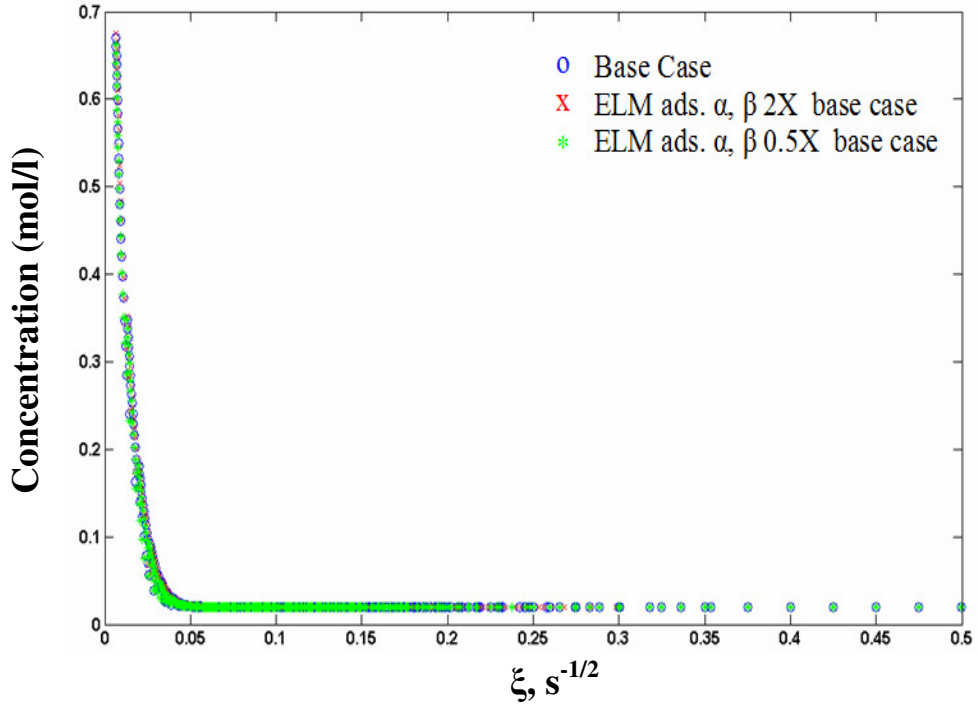

Figure 2-21: Impact of ELM adsorption parameters on the characteristic curves for CO_2; L=10mm; $Đ_{13}$=0.05 mm^2/s; $Đ_{12}$=0.06 mm^2/s; $Đ_{23}$=0.03 mm^2/s.

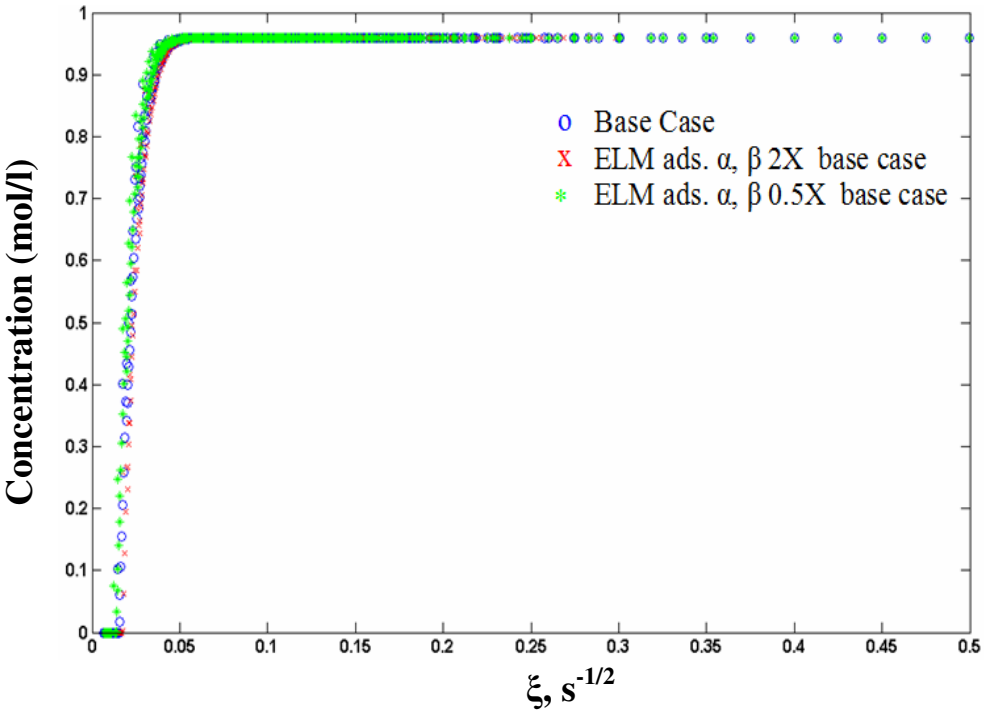

Figure 2-22: Impact of ELM adsorption parameters on the characteristic curves for CH_4; L=10mm; $Đ_{13}$=0.05 mm^2/s; $Đ_{12}$=0.06 mm^2/s; $Đ_{23}$=0.03 mm^2/s.

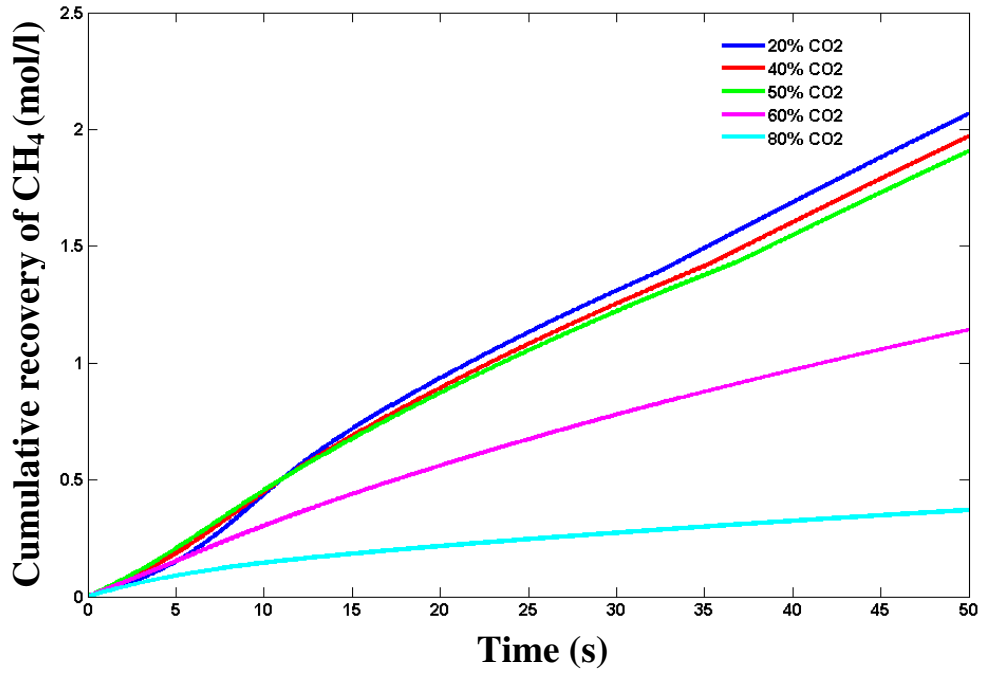

Figure 2-23: Impact of injection gas (N_2 and CO_2) composition on the CH_4 gas recovery; L=10mm; $Đ_{13} = Đ_{12} = Đ_{23} = 0.03\ mm^2/s$.

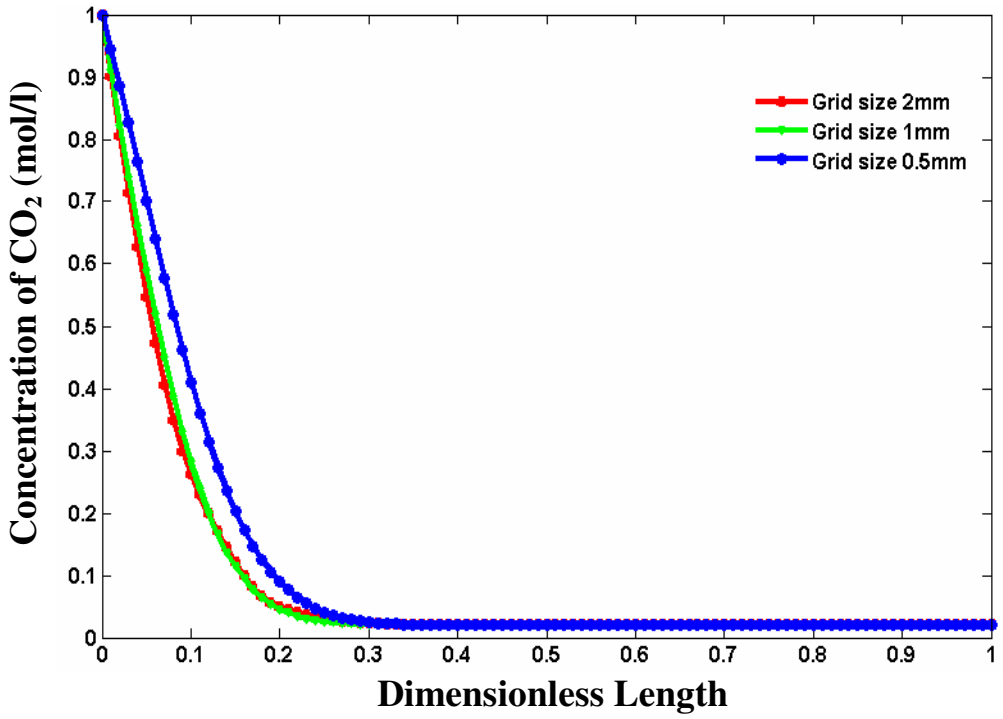

Figure 2-24: Grid size sensitivity on the CO_2 concentration profile at 20s using the ELM; $Đ_{13}=0.09\ mm^2/s$; $Đ_{12}=0.08\ mm^2/s$; $Đ_{23}=0.07\ mm^2/s$.

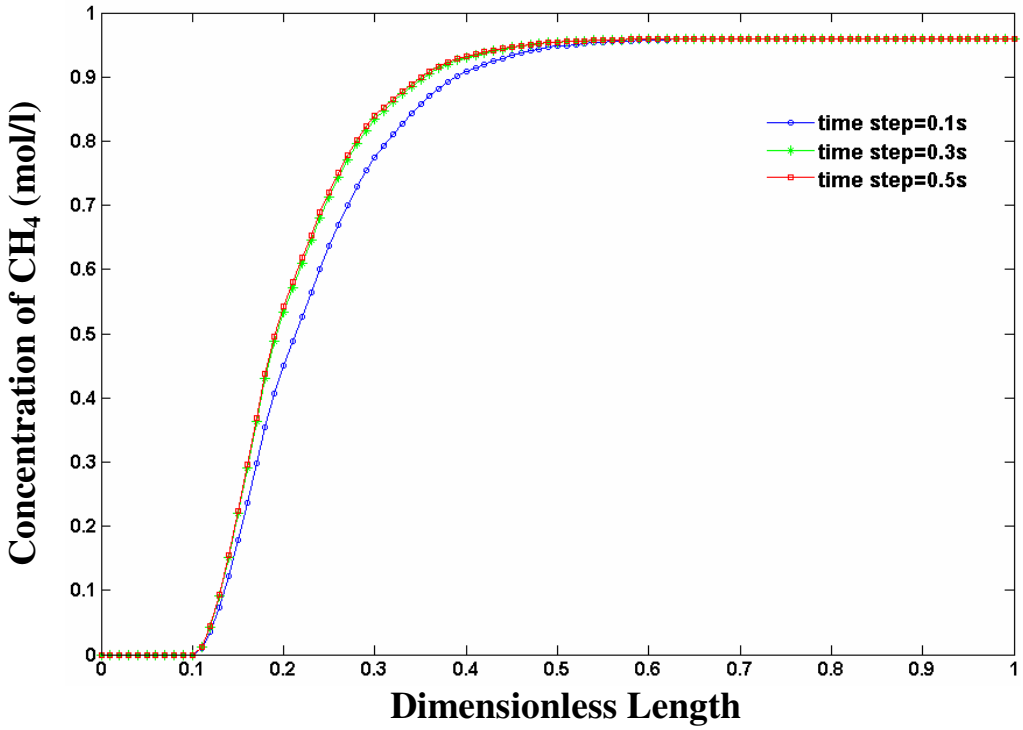

Figure 2-25: Time step size sensitivity on the CH_4 concentration profile at 20s using the ELM; $Đ_{13}$=0.09 mm^2/s; $Đ_{12}$=0.08 mm^2/s; $Đ_{23}$=0.07 mm^2/s.

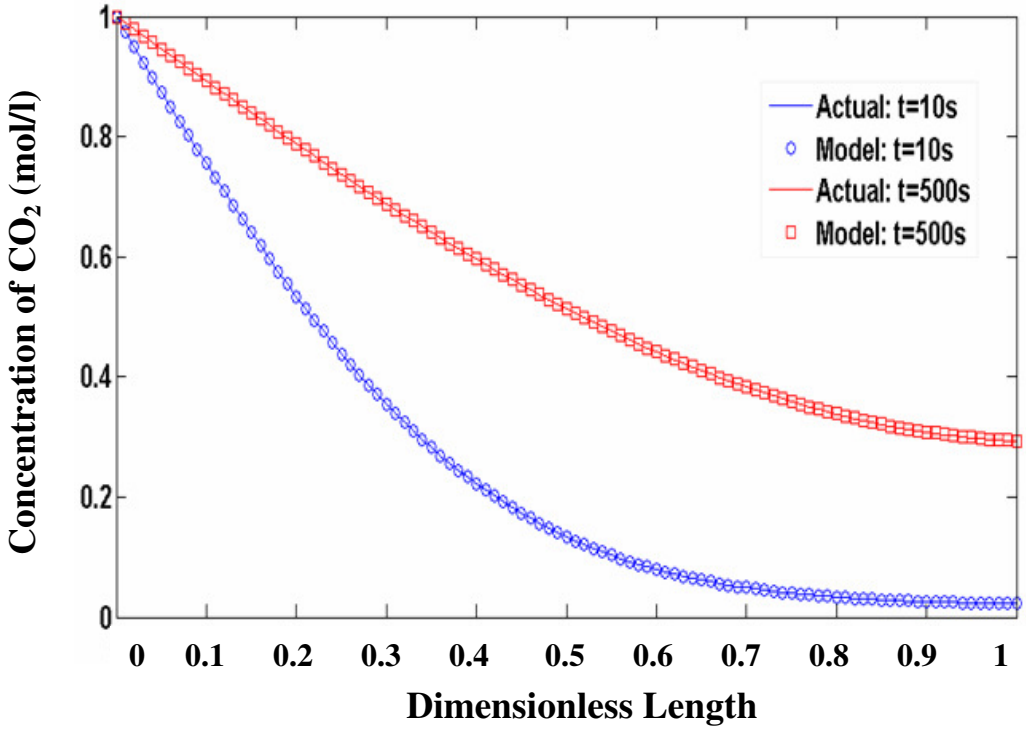

Figure 2-26: Comparison of concentration profiles for CO_2 for the reduced model case against the actual case using the ELM; D = 0.05 mm^2/s.

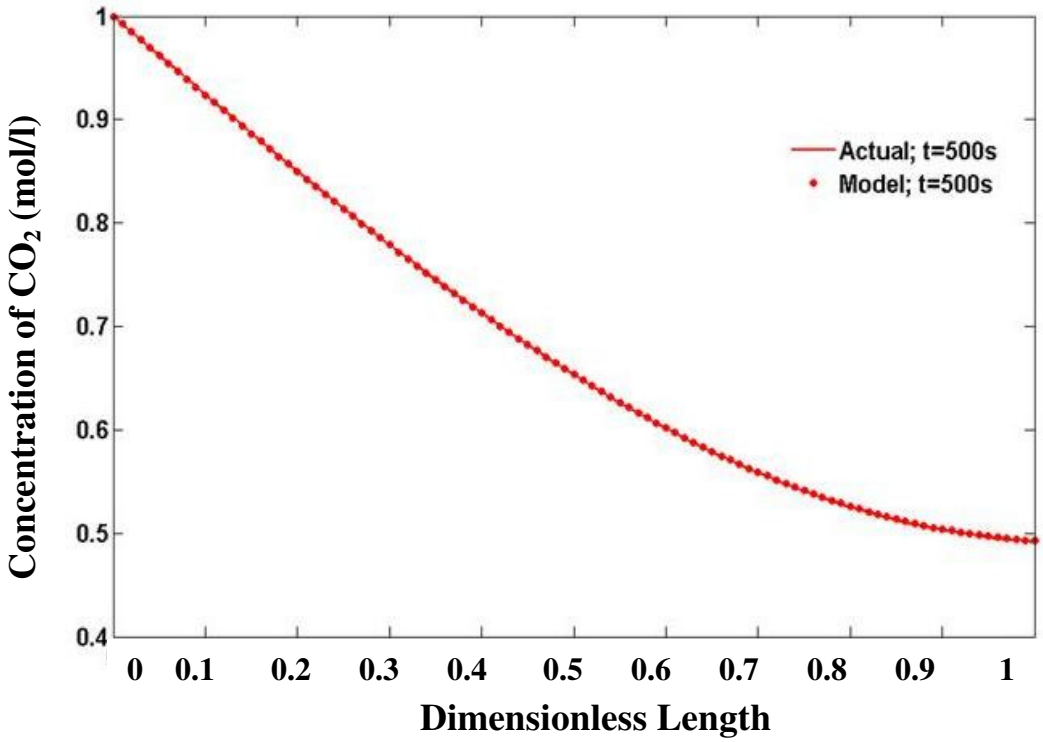

Figure 2-27: Comparison of late time concentration profiles for CO_2 for the reduced model case against the actual case using the ELM; D = 0.08 mm^2/s.

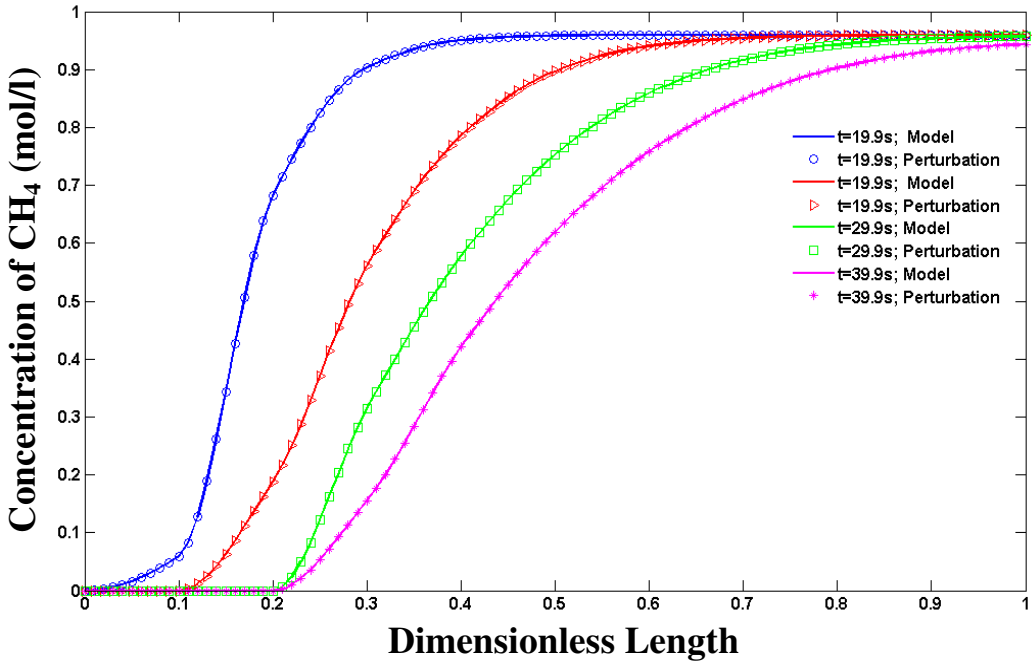

Figure 2-28: Comparison of concentration profiles for CH_4 using the model (analytical Jacobian) and the perturbation case (numerical Jacobian), ELM; $Đ_{13}= Đ_{12}= Đ_{23}=0.3$ mm^2/s.

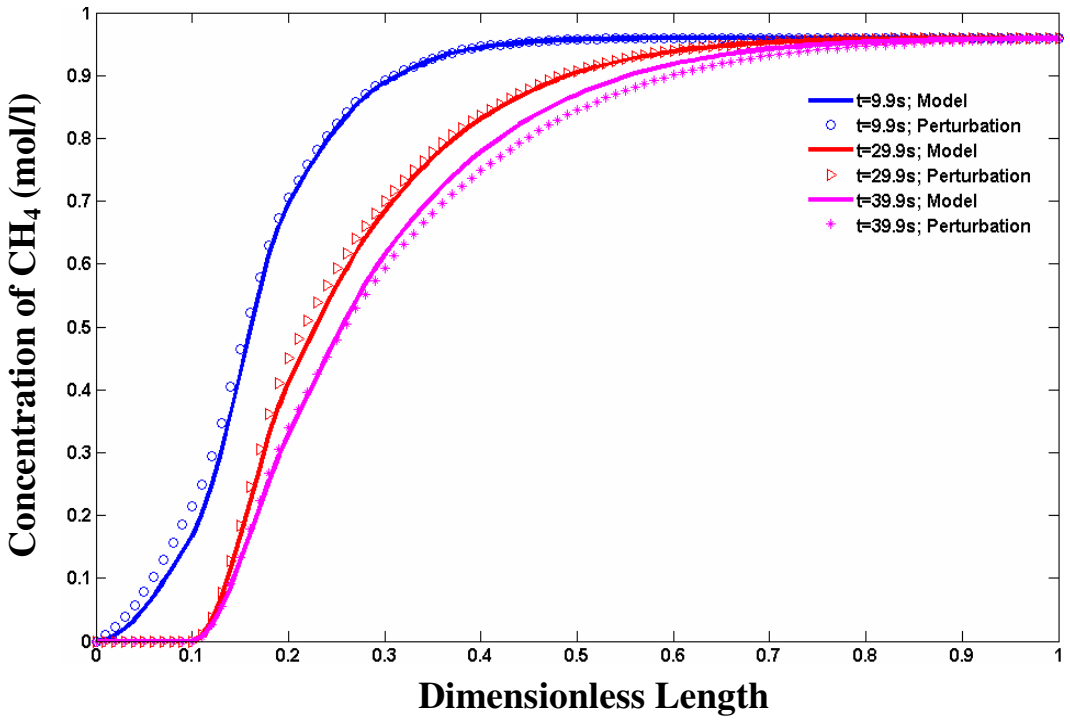

Figure 2-29: Comparison of concentration profiles for CH_4 using the model (analytical Jacobian) and the perturbation case (numerical Jacobian), ELM; $Đ_{13}$= 0.2 mm^2/s, $Đ_{12}$= 0.3 mm^2/s and $Đ_{23}$=0.1 mm^2/s.

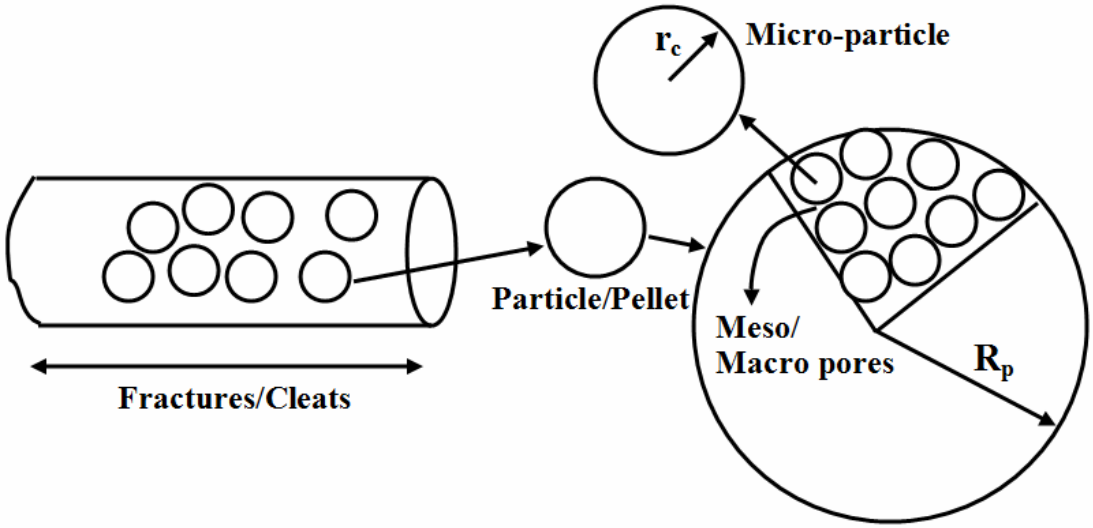

Figure 2-30: Schematic of a coalbed modeled using a cylindrical coal matrix. The matrix comprises of macropores and micropores (bidisperse pore model).

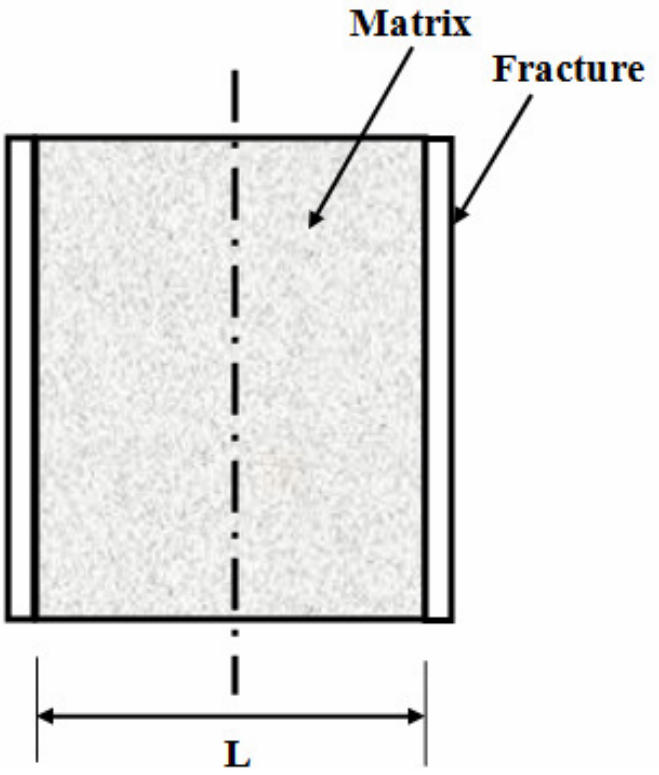

Figure 2-31: Schematic of a rectangular matrix block surrounded by one set of fractures.

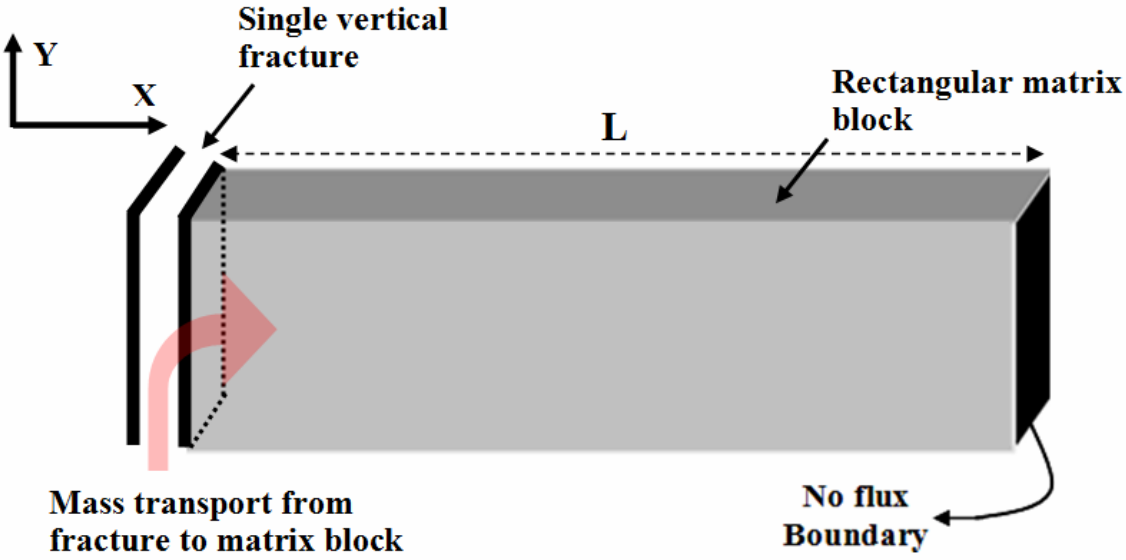

Figure 2-32: Schematic of a matrix-fracture geometry used in the shape factor investigation study.

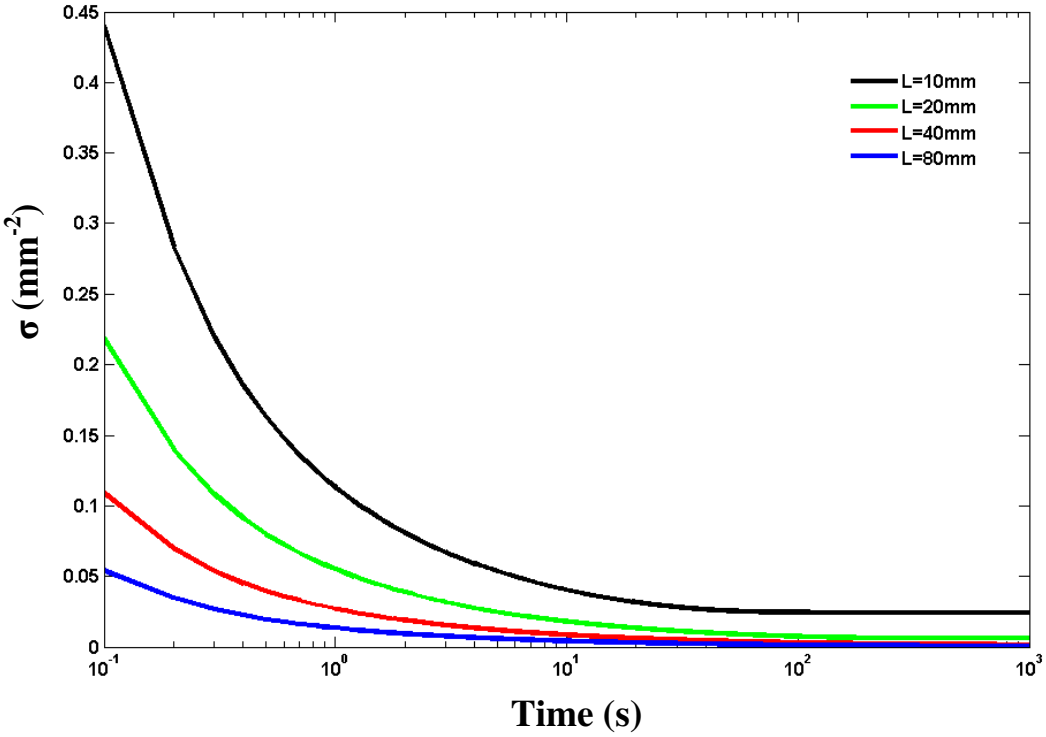

Figure 2-33: Semi-log plot showing the impact of length of matrix block on shape factor (σ) with time; D=0.3 mm^2/s.

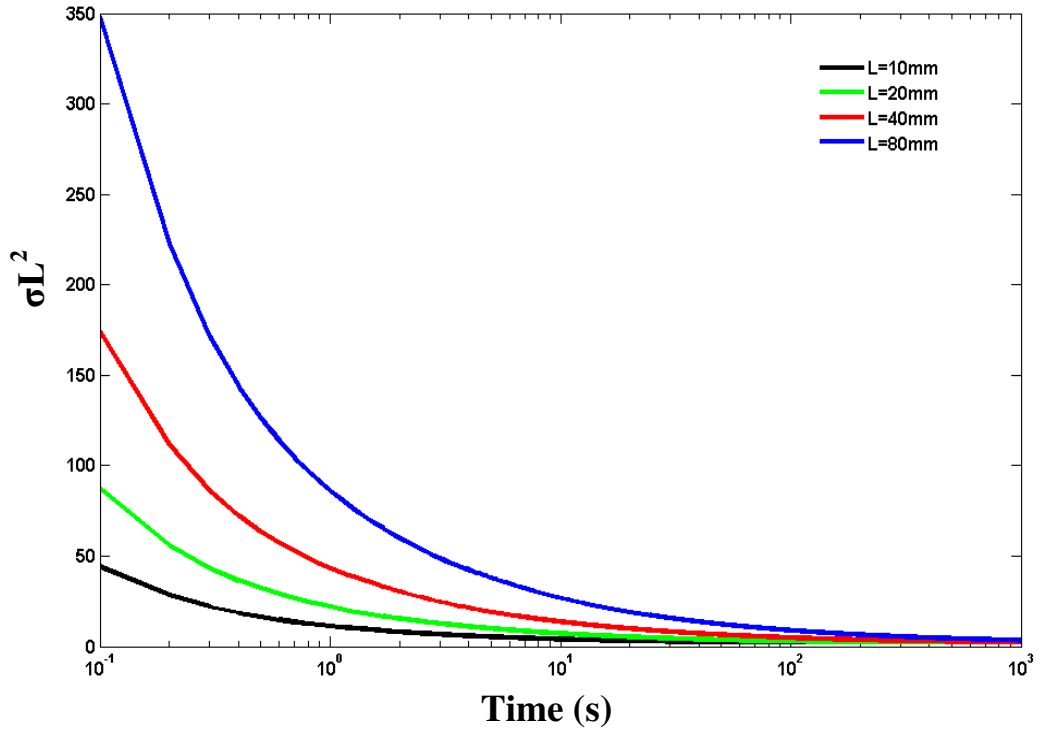

Figure 2-34: Semi-log plot showing the impact of length of matrix block on σL^2 (dimensionless) with time; D=0.3 mm^2/s.

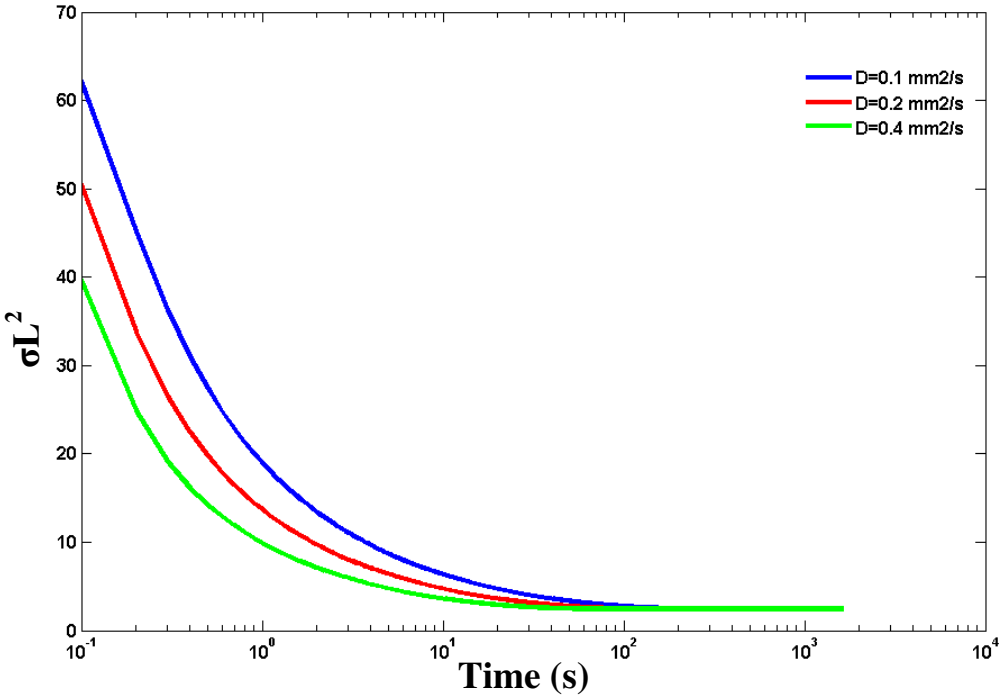

Figure 2-35: Semi-log plot showing the impact of Fickian diffusivity on σL^2 (dimensionless) with time; L=10mm.

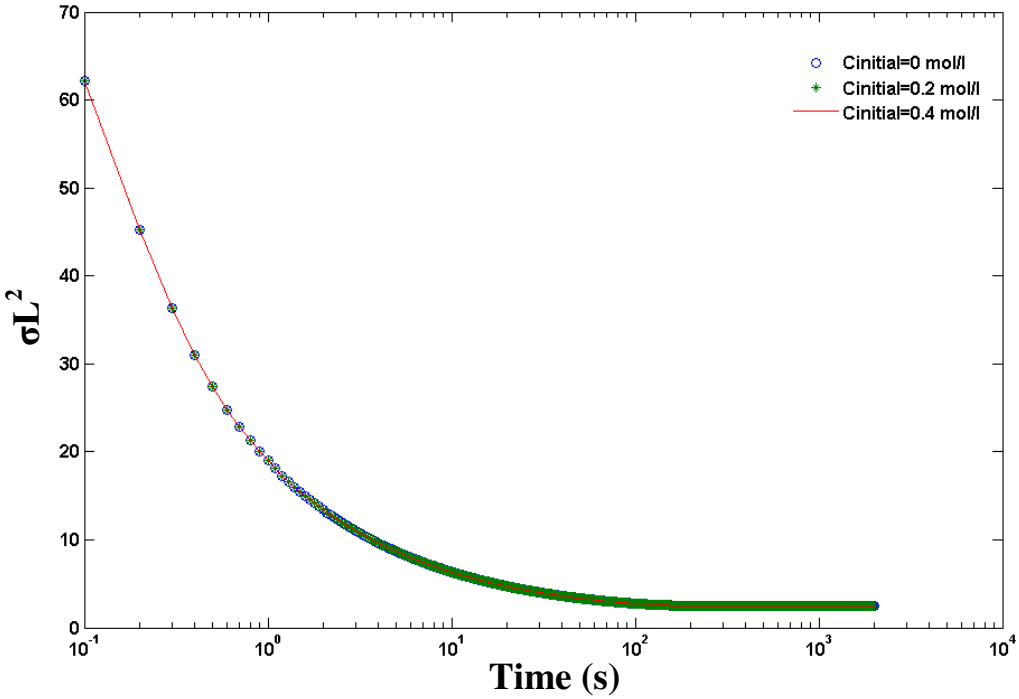

Figure 2-36: Semi-log plot showing the impact of initial condition on σL^2 (dimensionless) with time; L=10mm, D=0.1 mm^2/s.

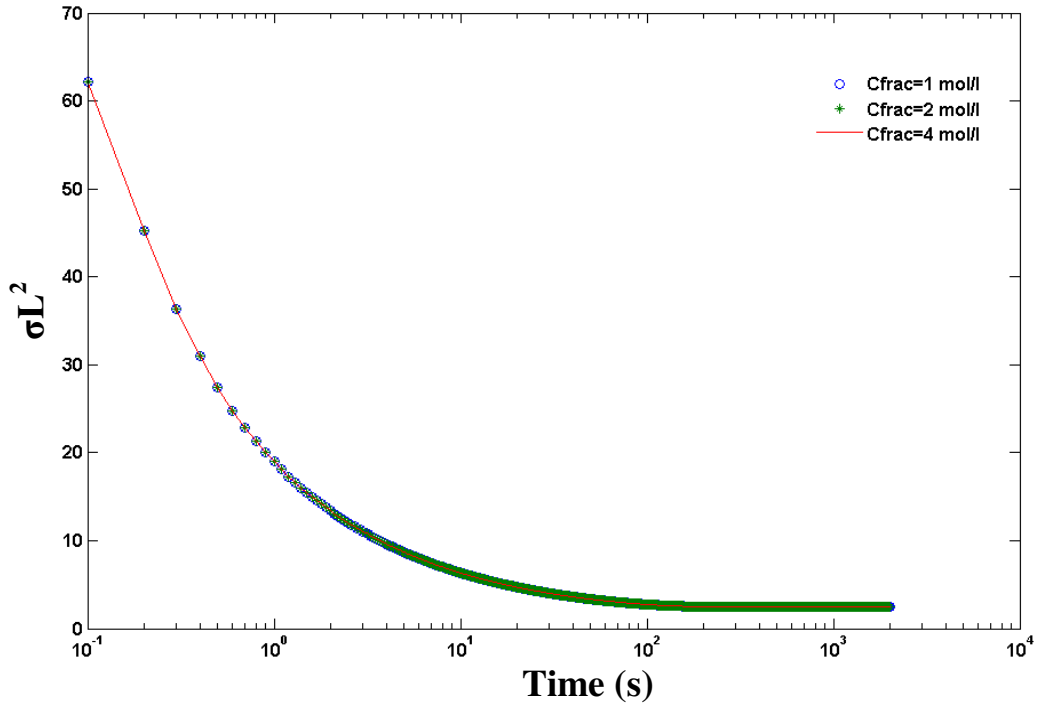

Figure 2-37: Semi-log plot showing the impact of boundary condition on σL^2 (dimensionless) with time; L=10mm, D=0.1 mm^2/s.

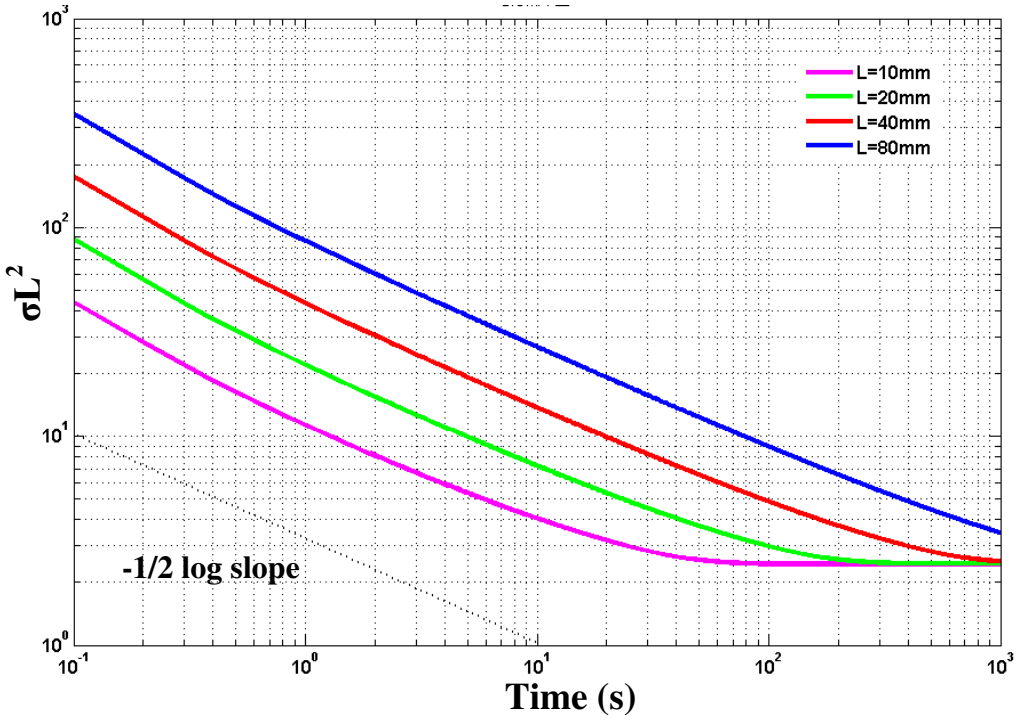

Figure 2-38: Log-log plot showing the impact of length of matrix block on σL^2 (dimensionless) with time. In the early transient phase, the shape factors show linear behavior with a log slope of -1/2 on the log-log plot; D=0.3 mm^2/s.

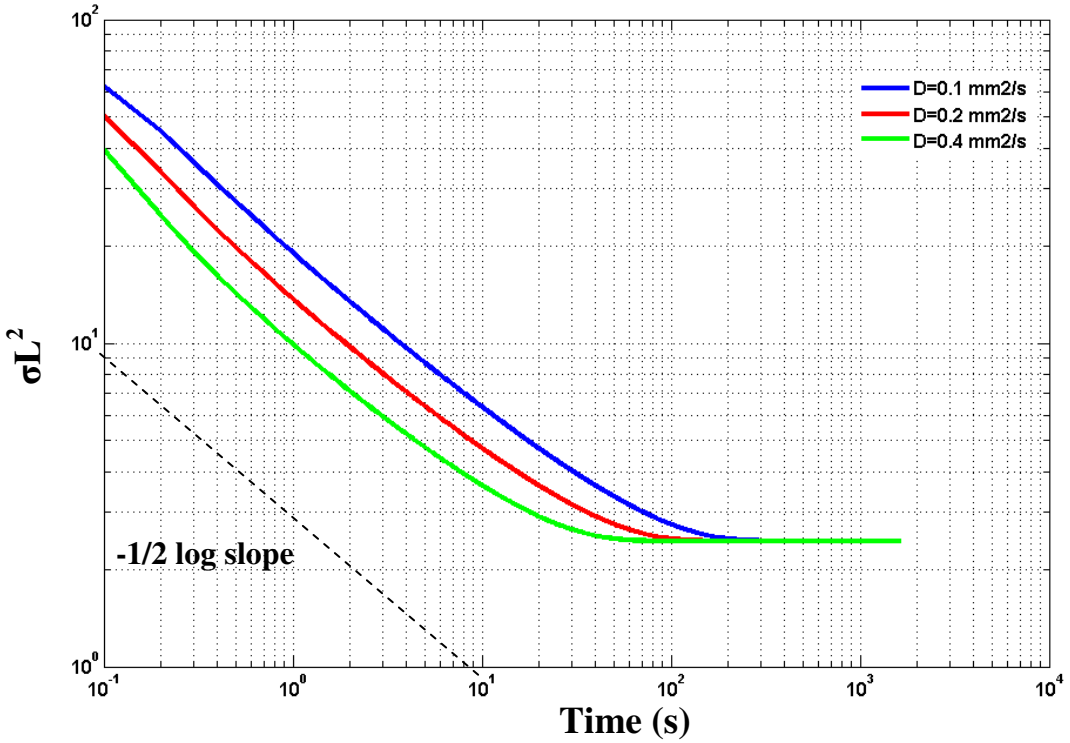

Figure 2-39: Log-log plot showing the impact of Fickian diffusivity on σL^2 (dimensionless) with time. In the early transient phase, the shape factors show linear behavior with a log slope of -1/2 on the log-log plot; L=10mm.

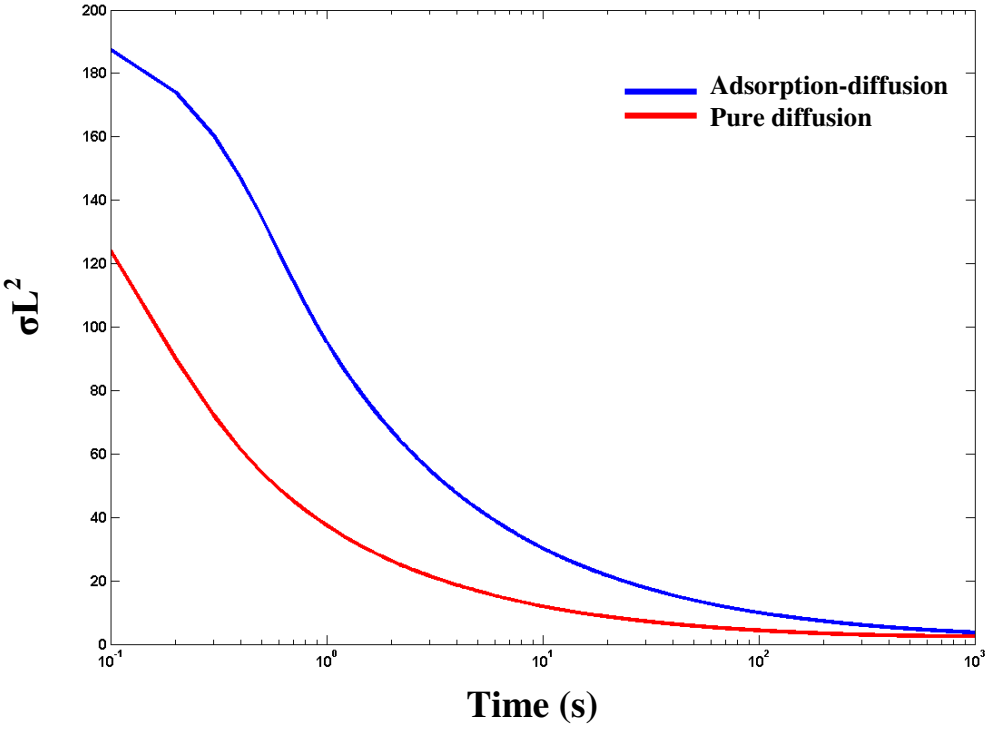

Figure 2-40: Semi-log plot comparing σL^2 (dimensionless) for the pure diffusion case against the adsorption-diffusion case; L=20mm, D=0.1 mm^2/s.

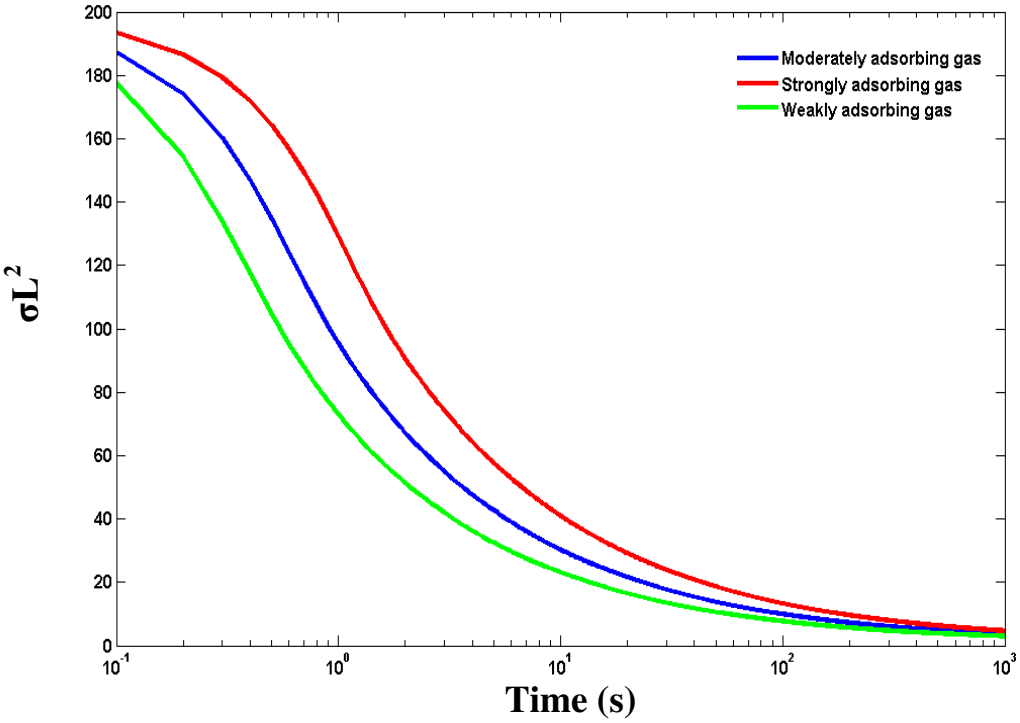

Figure 2-41: Semi-log plot comparing σL^2 (dimensionless) for gases with varying adsorption tendencies; L=20mm, D=0.1 mm^2/s.

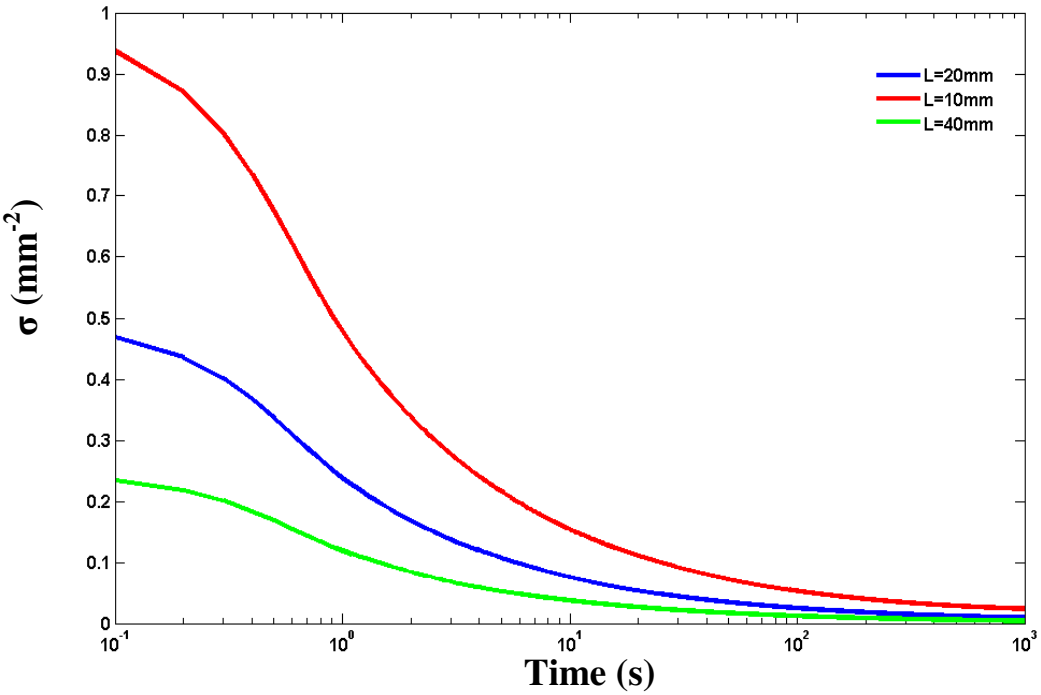

Figure 2-42: Semi-log plot showing the impact of length of matrix block on shape factor (σ) with time; D=0.1 mm^2/s.

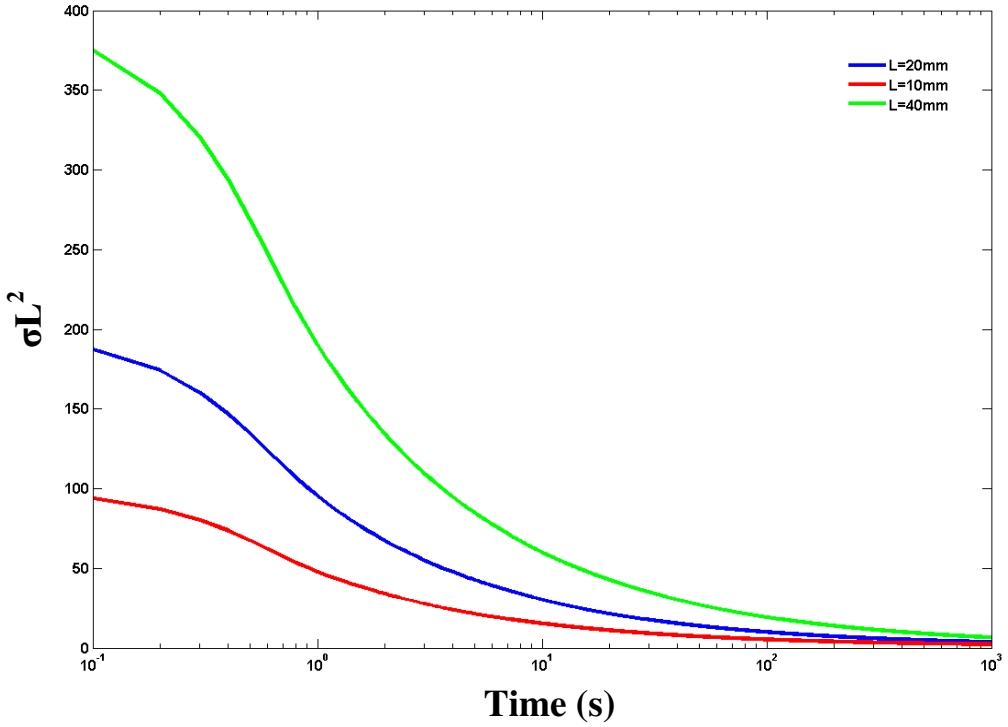

Figure 2-43: Semi-log plot showing the impact of length of matrix block on σL^2 (dimensionless) with time; D=0.1 mm^2/s.

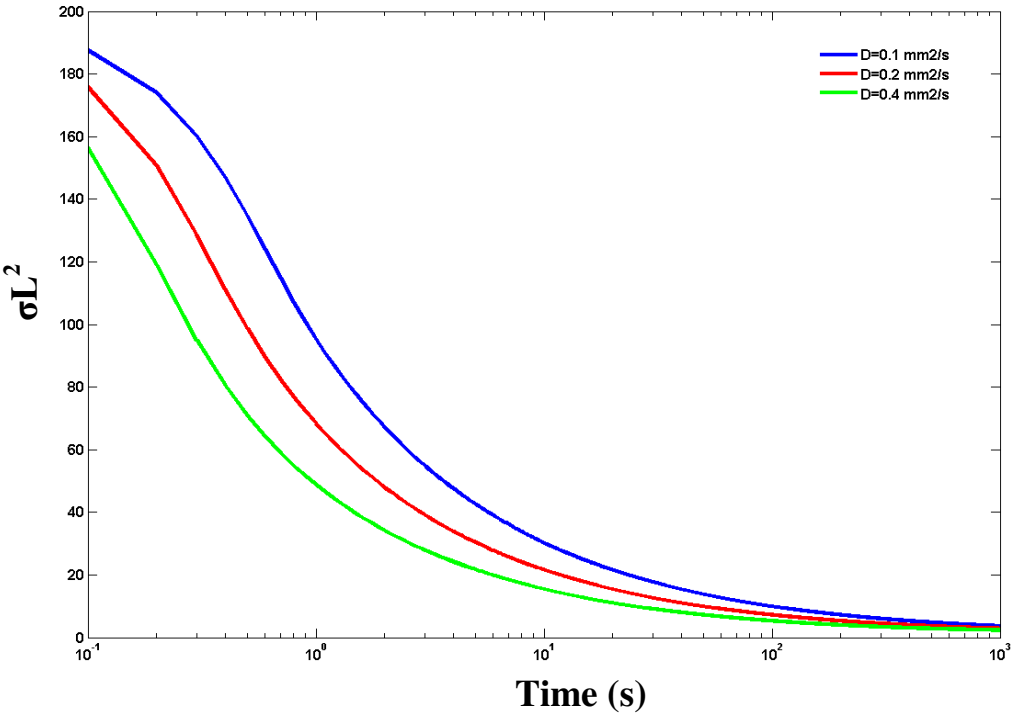

Figure 2-44: Semi-log plot showing the impact of Fickian diffusivity on σL^2 (dimensionless) with time; L=20mm.

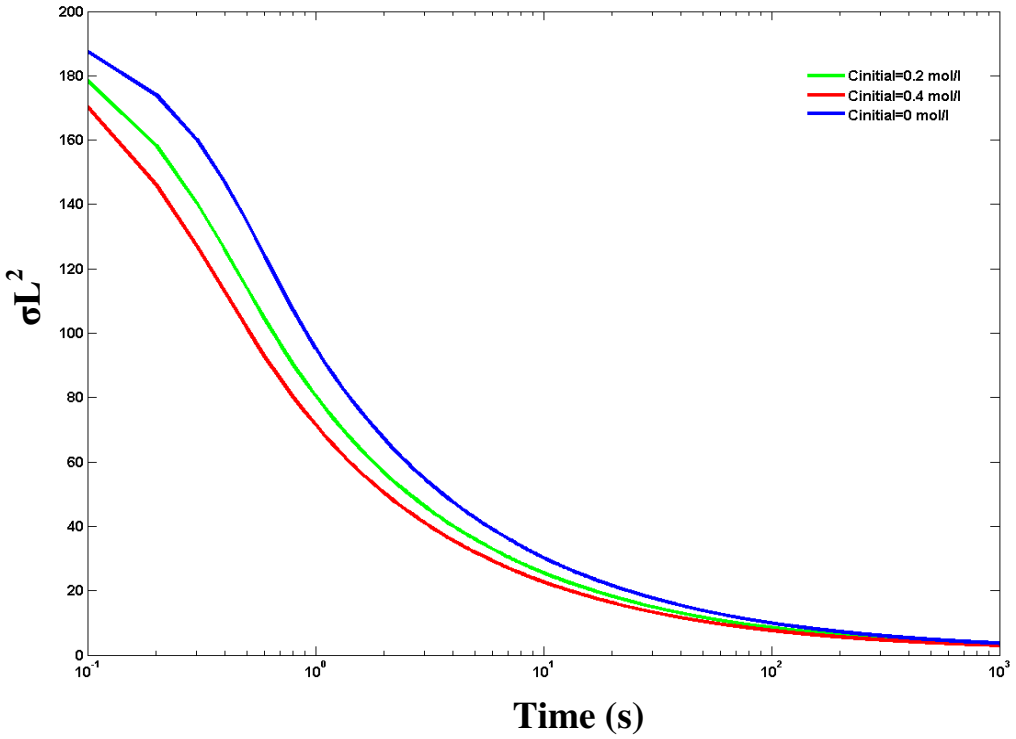

Figure 2-45: Semi-log plot showing the impact of initial condition on σL^2 (dimensionless) with time; L=20mm, D=0.1 mm^2/s.

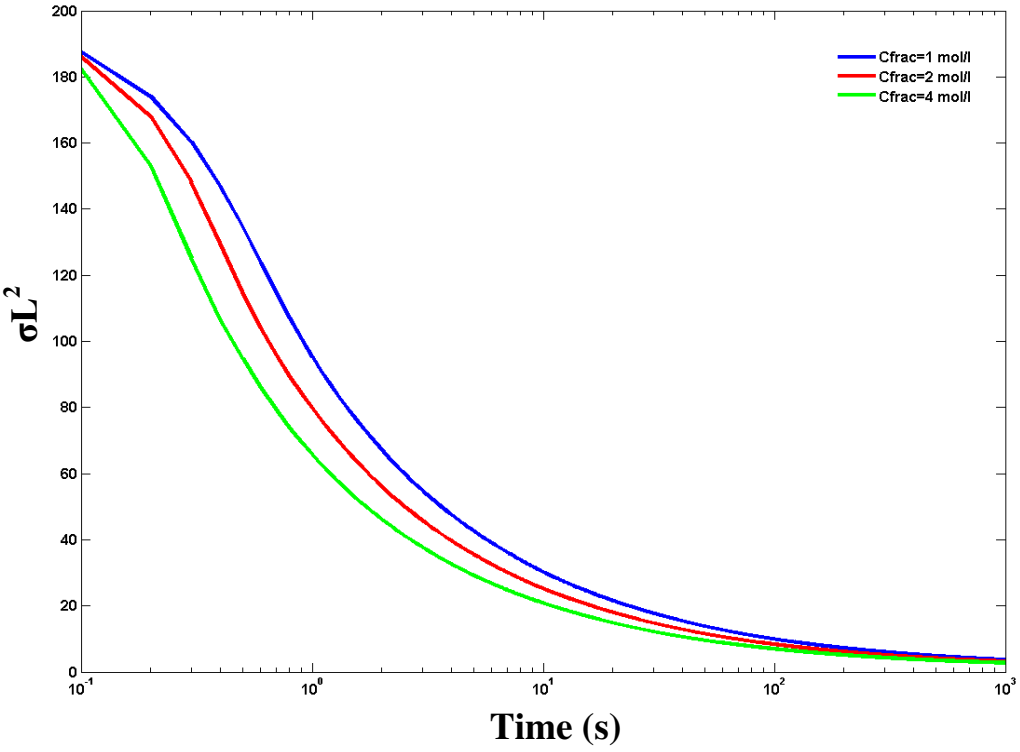

Figure 2-46: Semi-log plot showing the impact of boundary condition on σL^2 (dimensionless) with time; L=20mm, D=0.1 mm^2/s.

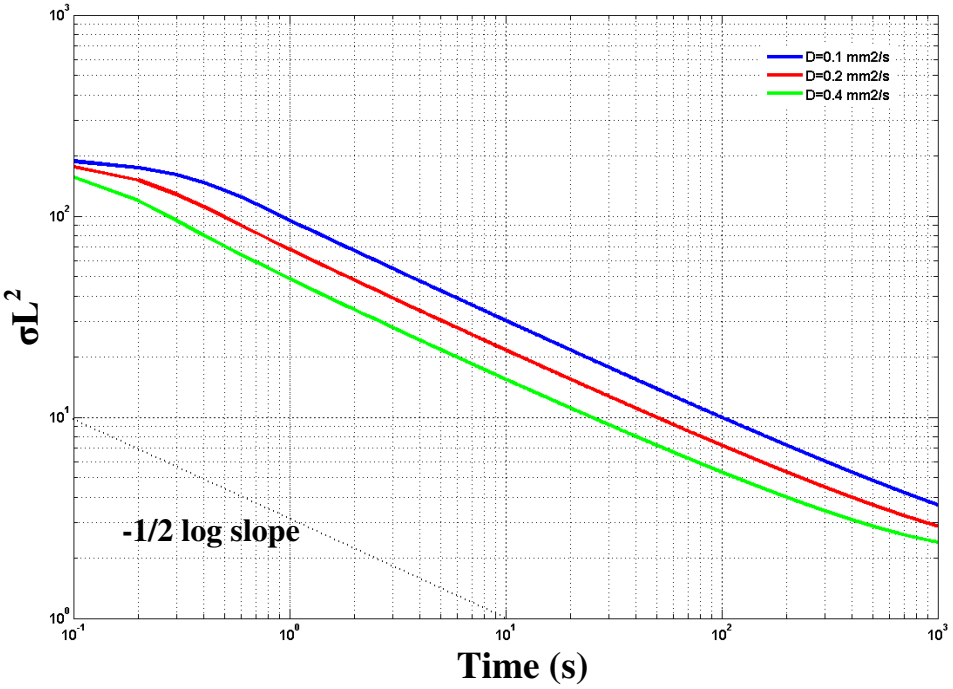

Figure 2-47: Log-log plot showing the impact of Fickian diffusivity on σL^2 (dimensionless) with time. In the early transient phase, the shape factors show linear behavior with a log slope of -1/2 on the log-log plot; L=20mm.

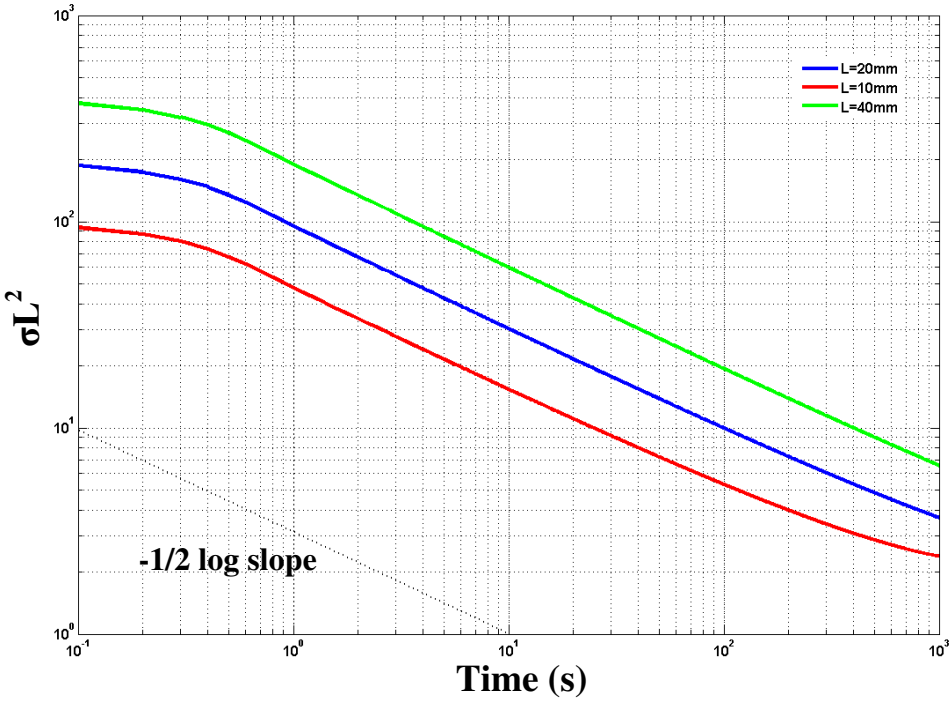

Figure 2-48: Log-log plot showing the impact of length of matrix block on σL^2 (dimensionless) with time. In the early transient phase, the shape factors show linear behavior with a log slope of -1/2 on the log-log plot; D=0.1 mm^2/s.

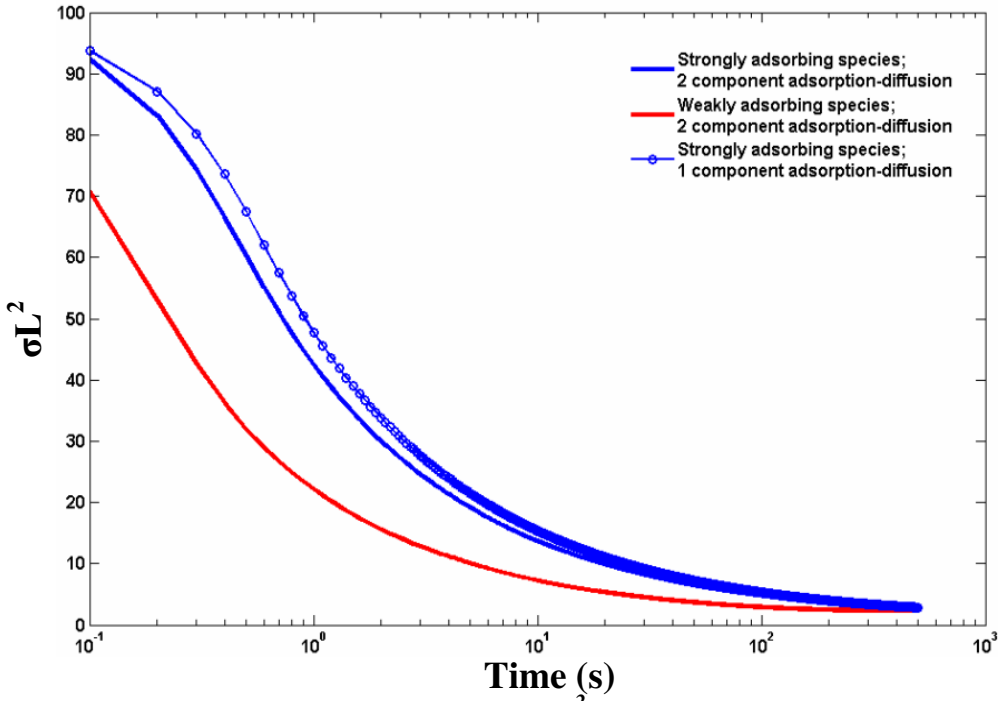

Figure 2-49: Semi-log plot comparing the σL^2 (dimensionless) values for the single component versus two component adsorption-diffusion case; L=10mm, D=0.1 mm^2/s.

Chapter 3

3. Experimental study of fluid flow in coal using CT scan

The objective of the experiments is to observe transient gas diffusion through bulk coal to ground truth some aspects of the modeling effort. The experimental study concentrates on the use of X-ray computed tomography (CT) for observing single and multiphase fluid flow within porous media interior. X-ray CT is a non-destructive, non-invasive technique that is applied here to visualize the internal structure of coal and the diffusion of tracer gas into these structures. The basic principle underlying CT scanning is the differential attenuation of a beam of X-rays as it passes through layers of varying thickness and density difference (Akin and Kovscek, 2003). Thus CT images are digital images of the effective X-ray attenuation coefficient for elementary volumes (voxels) within the sample. The CT number for each voxel is related to the experimental effective attenuation coefficient (μ) for that volume by the relationship (Akin and Kovscek, 2003):

$$CT = 1000\frac{(\mu - \mu_{water})}{\mu_{water}} \tag{3-1}$$

The units of Eq. 3-1 are Hounsfield (H). The linear attenuation coefficient is a function of the electron density, bulk density and effective atomic number. The CT number for a particular volume of the imaging space is affected by the amount and density of the coal present which is a function of fluid saturation, the minerals present and the void space in that volume. As a result, CT scans generating cross-sectional images of the coalpack assist in transient front tracking and flow profiling that otherwise is practically undetectable by standard practices. CT scanning also determines the dynamic two/three phase saturations.

3.1. Experimental set-up

A fast accurate and non destructive way to visualize a fluid flow inside a core is to use an X-ray CT scanner (Akin and Kovscek, 2003). The scanner employed was a Picker Synerview 1200 SX. The X-ray tube and the detectors rotate around the apparatus containing the core. The tube emits an X-ray beam that penetrates a thin volumetric slice of the core. The detector records the attenuated X-day beam and produces an electrical signal. Finally, the computer transforms this signal into a picture showing a slice of the core. Because the X-ray tube moves around the apparatus in a circular path and reconstruction algorithms assume symmetric paths, pictures have a better resolution when

the scanned object has a circular cross-section (Le Guen and Kovscek, 2005). The coal holder is kept inside a water jacket in order to minimize beam hardening effects that can introduce some artifacts in the CT images. Such effects result because photons of lower energy are more attenuated than those of greater energy (Schembre et al., 1998; Akin at al., 2000). The voltage of the scanner was fixed at 130 keV and the tube current at 95 mA.

The pore structure of coal and diffusion phenomenon of a gas inside coal was examined by injecting xenon gas into the sample at room temperature (25˚C). Xenon was chosen because of its relatively inert nature and because it is strong X-ray absorber. The presence of xenon should therefore be detectable against the coal background.

Figure 3-1 shows the CT image of the experimental setup. The core holder has 3 separate pieces of coal stacked on top of each other, the gap between the three mimicking cleats and fractures in coal. Once the coal pieces were stacked in the core holder, it was connected to a vacuum pump and allowed to dry for approximately two weeks. Once dry, the core holder was inserted vertically in the water jacket. After closing the whole assembly, the water jacket is filled with water. The core holder is sealed at one end (no flow/flux boundary) while the penetration of xenon into the coal was carried out by exposing the other end (base of core holder) to xenon at a pressure of 15 psia. High pressure (70 psia) N_2 serves as the confining pressure.

3.2. Results

With time, xenon gas diffuses into the coal matrix and as a result its concentration in the coal matrix increases with time. The idea of the experimental study is to capture this dynamic flow profile of xenon involving diffusion and advection in coal via CT scan images and attempt to measure the diffusivity of xenon in coal. The experiment was allowed to run for 44 hours. An increase in CT numbers with time implies a proportional increase in the xenon concentration in coal. The CT image produced by the computer attached to the scanner is a matrix of CT numbers in Hounsfield units. A MATLAB code was used to do image processing on these CT images. Figures 3-2 (a), (b), (c) and (d) are the CT scan images for the middle coal piece at different times. From these, one observes the slow penetration of xenon via diffusion inside coal.

The concentration of xenon inside coal is directly proportional to the increase in CT number; as a result the variation of CT number along the length of coal at different times is representative of the xenon concentration profile as a function of time. The CT numbers along the horizontal plane were averaged for each axial location, see Appendix B.2 for the MATLAB code.

Figure 3-3 shows the CT number variation with time along the length of coal. With time as the concentration of xenon builds up inside the coal pack, the CT number goes high. The variation of average CT number with time looks similar to the numerically simulated concentration profiles of CO_2 and/or N_2 diffusing inside coal matrix (Ch. 2).

The CT scan experiment can also be used to estimate the diffusivity of xenon in coal. This is based on the idea of curve matching, wherein we match the experimental data points (CT numbers) with the simulation results (xenon concentration). The diffusion of xenon inside coal, assuming no adsorption, is given by

$$\frac{\partial C_{xenon}}{\partial t} = D\frac{\partial^2 C_{xenon}}{\partial x^2} \tag{3-2}$$

We simulate the diffusion of xenon inside coal by using the above model using different values of xenon diffusivity (D) and plot the concentration profiles at certain time intervals. The initial and boundary conditions are kept the same as the experiment:

- At t=0 [xenon] = 0 mol/l (dry coal) for all x
- At x=0 [xenon] = 0.0417 mol/l (from ideal gas law: P_{xenon}=15 psia and T=298K)
- At x=L No flux

For the same time intervals, we overlay the CT profiles with the concentration profiles on the same plot. The middle part of the coal assembly, shown by the dotted area in Figure 3-1 was used for this analysis. In our case, the concentration buildup of xenon inside the core is primarily via diffusion phenomenon and the rate dictated by the diffusivity parameter, D. With time, the CT number varies inside the core because of the change in the concentration of xenon, the impact being one on one. Thus, making use of the above property of CT scans, "curve matching" can be performed to compute the diffusivity of xenon in coal. This is done by overlaying the average CT profile and concentration profile at a given time instant, on the same plot. From Figures 3-4 and 3-5 one can see that the concentration profile numerically simulated using a diffusivity of 3 mm^2/s matches pretty well with the experimental CT profiles for the two times.

The other matching technique that was used is based on the concept of self-similar solution of certain PDE's. The self-similarity method reduces the number of independent variables by introducing what are called "similarity variables". The parabolic diffusion equation (Eq. 3-2) is transformed into an ordinary differential equation by introducing the self-similar variable (Chen et al., 1990):

$$\xi = \frac{x}{\sqrt{t}} \tag{3-3}$$

The concentration and CT profiles are transformed into characteristic curves by plotting the concentration and CT numbers vs. the self similar variable defined by Eq. 3-3. From Figure 3-4 and 3-5, we got an idea about the diffusivity of xenon (D=0.3 mm^2/s). Reduction of the numerical solutions to the characteristic curves is illustrated in Figure 3-6. From the figure, one can see that the experimental data points plotted vs. ξ are centered on the characteristic curves. This also verifies that the diffusivity of xenon used in the numerical simulations is the value dictating the evolution of CT profiles with time.

With this we conclude that the diffusivity of xenon in coal at 298 K and atmospheric pressure is **3 mm^2/s**.

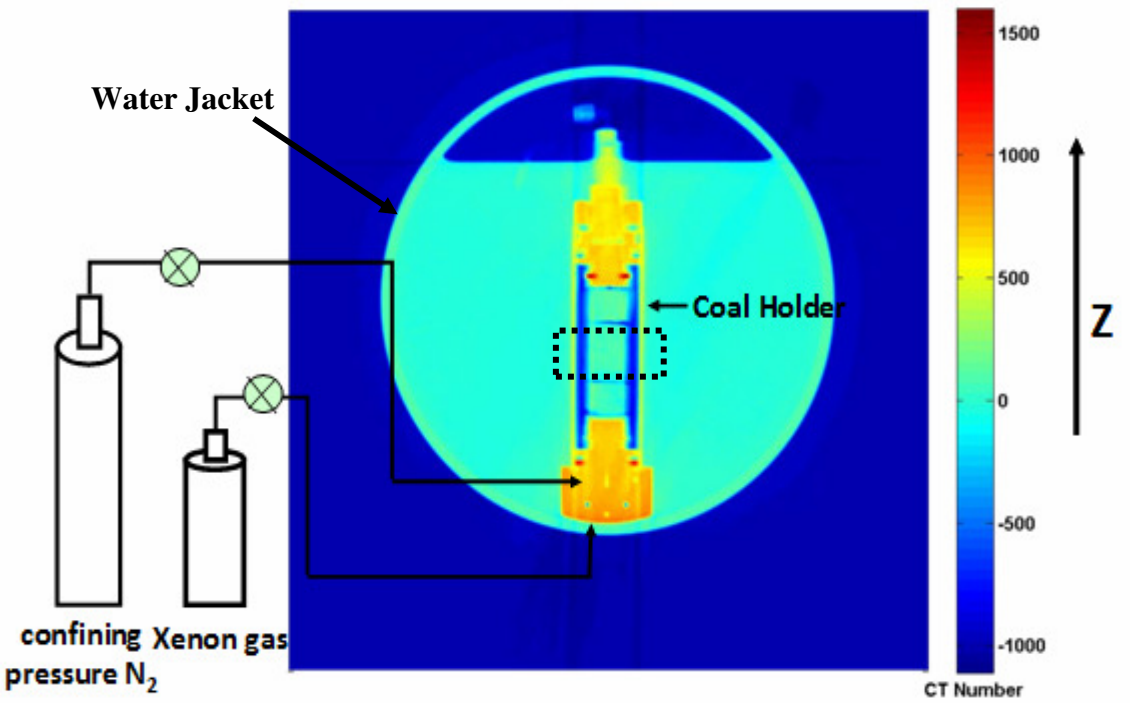

Figure 3-1: CT scan image of the experimental setup. Dashed box illustrates the portion of the core shown in detail in Figure 3-2.

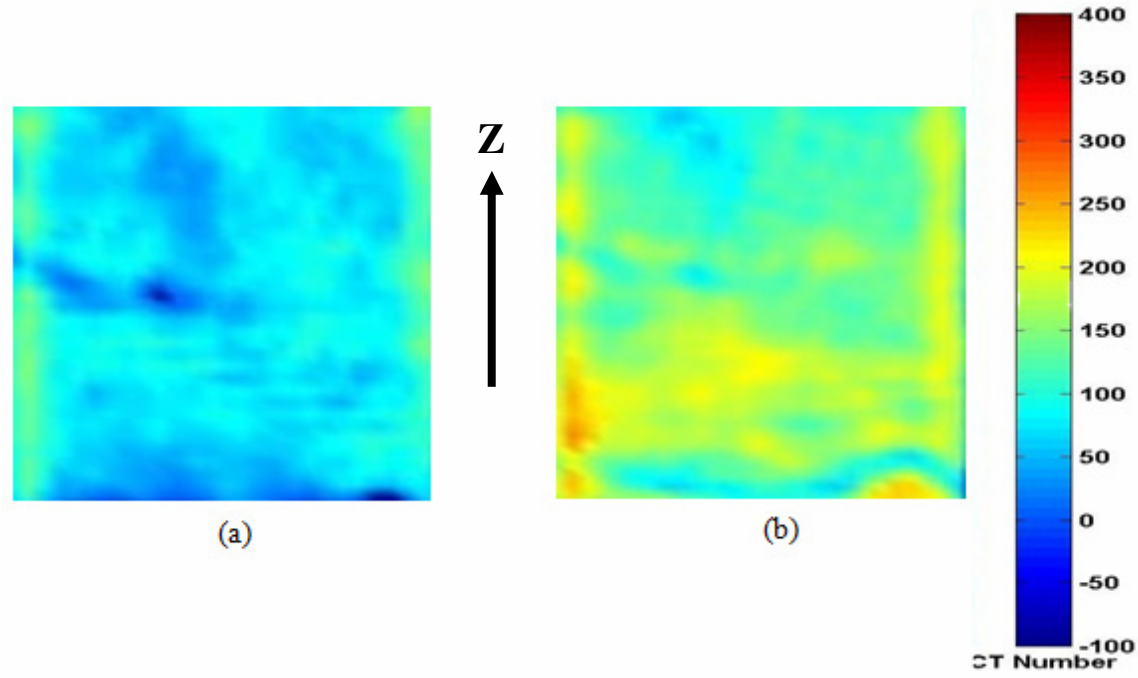

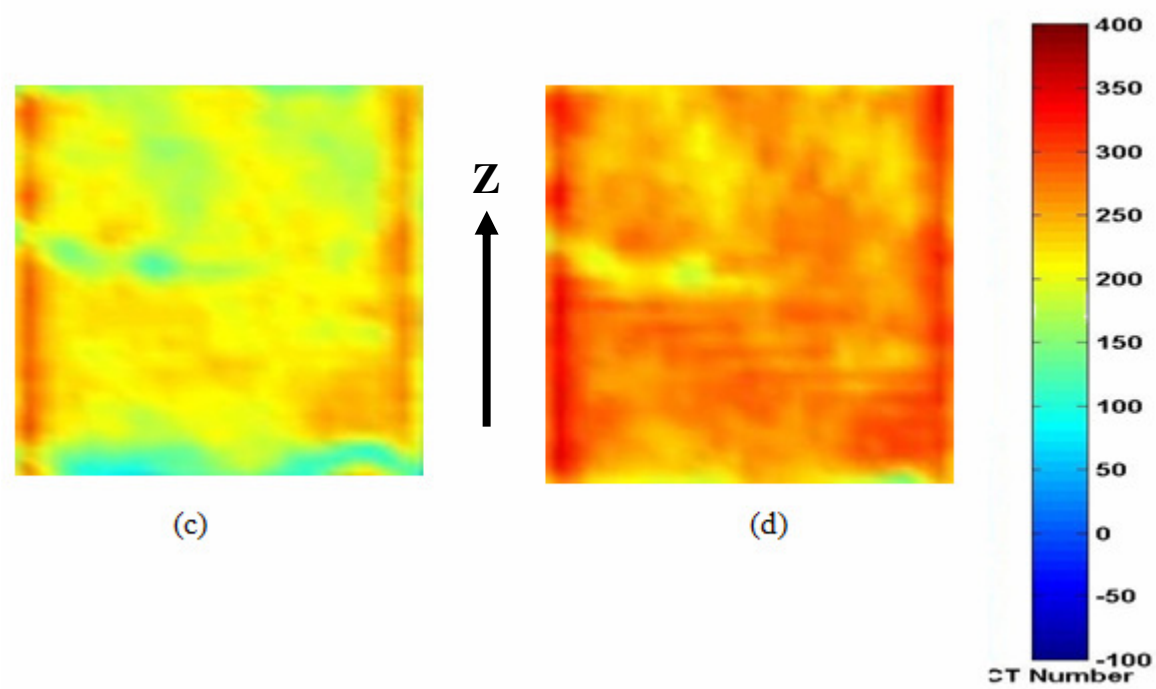

Figure 3-2: Zoomed CT scan images of the central coal piece shown by the dashed box in Figure 3-1 at (a) t=0 (b) t=51 mins (c) t=8hr33mins and (d) t=44hrs.

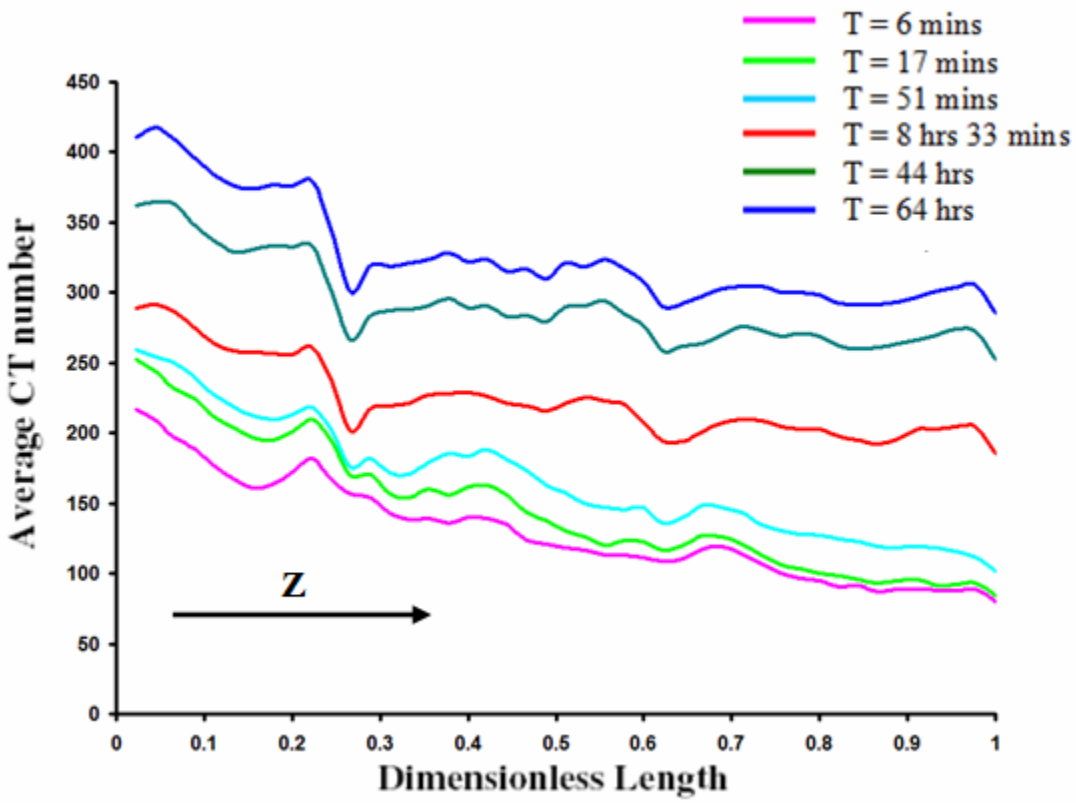

Figure 3-3: CT number variation along the length of coal with time.

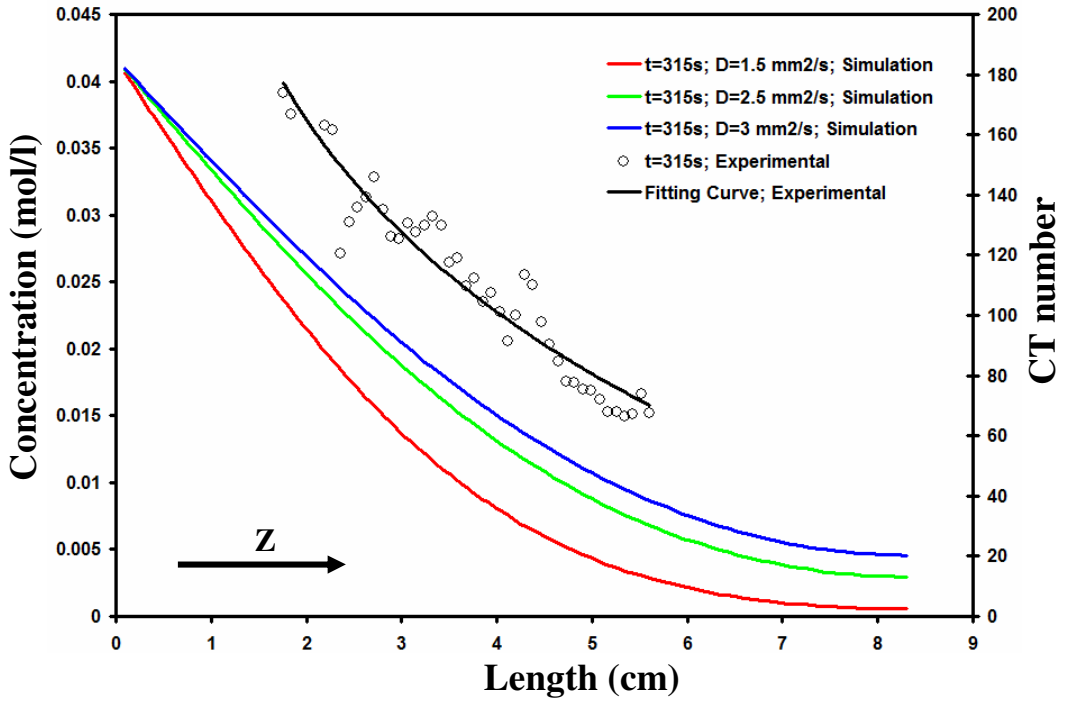

Figure 3-4: Plot overlaying the concentration profiles for different diffusivity values generated by simulation and experimental CT numbers at t=315 s.

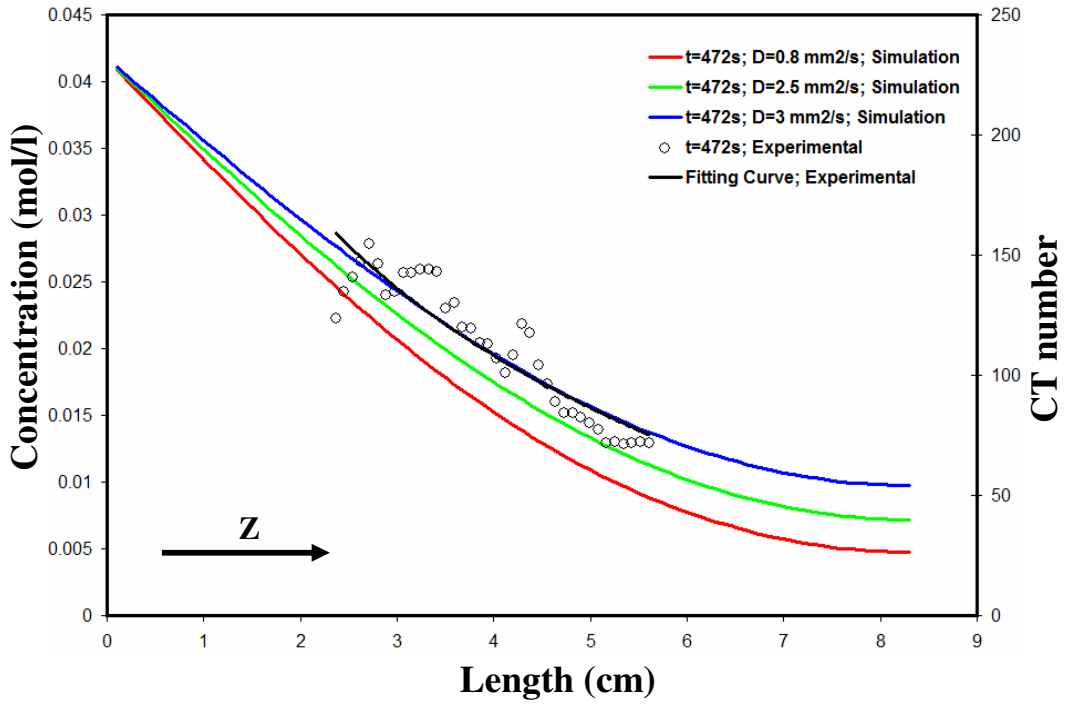

Figure 3-5: Plot overlaying the concentration profiles for different diffusivity values generated by simulation and experimental CT numbers at t=472 s.

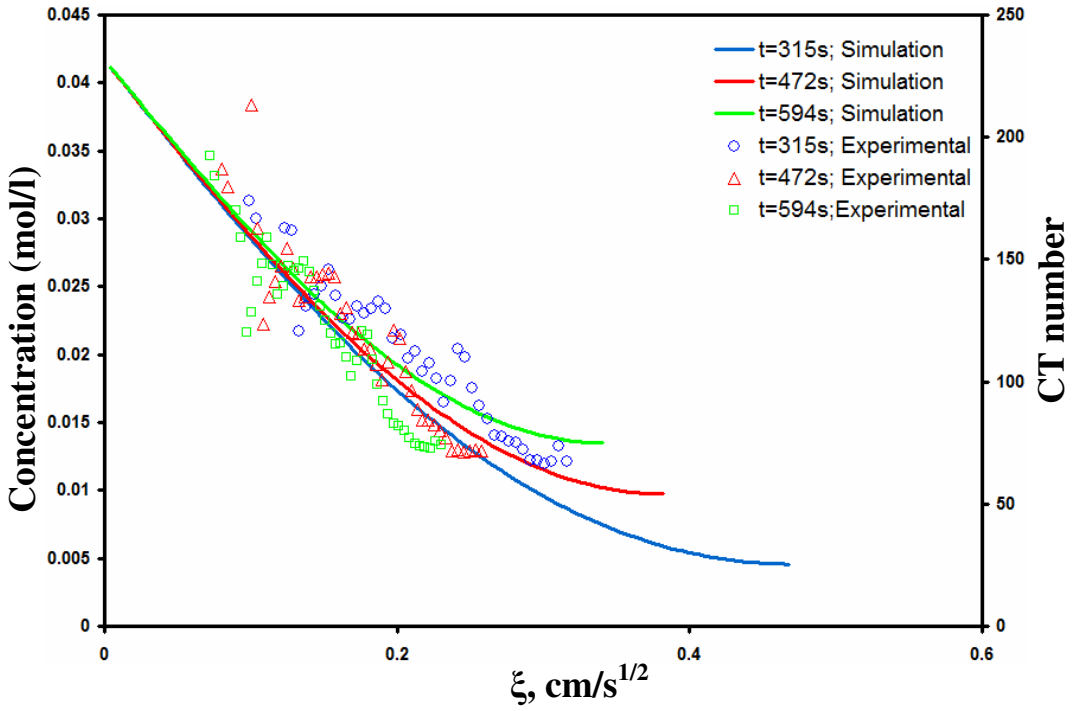

Figure 3-6: Reduction of numerical solutions using D=3 mm^2/s to the characteristic curves. The experimental CT numbers are centered on these characteristic curves.

Chapter 4

4. Conclusions

The primary focus of the work presented in this thesis has been the development of simulation models and algorithms for the study of ECBM recovery. The overall conclusions of the work are summarized in this chapter.

The motivation for addressing this topic has been the high potential of ECBM recovery by injection of CO_2 or by injection of CO_2 and N_2 to recover additional natural gas resources (CH_4) while at the same time sequestering CO_2 in the subsurface. Conventional numerical simulators, however, have limited predictive capabilities for the design and development of ECBM field projects because they neglect certain physical mechanisms intrinsic to the technique and its application in coalbeds. The Warren-Root approach is the industry standard procedure to explaining gas migration in dual-porosity media, implemented in many CBM simulators. The gas diffusion and adsorption dynamics have been, almost exclusively modeled using the quasi-steady state Fickian diffusion equation together with Langmuir equation. However, the interspecies interactions as described by the generalized Fick's law are neglected in the conventional simulators. The MS equation offers a more rigorous theoretical treatment of multicomponent diffusion in coalbeds by taking into account the interactions between the different gas components in the system.

The transport mechanism is primarily molecular/bulk diffusion in the matrix. From our calculation of the mean free path of gas molecules and from literature survey, one can conclude that the contribution of Knudsen diffusion in the gas transport within coal matrix, if at all, will be very less as compared to molecular/bulk diffusion. In our modeling approach, the simplicity of the Fick's diffusion expression has been retained but at the same time the MS approach has been incorporated to describe the transient multicomponent gas diffusion dynamics. The MS diffusivities ($Đ_{ij}$) are used to compute the Fickian diffusivities. Our modeling effort is targeted towards capturing the physics of the ternary (three component) gas adsorption-diffusion dynamics. The idea is to understand the impact of intermolecular interactions and mass transfer limitations on the CH_4 production prediction. A model very similar to the unipore diffusion model has been implemented. The only difference is that in this case, unlike the unipore diffusion model, gas can co-exist as a free gas and as an adsorbed state in the coal matrix.

A fully implicit solution method has been developed to model the ternary adsorption-diffusion transport problem. The Fickian diffusivities in our case are computed rigorously from MS diffusivities and composition. From the numerical examples, we observed that these Fickian diffusivities can sometimes vary significantly with time (Figure 2-11) and consequently have an important bearing on the gas adsorption-diffusion dynamics. The

counter diffusion between CO_2/N_2 and CH_4 results in the depletion of CH_4 in the matrix pores. As a result, very small concentration gradients for CH_4 develop in the vicinity of the CH_4 gas exit. Since the molecular diffusion is driven by concentration gradient, these low CH_4 concentrations near the boundary would create mass transfer resistance, thus curtailing the production of CH_4.

One important aspect of ECBM recovery is the adsorption and desorption behavior of gas mixtures on coalbeds. Conventional simulation tools use the ELM for predicting the sorption behavior of mixtures of CH_4, CO_2 and N_2 on the coal surface. From literature survey, it has been found that the ELM is unable to describe the behavior of ternary $CO_2/N_2/CH_4$ displacements. In our case, we started off with the ELM adsorption model and then developed a separate algorithm, incorporating the IAS adsorption model into the gas transport equations. The IAS model introduces an additional variable P_i^o (pure adsorbate pressure) which makes the IAS model more complicated than the ELM. As a result, the IAS model requires a nested iterative scheme to solve for gas compositions. Accordingly, the IAS model is more computationally expensive than the traditional approaches. A comparison of the concentration profiles predicted using the ELM and IAS models showed that there is substantial mismatch in prediction in the early transient phase. It was observed that the mismatch is more prominent for the most strongly adsorbed components which in our case are CO_2 and CH_4. This suggests that probably the IAS model is more sensitive to dynamic changes in pressure and composition than the ELM model.

We performed a sensitivity study on the recovery of CH_4 under varying rates of diffusion and adsorption and for varying gas compositions. CH_4 recovery is not sensitive to the total loading of the surface as influenced by the ELM adsorption parameters. The diffusivity parameters on the other hand substantially affect the concentration profiles of gases; greater diffusivities lead to rapid depletion of CH_4 gas. The injection gas composition study revealed that a greater composition of N_2 augments the rate of CH_4 recovery for the shorter time scales that we have considered. CH_4 on the other hand, leads a more complete displacement (Jessen et al., 2007). The reason is in the later stage, CO_2 saturates the coal surface owing to its strong adsorption tendency and as a result strips the CH_4, thereby leading to more uniform displacement.

The grid size and time step size sensitivity study shows that the solution method is stable and it converges for a wide range of MS diffusivity values. The numerical method was later tuned to make it more robust. “shoe-horn” method was found to be most suitable and thereby implemented in the solution algorithm. The solution method was then validated by two mutually exclusive test cases. In one case, the ternary adsorption-diffusion case was reduced to a single component pure diffusion case. For the other validation test, the full multicomponent transport problem was solved using a “numerical perturbation” technique. The derivatives required in the Jacobian of the fully coupled implicit system were approximated by numerical differences. In our case, an adaptive algorithm is implemented to decide upon the optimal perturbation size. The simulation results from the two test cases seemed to agree well with those from the numerical model,

thus validating the solution method. In addition, it was observed that the numerical model in comparison to the perturbation technique is much faster even under finer scale grid resolution.
We then investigated the matrix-fracture transfer function dictating mass transport from matrix to fracture or vice versa. Coalbeds are NFR comprising an interconnected fracture system that forms larger scale porous structures through which pressure driven flow travels according to Darcy's law and matrix blocks between those fractures with fine pores within which diffusion takes place. Flow between the matrix block and fracture is fundamental to the productivity of CH_4 gas from coal seams. In the dual-porosity model, these matrix-fracture interactions are modeled through a "transfer function" incorporating a "shape factor" (σ). With respect to CBM models, the standard industry practice is to use the Warren and Root approach which is based on a pseudo-steady state assumption. The conventional CBM simulators define a sorption/diffusion time which involves a constant effective diffusivity and a constant shape factor, both of which are not true in complete sense.

We developed an algorithm to compute numerically the shape factors for both pure diffusion and for adsorption-diffusion cases. In the derivation of shape factor, we do not invoke the pseudo-steady state assumption and thereby capture the transient matrix-fracture interactions. In the early transient phase, the shape factor is a large value because the concentration gradient driving mass into the matrix from fracture is maximum progressively decreasing with time. During this transient phase, the shape factor calculation is very sensitive to grid resolution, see Figure 4-1. From the sensitivity study, we found that during the early transient phase, the shape factor is a function of both the geometry of the system and the physics of mass transfer and concentration gradients in the matrix. The study verified that at late times and under pseudo- steady state conditions, the shape factor is a governed only by the geometry of the system and thereby a constant value. In our case, at late times the product of the shape factor and square of the length of matrix block (σL^2) for the given coalbed geometry and for the single component diffusion case comes out to be 2.443.

Compared to the pure diffusion case, it was observed that when adsorption occurs, the shape factor value is greater and there is a prolonged transition period (gradual slope) before attaining pseudo-steady state. This means that the assumption of constant shape factor based on the geometric parameters of the matrix block can presumably lead to significant deviations in the gas productivity prediction in conventional CBM models (based on constant shape factors). In fact, the deviations would be more significant for strongly adsorbing gas species such as CO_2 and/or CH_4. At late times, however, the shape factor appears to converge to the pure diffusion value. The sensitivity study revealed that the log-log plot of σL^2 with time during the early transient phase results in straight lines with a -1/2 log slope.

We also conducted experiments to observe transient diffusion dynamics for flow through bulk coal to ground truth some aspects of the modeling effort. The experimental study concentrates on the use of X-ray Computed Tomography (CT) for observing single phase

fluid flow in coal. The pore structure of coal and diffusion phenomenon of a gas inside coal was examined by injecting xenon gas into coal at room temperature (25˚C). Xenon was chosen because of its relatively inert nature and because it is a strong X-ray absorber. Differential rates of mass transport involving diffusion and advection showed up on the CT scans and this indicated the presence of heterogeneity inside coal.

In our case, the concentration buildup of xenon inside the core is primarily via diffusion phenomenon and the rate dictated by the diffusivity parameter, D. The concept of "curve matching" was used to compute the diffusivity of xenon in coal. This involved overlaying the experimental CT scan data set and the simulation results at a given time on the same plot. Two matching techniques have been illustrated, one of them based on the concept of "self-similarity". Using both the approaches, we found that the diffusivity of xenon in dry coal sample at 298 K and atmospheric pressure is 3 mm^2/s. There is no direct reference to xenon diffusivity value in dry coal in the literature, however its order of magnitude is consistent with the experimental binary gas diffusivity data tabulated by Hirschfelder et al. (1954) and Reid et al. (1977) for different gas pairs.

Suggestions for future work

The MS diffusion formulation that we considered invoked the assumption that fluids exhibited ideal behavior. The MS equations in a non ideal case would include a thermodynamic factor which takes into account the activity and fugacity coefficients. Computing the thermodynamic factor will require the evaluation of the derivatives of fugacities. The solution strategy will then become more complicated because it requires flash calculation to solve the equation of state.

There are different forms of representing the multicomponent flux equation such as the generalized Fick's law, Onsager-Fuoss, Darken, Nernest-Planck and Lattice Density Functional Theory (LDFT) equations (Matuszak and Donohue, 2005). Using inversion techniques, one can convert these multicomponent diffusion equations to the MS form. The generalized Fick's equation has been used in our case along with MS formulation, but it would be interesting to try out the other forms of multicomponent flux equations and compare the predictions against the standard Fick's law.

In our simulation study, we have successfully modeled matrix-fracture interactions and numerically computed the shape factor, but all of this was based on the assumption that the fracture compositions remained constant. If this is not the case, the Darcy flow equations in the fractures need to be solved simultaneously with the matrix adsorption-diffusion equations. Moreover, water is usually present in the cleats and fractures and this will make the modeling task even more challenging. Thus, as a future task one can model the above coupled fracture and matrix transport problem.

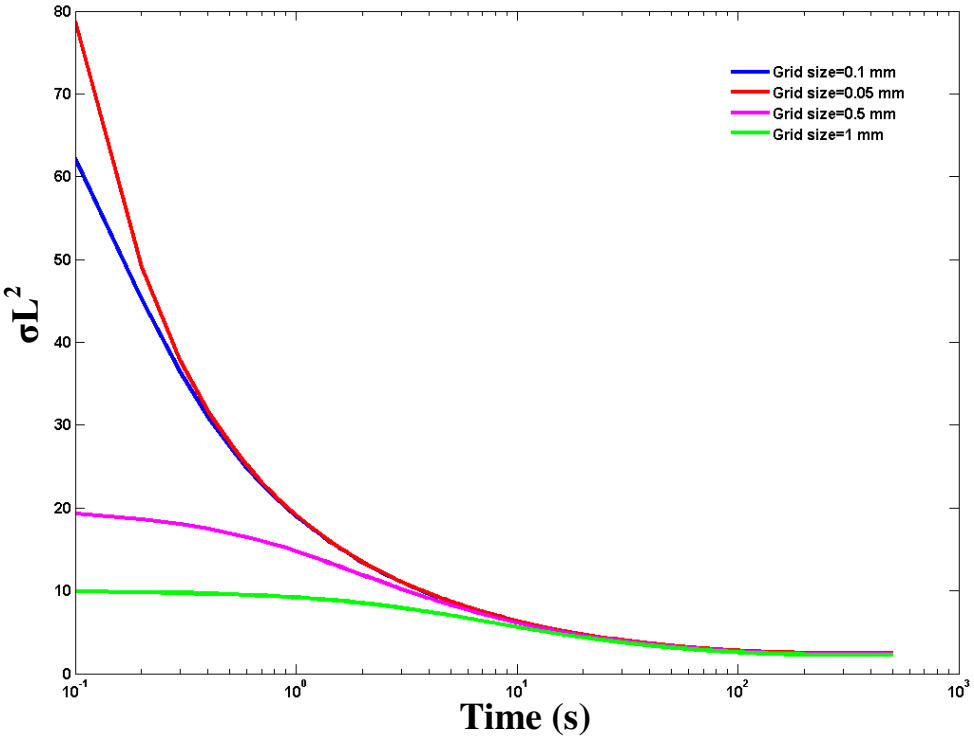

Figure 4-1: Semi-log plot showing the impact of grid resolution on σL^2 (dimensionless) with time for the pure diffusion case; Δt=0.1s, L=10mm, D=0.1 mm^2/s.

Nomenclature

a	Molar concentration of the adsorbed component
B	ELM parameter
c	Fluid compressibility
C	Gas composition
d_F	Driving force for diffusion
d	Pore diameter
M	Molecular weight
[**D**]	Diffusivity matrix
D	Fickian diffusivity
D_K	Knudsen diffusivity
Đ	MS diffusivity
D_{eff}	Effective diffusion coefficient
F	Residual vector
J_{ij}	Jacobian element
J	Diffusive flux
[J]	Jacobian matrix
k_B	Boltzmann constant
k_f	Fracture permeability
k_m	Matrix permeability
L	Length of matrix block
n	Specific amount adsorbed
n_C	Number of components
N	Number of grid points
P	Pressure
P^o	Pure adsorbate pressure
q	Rate of matrix-fracture transfer
r_C	Radius of microporous particle
R_p	Radius of macroporous particle
R_g	Universal gas constant
T	Temperature
u	Diffusive velocities

V_m ELM parameter

V Average remaining gas content in coal matrix

V_E Gas content in equilibrium with cleat gas pressure

V_b Liquid molar volume at normal temperature

V_c Critical volume

x Mole fraction in adsorbate phase

y Mole fraction in gas phase

Z Gas compressibility factor

Δx Grid size

Δt Time step size

δy Vector of unknowns

α Separation factor

ρ Density

π Spreading pressure

ζ Friction coefficient

α' Modified ELM parameter

β' Modified ELM parameter

σ_{AB} Collision diameter

σ Shape factor

Ω_D Diffusion collision diameter

Σ_v Sum of atomic diffusion volumes

τ Sorption time

ξ Similarity variable

μ Attenuation coefficient

μ_f Viscosity of fluid

ϕ_f Fracture porosity

ϕ Matrix porosity

Θ Accumulation in the matrix

ε Energy of interactions

λ Mean free path

References

Akin, S., Schembre, J.M., Bhat, S.K., and Kovscek, A.R.: "Spontaneous imbibition characteristics of diatomite, Journal of Petroleum Science and Engineering, 25, 149-165 (2000).

Akin, S., and Kovscek, A.R.: "Computed Tomography in Petroleum Engineering Research", Geological Society, London, Special Publications 23-38 (2003).

Bird, R.B., Stewart, W.E., and Lightfoot, E.N.: "Transport Phenomena, 2nd Edition", John Wiley & Sons, Inc. (2002).

Burchard, J.K., and Toor, H.L.: "Diffusion in an Ideal Mixture of Three Completely Miscible Non Electrolytic Liquids- Toluene, Chlorobenzene, Bromobenzene" J. Phys. Cem., 66, 2015-2022 (1962).

Barenblatt, G.E., Zheltov, I.P., and Kochina, I.N.: "Basic Concepts in the Theory of Homogeneous Liquids in Fissured Rocks", Journal of Applied Mathematical Mechanics 24: 1286-1303 (1960).

Bustin, R.M., and Clarkson, C.R.: "Free gas storage in matrix porosity: A potentially significant coalbed resource in low rank coals", paper 9956 presented at the 1999 Intl. Coalbed Methane Symposium, Tuscaloosa, Alabama, (1999).

Beckner, B.L.: "Improved Modeling of Imbibition Matrix/Fracture Fluid Transfer in Double Porosity Simulators. PhD dissertation. Stanford, California, Stanford U (1990).

Clarkson, C.R., and Bustin, R.M.: "Binary gas adsorption/desorption isotherms: effect of moisture and coal composition upon carbon dioxide selectivity over methane", Intl. Journal of Coal Geology 42: 241-271 (2000).

Cussler, E.L.: "Diffusion Mass Transfer in Fluid System", Cambridge University Press (1984).

Cervik, J.: "Behavior of Coal-Gas Reservoirs," presented at the 1967 SPE Eastern Regional Conference, Pittsburgh, (1973).

Clarkson, C.R. and Bustin, R.M.: "The Effect of Pore Structure and Gas Pressure upon the Transport Properties of Coal: a Laboratory and Modeling Study. 2. Adsorption rate modeling", Fuel 78: 1345-1362 (1999).

Crosdale, P.J., Beamish, B.B., and Valix, M.: "Coalbed Methane Sorption related to Coal composition", Intl J of Coal Geology 35, 147-158 (1998).

Chen, Z.X., Bodvarsson, G.S., and Witherspoon, P.A.: " An Integral equation formulation for two- phase flow and other nonlinear flow problems through porous media", SPE

20517, 447-457, presented at the 65th Annual Technical Conference and Exhibition of the Society of Petroleum Engineers held in New Orleans, Louisiana, U.S.A., September pp. 23-26 (1990).

Chang, M.: "Deriving the Shape Factor of a Fractured Rock Matrix", Technical Report NIPER-696 (DE93000170). Bartlesville, Oklahoma: NIPER (1993).

Chapman, S., and Cowling, T.G.: "The Mathematical Theory of Non-Uniform Gases, 3rd Edition", Cambridge University Press (1970).

Danner, R.P., and Daubert, T.E.: "Manual for Predicting Chemical Process Design Data", AIChE, New York (1983).

Dawson, R., Khoury, F., Kobayashi, R.: "Self Diffusion Measurements in Methane by Pulsed Nuclear Magnetic Resonance", AIChE J. 16, 725 (1970).

Do, D.D.: "Adsorption Analysis: Equilibria and Kinetics -Vol. 2", Imperial College Press. (1998).

Fathi, E., and Akkutlu, I.Y.: "Counter-Diffusion and Competitive Adsorption Effects During CO_2 Injection and Coalbed Methane Production", SPE 115482, paper presented at the 2008 SPE Annual Technical Conference and Exhibition held in Denver, Colorado, USA (2008).

Fuller, E.N., Shettler, P.D., and Giddings, J.C.: Ind. Eng. Chem., 58(5): 18 (1966).

Fuller, E.N., and Giddings, J.C.: J. Gas Chromatogr., 3: 222 (1965).

Fuller, E.N., Ensley, K., and Giddings, J.C.: J. Phys. Chem., 73: 3679 (1969).

Gale et al.: "Carbon Dioxide Capture and Storage", Intergovernmental Panel on Climate Change (IPCC) Special Report held in Montreal, Canada (2005), published by Cambridge University Press. http://www.ipcc.ch/ipccreports/srccs.htm.

Ghorayeb, K., and Firoozabadi, A.: "Modeling Multicomponent Diffusion and Convection in Porous Media", SPE 62168, paper presented at the 1999 SPE Reservoir Simulation Symposium held in Houston, USA (1999).

Gamson, P.D., Beamish, B.B., and Johnson D.P.: "Coal Microstructure and Micropermeability and Their Effects on Natural Gas Recovery", Fuel 72, 87-99 (1993).

Gamson, P.D., Beamish, B.B., and Johnson, D.P.: "Coal Microstructure and Secondary Mineralization: Their Effect on Methane Recovery", Geological Society of London; 165-179 (1996).

Gasem, K.A.M., Pan, Z., Fitzgerald, J.E., and Sudibandriyo, M.: "Adsorption Modeling Update. Present at the Second International Forum on Geological Sequestration of CO2 in deep unmineable coal seams (Coal-Seq II)", Washington DC, (2003).

Hoteit, H., and Firoozabadi, A.: "Numerical Modeling of Diffusion in Fractured Media for Gas Injection and Recycling Schemes", SPE 103292, paper presented at the 2006 SPE Annual Conference held in San Antonio, Texas, USA (2006).

Harris, J, Kovscek, A.R., Orr, F.M., and Zoback, M.D.: "Geologic Storage of Carbon Dioxide" 2007-08 Technical Report of the Global Climate and Energy Project, Stanford University http://gcep.stanford.edu/research/technical_report/20012.html.

Hirschfelder, J., Curtiss, E.L., and Bird, R.B.: "Molecular Theory of Gases and Liquids", Wiley, New York (1954).

Jessen, K., Lin, W., and Kovscek, A.R.: "Multicomponent Sorption Modeling in ECBM Displacement Calculations", SPE 110258, presented at the 2007 SPE Annual Technical Conference and Exhibition held in Anaheim, CA U.S.A., (2007).

Kazemi, H., Merrill, L.S. Jr., Porterfield, K.L., and Zeman, P.R.: "Numerical Simulation of Water-Oil Flow in Naturally Fractured Reservoirs. SPEJ 23 (4): 695-707. SPE-10511-PA (1976).

Leahy-Dios, A., and Firoozabadi, A.: "Unified Model for Non-Ideal Multicomponent Molecular Diffusion Coefficients", AIChE J. 53(11), 2932-2939 (2007).

Le Guen, S.S., and Kovscek, A.R.: "Non-equilibrium Effects during Spontaneous Imbibition" Transport in Porous Media, 63: 127-146 (2006).

Lu, M., and Connell, L.D.: "A Multi-Component Dual-Porosity Model for Gas Reservoir Flow with Adsorption Behavior", SPE 101113, paper presented at the 2006 SPE Asia Pacific Oil & Gas Conference and Exhibition held in Adelaide, Australia (2006).

Lin, W., Tang, G.-Q., and Kovscek, A.R.: "Sorption-Induced Permeability Change of Coal during Gas-Injection Processes", SPE 109855, presented at the 2007 SPE Annual Technical Conference and Exhibition held in Anaheim, CA U.S.A., (2007).

Laxminarayana, C., and Crosdale, P.J.: Role of coal type and rank on methane sorption characteristics of Bowen Basin, Australia, Intl J of Coal Geology 40, 309-325 (1990).

Lim, K.T., and Aziz, K. "Matrix-fracture transfer shape factors for dual-porosity simulators", Journal of Petroleum Science and Engineering, 13: 169-178 (1995).

Markham, E.C., and Benton, A.F.: "The Adsorption of Gas Mixtures by Silica", J. Amer. Chem. Soc. 53, 497-507 (1931).

Matuszak, D., and Donohue, M.D.: "Inversion of multicomponent diffusion equations", Ch. Eng. Sc. 60: 4359-4387 (2005).

Myers, A.L., and Prausnitz, J.M.: "Thermodynamics of Mixed-Gas Adsorption", AIChE Jr. 11, 121-127 (1965).

Mather, G and Thodos, G.: "The self diffusivity of substances in the gaseous and liquid states", AIChE J. 11, 613 (1965).

Moore, W.R.: "Geothermal Gradient of the Powder River Basin, Wyoming", presented at the AAPG Annual Meeting, Salt Lake City, UT U.S.A. 11-14 (2003).

Muckenfuss, C.: "Stefan-Maxwell Relations for Multicomponent Diffusion and Chapman Enskog Solution of the Boltzmann Equations" J. Chem. Phys. 59, 1747-1752 (1973).

Myers, A.L., and Prausnitz, J.M.: "Thermodynamics of Mixed-Gas Adsorption", AIChE J., 11: 121 (1965).

Perry, R.H., and Green, D.W.: "Perry's Chemical Engineers' Handbook (7^{th} Edition)", McGraw-Hill Company, Inc. (1997).

Remner, D.J., Ertekin, T., and King, G.R.: "A Parametric Study of the Effects of Coal Seam Properties on Gas Drainage Efficiency", paper SPE 13366, Proceedings, SPE Eastern Regional Meeting, Charleston, WV, (!984).

Rangel-German, E.R., and Kovscek, A.R.: "Time-dependent matrix-fracture shape factors for partially and completely immersed fractures", Journal of Petroleum Science and Engineering, 54, 149-163 (2006).

Riazi, M.R., and Whitson, C.H.: "Estimating Diffusion Coefficients of Dense Fluids", Ind. Eng. Chem. Res. 32, 3081 (1993).

Reid, R.C., Sherwood, T.K., and Prausnitz, J.M.: "The Properties of Gases and Liquids, 3rd Edition", McGraw-Hill, New York (1977).

Rice, D.D.: "Composition and origins of coalbed gas. In: Law, B.E., Rice, D.D. (Eds), Hydrocarbons from Coal. AAPG Studies in Geology, 38, 159-185 (1993).

Ruthven, D.M.: "Principles of Adsorption and Adsorption Processes", Wiley, New York (1984).

Smith, D.M., and Williams, F.L.: "Diffusional Effects in the Recovery of Methane From Coalbeds", Society of Petroleum Engineers of AIME (1984).

Stevens, S.H., Spector, D., and Reimer, P.: "Enhanced Coalbed Methane Recovery Using CO2 Injection: Worldwide Resources and CO2 Sequestration Potential", SPE 48881, presented at the 1998 SPE International Conference and Exhibition held in Beijing, China, (1998).

Shi, J.Q., and Durucan, S.: "A bidisperse pore diffusion model for methane displacement desorption in coal by CO2 injection", Fuel, Vol 82, 1219-1229 (2003).

Sengul, M.: "CO2 Sequestration – A Safe Transition Technology", SPE 98617, presented at the SPE International Conference on Health, Safety, and Environment in Oil and Gas Exploration and Production held in Abu Dhabi, U.A.E., (2006).

Sigmund, P.: "Prediction of Molecular Diffusion at Reservoir Conditions. Part 1- Measurements and Prediction of Binary Dense Gas Diffusion Coefficients", J. of Canadian Petro. Tech. 48 (1976a).

Sigmund, P.: "Prediction of Molecular Diffusion at Reservoir Conditions. Part 2- Estimating the Effect of Molecular Diffusion and Convective Mixing in Multicomponent Systems", J. of Canadian Petro. Tech. 53 (1976b).

Sharkey, A.G., Jr. and McCartney, J.T.: "Chemistry of Cal Utilization", Second Supplementary Volume, Elliott, M.A. Ed. John Willey & Sons Inc., 159-283 (1981).

Saulsberry, J.L., Schafer, P.S., and Schraufnagel, R.A.: "A Guide to Coalbed Methane Reservoir Engineering", Gas Research Institute, Chicago, USA (1996).

Schembre, J.M., Akin, S., Castanier, L.M., and Kovscek, A.R.: "Spontaneous water imbibition into diatomite", Proceedings of the 68th Annual Society for Petroleum Engineers Western Regional Meeting, Bakersfield, CA, SPE 46211 (1998).

Shi, J.Q., and Durucan, S.: "Modeling Mixed-Gas Adsorption and Diffusion in Coalbed Reservoirs", SPE 114197, paper presented at the 2008 SPE Unconventional Reservoirs Conference held in Keystone, Colorado, USA (2008).

Shi, J.Q., and Durucan, S.: "Gas Storage and Flow in Coalbed Reservoirs: Implementation of a Bidisperse Pore Model for Gas Diffusion in a Coal Matrix", SPE

84342, paper presented at the 2003 SPE Annual Technical Conference and Exhibition, Denver, USA (2005).

Tang, G.-Q., Jessen, K, and Kovscek, A.R.: "Laboratory and Simulation Investigation of Enhanced Coalbed Methane Recovery by Gas Injection", SPE 95947, presented at the 2005 SPE Annual Technical Conference and Exhibition held in Dallas, TX U.S.A., (2005).

Taylor, R. and Krishna, R.: "Multicomponent Mass Transfer", Wiley Series in Chemical Engineering, U.S.A (1993).

Takahashi, S.: "Preparation of Generalized Chart for the Diffusion Coefficients of Gases at High Pressures", J. Chem. Eng. Jpn 7, 417 (1974).

Tyn, M.T., and Calus, W.F.: "Diffusion Coefficients in Dilute Binary Liquid Mixtures:, J. Chem. Eng. Data, 20: 106-109 (1975a).

Tyn, M.T., and Calus, W.F.: "Temperature and Concentration Dependence of Mutual Diffusion Coefficients of Some Binary Liquid Systems", J. Chem. Eng. Data, 20: 310-316 (1975b).

Wong, S., Gunter, W.D., and Mavor, M.J.: "Economics of CO2 Sequestration in Coalbed Methane Reservoirs", SPE 59785, presented at the 2000 SPE/CERI Gas Technology Symposium held in Calgary, Alberta Canada, (2000).

Wesselingh, J.A., and Krishna, R.: "Mass Transfer in Multicomponent Mixtures", Delft University Press, Netherlands (2000).

Warren, J.E., and Root, P.J.: "The Behavior of Naturally Fractured Reservoirs. SPE J. 3, 235-255 (1963).

Wei, X.R., Wang, G.X., Massarotto, Golding, S.D., and Rudolph, V.: "Numerical simulation of multicomponent gas diffusion and flow in coals for CO_2 enhanced coalbed methane recovery", Chem. Eng. Sc. 62: 4193-4203 (2007).

Wei, X.R., Wang, G.X., Massarotto, and Golding, S.D.: "A Case Study on the Numerical Simulation of Enhanced Coalbed Methane Recovery", SPE 101135, paper presented at the 2006 SPE Asia Pacific Oil & Gas Conference and Exhibition held in Adelaide, Australia (2006).

Wilke, C.R., and Lee, C.Y.: "Estimation of Diffusion Coefficients for Gases and Vapors", Ind. Eng. Chem., 47: 1253-1257 (1955).

Yang, R.T.: "Gas Separation by Adsorption Processes", Butterworth, London (1987).

Appendix A

A.1 Estimation of Diffusion Coefficients

The following example illustrates in detail the procedure to compute the binary diffusivities. For a given set of pressure and temperature data, the binary diffusivities are computed. From the computed diffusivity numbers, one can get an idea of the order of magnitude of diffusivities associated with multicomponent gas mixtures (which is otherwise not available). Of course, the binary diffusivity is a function of the total pressure and temperature and as it will become evident from the example; the order of magnitude of diffusivity values can change significantly over varying temperature and pressure ranges. For this example, the following temperature and pressure conditions have been chosen: T= 305K (32 ˚C) & P= 27.6 bars (400 psia). For ease of representation, the components are numbered as 1: CO_2 2: N_2 3: CH_4
The molecular weights are:
M_1 = 44 g/mol M_2 = 28 g/mol M_3 = 16g/mol

Using Fuller et al. (1965, 1966, 1969) method

$$D_{AB} = \frac{0.00143T^{1.75}}{PM_{AB}^{1/2}[(\Sigma_v)_A^{1/3} + (\Sigma_v)_B^{1/3}]^2}$$

$$M_{AB} = 2\left[(1/M_A) + (1/M_B)\right]^{-1}$$

Table A.1.1: Σ_v data from the table given by Fuller et al., 1969

Diffusion Volume	**CO_2**	**N_2**	**CH_4**
Σ_v	26.9	18.5	25.14

M_{12} =34.22 g/mol

$$Đ_{1,2} = \frac{0.00143\times 305^{1.75}}{27.6\times 34.22^{1/2}[(26.9)_{CO2}^{1/3} + (18.5)_{N2}^{1/3}]^2} = 0.0062 \text{ cm}^2/\text{s}$$

M_{13} =23.47 g/mol

$$Đ_{1,3} = \frac{0.00143\times 305^{1.75}}{27.6\times 23.47^{1/2}[(26.9)_{CO2}^{1/3} + (25.14)_{N2}^{1/3}]^2} = 0.00678 \text{ cm}^2/\text{s}$$

M_{23} =20.364 g/mol

$$Đ_{2,3}= \frac{0.00143\times 305^{1.75}}{27.6\times 20.364^{1/2}[(18.5)_{CO2}^{1/3}+(25.14)_{N2}^{1/3}]^2} = 0.00822 \text{ cm}^2/\text{s}$$

Using the empirical method Wilke and Lee (1955)

$$D_{AB} = \frac{[3.03-(0.98/M_{AB}^{1/2})](10^{-3})T^{3/2}}{PM_{AB}^{1/2}\sigma_{AB}^2\Omega_D}$$

$$M_{AB} = 2\left[(1/M_A) + (1/M_B)\right]^{-1}$$

The collision integral (Ω_D) is found using the formulation outline by Neufeld et al. (1972):

$$\Omega_D = \frac{1.06036}{(T^*)^{0.15610}} + \frac{0.19300}{\exp(0.47635T^*)} + \frac{1.03587}{\exp(1.52996T^*)} + \frac{1.76474}{\exp(3.89411T^*)}$$

where $T^* = k_BT/\varepsilon$ (k_B being the Boltzmann constant and ε the energy of interaction)

$\sigma = 1.18\ V_b^{1/3}$; V_b is the liquid molar volume at normal temperature

$\varepsilon/k_B = 1.15T_b$; T_b is the normal boiling temperature

$\varepsilon_{AB} = (\varepsilon_A\ \varepsilon_B)^{1/2}$ and $\sigma_{AB} = (\sigma_A + \sigma_B)/2$

In order to find V_b, the Tyn and Calus Method (1975) has been used wherein V_b is expressed as a function of critical volume (V_c).

$V_b = 0.285V_c^{1.048}$, both the units being in cc/gm mole

The critical volumes and normal boiling temperatures of the three components are known values (Perry and Green, 1997) and using the above correlations, the collision diameter (σ) and interaction energy (ε) can be estimated (Table 2).

Table A.1.2: Empirical model parameters (based on Wilke and Lee)

Component	**V_c (cc/mol)**	**T_b (K)**	**$V_b = 0.285V_c^{1.048}$ (cc/mol)**	**$\sigma=1.18\ V_b^{1/3}$**	**$\varepsilon/k_B=1.15T_b$**
CO_2 (1)	95	194.5	33.7	3.81	223.7
N_2 (2)	89	77.2	31.46	3.72	88.78
CH_4 (3)	99	111.6	35.2	3.87	128.34

$\varepsilon_{12} / k_B = 140.92$
$\sigma_{12} = 3.765$
$T^* = T/(\varepsilon_{12} / k) = 2.164$
$\Omega_D = 1.047$
$M_{12} = 34.22$ g/mol

$$Đ_{1,2} = \frac{[3.03 - (0.98 / 34.22^{1/2})](10^{-3})305^{3/2}}{27.6 \times 34.22^{1/2} \times 3.765^2 \times 1.047} = 0.00636 \text{ cm}^2/\text{s}$$

$\varepsilon_{13} / k_B = 169.44$
$\sigma_{13} = 3.84$
$T^* = 1.82.164$
$\Omega_D = 1.1168$

$M_{13} = 23.47$ g/mol

$$Đ_{1,3} = \frac{[3.03 - (0.98 / 23.47^{1/2})](10^{-3})305^{3/2}}{27.6 \times 23.47^{1/2} \times 3.84^2 \times 1.1168} = 0.00684 \text{ cm}^2/\text{s}$$

$\varepsilon_{23} / k_B = 106.74$
$\sigma_{23} = 3.795$
$T^* = 2.857$
$\Omega_D = 0.9627$
$M_{23} = 20.364$ g/mol

$$Đ_{2,3} = \frac{[3.03 - (0.98 / 20.364^{1/2})](10^{-3})305^{3/2}}{27.6 \times 20.364^{1/2} \times 3.795^2 \times 0.9627} = 0.008676 \text{ cm}^2/\text{s}$$

The values of the binary diffusion coefficients calculated using the two correlations come pretty close to each other, see Table 3.

Table A.1.3: Comparison of binary diffusivity values obtained using the two empirical approaches for T= 305 K (32 ˚C) & P= 27.6 bars (400 psia)

Correlations	**$Đ_{1,2}$ (cm^2/s)**	**$Đ_{1,3}$ (cm^2/s)**	**$Đ_{2,3}$ (cm^2/s)**
Fuller et al.	0.0062	0.00678	0.00822
Wilke and Lee	0.00636	0.00684	0.008676

A.2 Estimation of Mean Free Path

The mean free path can be estimated using the following equation:

$$\lambda = \frac{k_B T}{\sqrt{2}(\pi \sigma^2_{ii} P)}$$

The method of Chung, et al. (1984, 1988) is used to calculate the value of collision diameter σ_{ii}:

$$\sigma_{ii} = 0.809 V_C^{1/3}$$

where σ_{ii} is in Å and V_C (critical volume) in cm^3/mol. The critical volumes of the three components are known values (Perry and Green, 1997) and using the above correlation, the collision diameter can be estimated (Table 4).

Table A.2.1: V_C and σ_{ii} data for the three gas components

	CO_2	**N_2**	**CH_4**
V_C (cc/mol)	95	89	99
σ_{ii} (Å)	3.69	3.612	3.742

For this example, the following temperature and pressure conditions have been chosen: T= 305K (32 ˚C) & P= 27.6 bars (400 psia). Substituting the values of P, T and σ_{ii}, the mean free path can be computed, see Table 5.

Table A.2.2: Mean free path (λ) for the three gas components

Mean Free Path	**CO_2**	**N_2**	**CH_4**
λ (nm)	2.53	2.64	2.46

Appendix B

B.1 Adaptive Perturbation Technique

The following is the part of the MATLAB code that computes the Jacobian elements by numerical perturbation technique.

```
function Jacob = num_jacob (C1temp,C2temp,C3temp,C1nu,C2nu,C3nu,i);
global D23 D12 D13 Csurf N phi delt delr alphap1 alphap2 alphap3 betap1 betap2 betap3
global jacob
%% This function constructs the Jacobian numerically by perturbation
%% technique

if   (i == 1)

% for inner block with adjacent neighbors
%% C1 residual equations jacobian terms

%% Finding jacob (3*i-2,3*i-2)

%%%%%   Beginning of "PERTURBATION TECHNIQUE"  %%%%%%
tol = 0.0001;
dx = 1.e-4; % initial perturbation
temp = dx;
C1pert = C1temp;
C1pert (i) = C1pert (i) + dx; % only change the i location value
fp1 = res1 (C1pert, C2temp, C3temp, C1nu, C2nu, C3nu, i); % computes the residual F using the
perturbed value
C1pert = C1temp;
C1pert (i) = C1pert (i) - dx; % only change the i location value
fn1 = res1 (C1pert, C2temp, C3temp, C1nu, C2nu, C3nu, i);% computes the residual F using the
perturbed value
fprime10 = (fp1 - fn1) /( 2*dx); % second order central difference

% The first "while" is to find the derivative dRC1/dC1
j = 0;
errorflag = 0;
while (1)
```

```
   % Test if minimum threshold is reached
   if   (dx/2 < 1.e-10) % This is the minimum threshold value
      errorflag = 1;
      break;
   end

   % Otherwise calculate new df/dx
   j = j + 1;
   C1pert = C1temp;
   C1pert (i) = C1pert (i) + dx/2;   % If tolerance not reached, bisect the perturbation size
    fp1 = res1 (C1pert, C2temp, C3temp, C1nu, C2nu, C3nu, i); % computes the residual F using
  the perturbed value
   C1pert = C1temp;
   C1pert (i) = C1pert (i) - dx/2;
   fn1 = res1 (C1pert, C2temp, C3temp, C1nu, C2nu, C3nu, i); % computes the residual F using
  the perturbed value
   fprime1N = (fp1 - fn1)/dx;

   % Test for convergence
   fprimediff1 = fprime1N - fprime10;
   nlength1 = length (fprimediff1);
   error1 = norm (fprimediff1)/sqrt(nlength1);
   if  (abs(error1)< tol)
      break
   end

   % dx/2 ---> dx and repeat
   dx = dx/2; % If tolerance not reached, bisect the perturbation size
   fprime10 = fprime1N;
end

% Print result
if  (errorflag)
   fprime1final = fprime10;
else
   fprime1final = fprime1N;
end
 %%%%%   End of "PERTURBATION TECHNIQUE"  %%%%%%

jacob (3*i-2,3*i-2) = fprime1final;
```

B.2 CT image processing code to generate CT profile (vector of CT numbers)

```
%% MATLAB code to generate CT profiles
% The computer connected to the scanner using reconstruction algorithms
% generates CT image which is a matrix of CT numbers in Hounsfield units
% The CT image is stored with an "IMG" extension

filename = '0466-06.IMG';  % CT image at a given time instant
fig = ReadCTData (filename); % reads the CT image using the function developed by Andres
Mantilla, 2002
imagesc (fig.Data); % Generates the image

% By zooming into this image, the X-Y “image” co-ordinates of the 3 coal pieces were found
% Compute the mean of the CT numbers in the X direction for a given Y

avgCT1 = mean (fig.Data (291:311,247:263), 2);  % CT profile for the bottom coal piece
avgCT2 = mean (fig.Data (245:287,247:263), 2);  % CT profile for the middle coal piece
avgCT3 = mean (fig.Data (218:241,247:263), 2);  % CT profile for the top coal piece
avgCT_total = vertcat (avgCT3, avgCT2, avgCT1); % Compiles CT numbers from top to bottom
```